

**LIPID BINDING PROTEINS: ROLES IN LIGAND TRANSFER  
AND ACTIVATION OF NUCLEAR RECEPTORS**

A Dissertation

by

ANCA DANIELA PETRESCU

Submitted to the Office of Graduate Studies of  
Texas A&M University  
in partial fulfillment of the requirements for the degree of  
DOCTOR OF PHILOSOPHY

May 2003

Major Subject: Toxicology

LIPID BINDING PROTEINS: ROLES IN LIGAND TRANSFER  
AND ACTIVATION OF NUCLEAR RECEPTORS

A Dissertation

by

ANCA DANIELA PETRESCU

Submitted to Texas A&M University  
in partial fulfillment of the requirements  
for the degree of

DOCTOR OF PHILOSOPHY

Approved as style and content by:

---

Friedhelm Schroeder  
(Chair of Committee)

---

Timothy D. Phillips  
(Member)

---

James E. Womack  
(Member)

---

Robert S. Chapkin  
(Member)

---

Glen A. Laine  
(Head of Department)

---

Timothy D. Phillips  
(Chair of Toxicology Faculty)

May 2003

Major Subject: Toxicology

**ABSTRACT**

Lipid Binding Proteins: Roles in Ligand Transfer and Activation of Nuclear Receptors. (May 2003)

Anca Daniela Petrescu B.S.; M.S., University of Bucharest;

Chair of Advisory Committee: Dr. Friedhelm Schroeder

Cholesterol and fatty acyl-coenzymeA thioesters are signalling molecules with role in regulation of genes involved in lipid and glucose transport and metabolism. The studies described herein focused on three proteins that bind lipids and have different cellular functions: steroidogenic acute regulatory protein (StAR), hepatocyte nuclear factor-4 $\alpha$  (HNF-4 $\alpha$ ) and acyl-CoA binding protein (ACBP). First, StAR mediates delivery of cholesterol to inner mitochondrial membrane in steroidogenesis by a poorly understood mechanism. In our studies, fluorescent NBD-cholesterol binding assays demonstrate that StAR binds cholesterol at two binding sites with 32 nM  $K_d$ s and circular dichroism spectra show that cholesterol binding results in changes of StAR secondary structure. Fluorescent sterol exchange assays between donor and acceptor mitochondrial membranes indicate that StAR significantly increased the formation of rapidly transferable cholesterol domains. Second, HNF-4 $\alpha$ , a nuclear receptor, had been shown to bind fatty acyl-CoAs as natural ligands with apparent low affinities obtained with radiolabeled ligand binding assays. Our fluorescence spectroscopy studies demonstrate that HNF-4 $\alpha$  ligand binding domain (HNF-4 $\alpha$ LBD) binds acyl-CoAs at a single binding site with  $K_d$ s of 1.6-4 nM. Fluorescence resonance energy transfer (FRET) between HNF-4 $\alpha$ LBD tryptophan residues and *cis*-parinaroyl-CoA yielded an intermolecular distance of 42 Å thus pointing to direct molecular interaction. Third, although ACBP has been detected in the nucleus, it is not known whether ACBP may directly and/or functionally interact with a nuclear acyl-CoA binding protein such as

HNF-4 $\alpha$  to regulate transcription. Our present studies in vitro and in intact cultured cells, including circular dichroism of HNF-4 $\alpha$  in the presence of ACBP, coimmunoprecipitation of HNF-4 $\alpha$ /ACBP complexes, ACBP and HNF-4 $\alpha$  colocalization in nuclei of cells by confocal microscopy demonstrate a physical association of ACBP and HNF-4 $\alpha$ . FRET microscopy data indicated an intermolecular distance of 53 Å between ACBP and HNF-4 $\alpha$  in rat hepatoma cells. Functional assays (transactivation of an HNF4 $\alpha$ -dependent reporter gene) showed significant increase in the presence of ACBP in two different cell lines. Expression of ACBP anti-sense RNA decreased HNF-4 $\alpha$ -mediated transactivation, pointing to a role of ACBP in co-regulating HNF-4 $\alpha$ -dependent transcription.

## ACKNOWLEDGEMENTS

I want to express my sincere gratitude to Dr. Friedhelm Schroeder and Dr. Ann B. Kier who have closely guided and supervised my graduate program, giving me not only the opportunity to work in a laboratory with outstanding equipment for science research but also a great sense of direction and confidence throughout my professional training.

I also want to thank all my colleagues who helped me on numerous occasions and generously shared their time, professional skills and knowledge during my graduate program. My special thanks go to (in alphabetical order): Barbara Atshaves, Amy Boedeker, Hsu Chao, Al Gallegos, Huan Huang, Avery McIntosh, Greg Martin, John Roths. I am very grateful to Dr. Bar-Tana and Dr. Rachel Hertz from the Hebrew University Medical School, who had important contributions to our projects on hepatocyte nuclear factor 4  $\alpha$ .

I express my appreciation to Dr. Timothy D. Phillips, Dr. James E. Womack, Dr. Robert S. Chapkin and Dr. Rajiv Sarin for their participation on the graduate committee and their scientific advice.

## TABLE OF CONTENTS

	Page
ABSTRACT.....	iii
ACKNOWLEDGEMENTS.....	v
TABLE OF CONTENTS.....	vi
LIST OF TABLES.....	xiii
LIST OF FIGURES.....	xiv
CHAPTER	
I    Theoretical Background on Lipid Binding Proteins with Roles in Lipid Transfer and Gene Regulation.....	1
1.1 Lipid Binding Proteins with Role in Intracellular Traffic of Cholesterol.....	1
1.1.1 General Characterization of Cholesterol Binding Proteins that Mediate Intracellular Transport of Cholesterol.....	1
1.1.2 Steroidogenic Acute Regulatory Protein (StAR): Structure/Function Relationship.....	3
1.2 Lipid Binding Proteins with Role in Intracellular Traffic of Fatty Acyl-CoAs.....	4
1.2.1 General Characterization of Intracellular Acyl-CoA Binding Proteins.....	5
1.2.2 Acyl-CoA Binding Protein (ACBP): Functions and Regulation.....	6
1.3 Nuclear Receptors.....	7
1.3.1 Classification and General Characterization of Nuclear Receptors.....	7
1.3.2 Hepatocyte Nuclear Factor-4 $\alpha$ : Functions, Regulation.....	11

CHAPTER	Page
1.3.3 Nuclear Receptors that Regulate Genes in Response to Cholesterol as Signal Molecule.....	13
1.3.4 Nuclear Receptors that Regulate Genes in Response to Fatty Acids and Acyl-CoAs Signal Molecules.....	16
1.3.5 Lipid Binding Proteins Interact with Nuclear Receptors and Coregulate Gene Expression.....	20
1.4 Present Research Objective.....	22
1.4.1 Studies on StAR Protein Ability to Bind Cholesterol and Modulate Sterol Domain Dynamics in Mitochondrial Membranes.....	22
1.4.2 Ligand Specificity and Conformational Dependence of HNF-4 $\alpha$ .....	22
1.4.3 Physical and Functional Interaction of ACBP and HNF-4 $\alpha$ .....	23
II Steroidogenic Acute Regulatory Protein Binds Cholesterol and Modulates Membrane Sterol Domain Dynamics.....	24
2.1 Introduction.....	24
2.2 Experimental Procedures.....	26
2.2.1 Materials.....	26
2.2.2 Recombinant Proteins.....	26
2.2.3 Cell Culture.....	27
2.2.4 Isolation of Mitochondria for Sterol Transfer Assay.....	28
2.2.5 Fluorescence Assay for Sterol Binding to StAR.....	28
2.2.6 Fluorescence Resonance Energy Transfer.....	29
2.2.7 Stern-Volmer Fluorescence Quenching.....	31
2.2.8 Circular Dichroism of StAR with and without Cholesterol....	31
2.2.9 Fluorescence Sterol Transfer Assays.....	32
2.2.10 Calculation of Molecular Sterol Transfer.....	34

CHAPTER	Page
2.3 Results.....	34
2.3.1 The Sterol Binding Site of StAR; NBD-Cholesterol Spectral Shifts and KI Quenching.....	34
2.3.2 StAR Binding of NBD-Cholesterol: Affinity and Stoichiometry.....	36
2.3.3 Binding of NBD-Cholesterol to the A218V Mutant Recombinant StAR.....	39
2.3.4 StAR Trp: Aqueous Accessible or Buried.....	40
2.3.5 Fluorescence Resonance Energy Transfer of StAR Trp to Bound NBD-Cholesterol; Quenching of StAR Trp Fluorescence Emission.....	42
2.3.6 Sterol Binding Parameters of StAR Determined by FRET and Sensitized Emission of Bound NBD-Cholesterol.....	44
2.3.7 Effect of Sterol Binding on StAR Conformation.....	48
2.3.8 Spontaneous Sterol Transfer from Mitochondrial Membranes...	51
2.3.9 StAR Preferentially Enhanced the Initial Rate of Molecular Sterol Transfer from Mitochondrial Membranes of Steroidogenic MA-10 Cells versus Fibroblasts.....	51
2.3.10 Effect of SCP-2 on Initial Rate of Molecular Sterol Transfer from Mitochondrial Membranes of Steroidogenic MA-10 Cells and Normal CWN Human Fibroblasts.....	53
2.3.11 Dynamic Analysis of Spontaneous Sterol Transfer from Mitochondrial Membranes.....	54
2.3.12 StAR Preferentially Alters the Sterol Kinetic Pools of Mitochondrial Membranes Isolated from Steroidogenic MA-10 Cells versus Fibroblasts.....	55
2.3.13 Effect of SCP-2 on Sterol Kinetic Pools of Mitochondrial Membranes Isolated from Steroidogenic MA-10 Cells versus Fibroblasts.....	56



CHAPTER	Page
2.4 Discussion.....	57
III Ligand Specificity and Conformational Dependence of the Hepatocyte Nuclear Factor-4 $\alpha$ (HNF-4 $\alpha$ ).....	65
3.1 Introduction.....	65
3.2 Experimental Procedures.....	67
3.2.1 Chemicals.....	67
3.2.2 Expression of Recombinant Rat HNF-4 $\alpha$ LBD.....	67
3.2.3 Purification, SDS-PAGE and Western Blotting of Recombinant HNF-4 $\alpha$ LBD.....	67
3.2.4 Synthesis and Purification of Fluorescent <i>cis</i> -Parinaroyl- CoA (cPNA-CoA).....	68
3.2.5 Direct Ligand Binding Assays.....	70
3.2.5.1 Fluorescent Ligands.....	70
3.2.5.2 Quenching of Intrinsic Fluorescence of HNF- 4 $\alpha$ LBD Aromatic Amino Acids Tyr/Trp or Trp .....	71
3.2.6 FRET Determination of Intermolecular Distance between the HNF-4 $\alpha$ LBD Trp and Bound <i>cis</i> -Parinaroyl-CoA.....	71
3.2.7 Circular Dichroism (CD) of HNF-4 $\alpha$ LBD.....	73
3.3 Results.....	73
3.3.1 Determination of the Binding Parameters of HNF-4 $\alpha$ LBD for a Naturally Occurring Fluorescent Fatty Acyl-CoA: <i>cis</i> -Parinaroyl- CoA Quenching of HNF-4 $\alpha$ LBD Trp.....	73
3.3.2 Molecular Interaction of <i>cis</i> -Parinaroyl-CoA with HNF-4 $\alpha$ LBD: Fluorescence Resonance Energy Transfer (FRET) .....	76
3.3.3 Calculation of the Intermolecular Distance between HNF- 4 $\alpha$ LBD and Bound <i>cis</i> -Parinaroyl-CoA by FRET.....	78

CHAPTER	Page
3.3.4	Determination of the Binding Parameters of HNF-4 $\alpha$ LBD for <i>cis</i> -Parinaroyl-CoA from FRET Data..... 82
3.3.5	Binding Specificity of HNF-4 $\alpha$ LBD for <i>cis</i> -Parinaroyl-CoA: Interaction with <i>cis</i> -Parinaric Acid and CoA..... 82
3.3.6	Binding of Nonfluorescent, Long Chain Fatty Acyl-CoA to HNF-4 $\alpha$ LBD..... 87
3.3.7	Binding Specificity of HNF-4 $\alpha$ LBD: Free Fatty Acids..... 87
3.3.8	HNF-4 $\alpha$ LBD Binds Peroxisome Proliferators as CoA-thioesters or Free Fatty Acids..... 91
3.3.9	Secondary Structure of HNF-4 $\alpha$ LBD and Effects of Fatty Acyl-CoAs: Circular Dichroism..... 93
3.4	Discussion..... 94
IV	Physical and Functional Interaction of Acyl-CoA Binding Protein (ACBP) and Hepatocyte Nuclear Factor-4 $\alpha$ (HNF-4 $\alpha$ ) ..... 101
4.1	Introduction..... 101
4.2	Experimental Procedures..... 103
4.2.1	Materials..... 103
4.2.2	Circular Dichroism (CD) of ACBP and HNF-4 $\alpha$ LBD..... 103
4.2.3	ACBP and HNF-4 $\alpha$ LBD Antisera for Coimmunoprecipitation, Western Blotting, and Immunocytochemistry..... 104
4.2.4	Coimmunoprecipitation of ACBP and HNF-4 $\alpha$ LBD..... 105
4.2.5	Western Blotting of ACBP and HNF-4 $\alpha$ ..... 105
4.2.6	Cell Culture..... 106
4.2.7	Preparation of Cells for Indirect Immunofluorescence Microscopy..... 106
4.2.8	Laser Scanning Confocal Microscopy (LSCM) and Image Analysis..... 107

CHAPTER	Page
4.2.9	Fluorescence Resonance Energy Transfer (FRET) Microscopy.....107
4.2.10	DNA Constructs and Plasmids Used in Transfection Assays...108
4.2.11	Functional Interaction of ACBP with HNF-4 $\alpha$ in Intact Cells: Transactivation Assay..... 109
4.2.12	Functional Interaction of ACBP with HNF-4 $\alpha$ in Intact Cells: Mammalian Two-Hybrid Assay.....109
4.3	Results.....110
4.3.1	ACBP/HNF-4 $\alpha$ Complex Formation <i>in Vitro</i> : Circular Dichroism.....110
4.3.2	ACBP/HNF-4 $\alpha$ Complex Formation <i>in Vitro</i> : Coimmunoprecipitation .....113
4.3.3	Colocalization of ACBP and HNF-4 $\alpha$ within the Nuclei of Fixed Hepatoma Cells..... 113
4.3.4	ACBP/HNF-4 $\alpha$ Intermolecular Distance in Fixed Cells: Fluorescence Resonance Energy Transfer (FRET) Microscopy .....116
4.3.5	ACBP/HNF-4 $\alpha$ Structural Interaction in Living cells: Mammalian Two-Hybrid Assay .....117
4.3.6	Expression of ACBP and HNF-4 $\alpha$ in COS-7 and Hepatoma Cells.....117
4.3.7	Intracellular Distribution of ACBP and HNF-4 $\alpha$ in Transfected COS-7 and Rat Hepatoma Cells Overexpressing ACBP and HNF-4 $\alpha$ .....121
4.3.8	Functional Significance of ACBP Expression on HNF-4 $\alpha$ Transcriptional Activity: Transactivation Assays.....123

CHAPTER	Page
4.3.9 Functional Significance of ACBP Expression on HNF-4 $\alpha$ Transcriptional Activity: LSCM Imaging of Luciferase Transactivation in Individual Cells.....	125
4.4 Discussion.....	128
V Summary and Conclusions.....	133
5.1 Steroidogenic Acute Regulatory Protein (StAR) Binds Cholesterol with High Affinity and Modulates the Dynamics of Mitochondrial Membrane Domains.....	133
5.2 Ligand Specificity and Conformational Dependence of the Hepatocyte Nuclear Factor-4 $\alpha$ (HNF-4 $\alpha$ ).....	134
5.3 Studies on Physical and Functional Interaction of Acyl-CoA Binding Protein (ACBP) and Hepatocyte Nuclear Factor-4 $\alpha$ (HNF-4 $\alpha$ ).....	135
REFERENCES.....	137
APPENDIX.....	153
VITA.....	154

## LIST OF TABLES

TABLE	Page
1.1	Transcription factors modulated by fatty acids and fatty acyl-CoAs are involved in regulation of lipid transport and metabolism..... 10
1.2	Target genes regulated by HNF-4 $\alpha$ and their functions in cellular physiology..... 12
1.3	Lipid binding proteins with role in coregulation of nuclear receptors..... 21
2.1	Forster energy transfer from N-62 StAR Trp to bound NBD-cholesterol..... 45
2.2	Initial rates of molecular sterol transfer from mitochondrial membranes isolated from normal CWN human fibroblasts and steroidogenic MA-10 Leydig cells..... 54
2.3	Mitochondrial membrane cholesterol domain dynamics..... 55
3.1	Chemical structures of fatty acids and peroxisome proliferators whose CoA thioesters as well as free fatty acid forms were tested for HNF-4 $\alpha$ LBD binding..... 74
3.2	Binding affinity of HNF-4 $\alpha$ LBD for <i>cis</i> -parinaroyl-CoA, CoA and <i>cis</i> -parinaric acid..... 77
3.3	Forster energy transfer from HNF-4 $\alpha$ LBD Trp to bound <i>cis</i> -parinaroyl-CoA..... 80
3.4	Specificity of HNF-4 $\alpha$ LBD for non-fluorescent ligands..... 90
3.5	Effect of CoA thioesters of long chain saturated and unsaturated fatty acids on the secondary structure of HNF-4 $\alpha$ LBD..... 96
4.1	Secondary structure of ACBP, HNF-4 $\alpha$ LBD and complexes of these two proteins..... 112

## LIST OF FIGURES

FIGURE	Page
1.1	Schematic presentation of a nuclear receptor modular structure.....8
1.2	Cholesterol and oxysterols are transcription factor modulators..... 15
1.3	Fatty acids and acyl-CoAs are transcription factor modulators.....17
2.1	Fluorescence emission spectra of NBD-cholesterol in the absence and presence of N-62 StAR or A218V N-62 StAR..... 35
2.2	Stern-Volmer quenching of N-62 StAR bound NBD-cholesterol and of N-62 StAR Trp residues..... 37
2.3	Fluorescence ligand binding assay for N-62 StAR (panel A) and the A218V mutant StAR (panel B).....38
2.4	Spectral overlap of N-62 StAR Trp fluorescence emission with NBD-cholesterol absorption (excitation).....41
2.5	Effect of FRET between N-62 StAR Trp and bound NBD-cholesterol... 43
2.6	Effect of FRET between N-62 StAR Trp/Tyr and bound NBD-cholesterol..... 46
2.7	Effect of cholesterol binding on circular dichroic spectra of N-62 StAR protein..... 48
2.8	Effect of N-62 StAR, A218V N-62 StAR, and SCP-2 on sterol transfer from mitochondrial membranes isolated from normal (CWN) human fibroblasts..... 50
2.9	Effect of N-62 StAR and SCP-2 on sterol transfer from mitochondrial membranes isolated from steroidogenic MA-10 Leydig cells..... 52
3.1	Purity of recombinant rat HNF-4 $\alpha$ LBD.....68
3.2	HPLC purification of <i>cis</i> -parinaroyl-CoA..... 69
3.3	Titration of HNF-4 $\alpha$ LBD with <i>cis</i> -parinaroyl-CoA: binding curves derived from quenching in HNF-4 $\alpha$ LBD fluorescence .....75

FIGURE	Page
3.4 Spectral overlap of HNF-4 $\alpha$ LBD Trp fluorescence emission with <i>cis</i> -parinaroyl-CoA absorption (excitation).....	78
3.5 Sensitized emission of HNF-4 $\alpha$ LBD-bound <i>cis</i> -parinaroyl-CoA and binding curves as resulted from FRET data.....	81
3.6 Titration of HNF-4 $\alpha$ LBD with CoA.....	83
3.7 Titration of HNF-4 $\alpha$ LBD with <i>cis</i> -parinaric acid.....	85
3.8 Binding of long chain fatty acyl-CoAs to HNF-4 $\alpha$ LBD.....	86
3.9 Binding of long chain free fatty acids to HNF-4 $\alpha$ LBD.....	88
3.10 Binding of peroxisome proliferators as CoA thioesters or free fatty acids, to HNF-4 $\alpha$ LBD.....	92
3.11 Circular dichroic spectral changes induced by fatty acyl-CoAs in HNF-4 $\alpha$ LBD.....	94
4.1 Circular dichroic spectrum of ACBP in the presence of HNF-4 $\alpha$ LBD indicates complex formation.....	111
4.2 Coimmunoprecipitation of ACBP and HNF-4 $\alpha$ LBD from an <i>in vitro</i> mixture.....	114
4.3 LSCM colocalization of ACBP and HNF-4 $\alpha$ in fixed hepatoma cells...	115
4.4 ACBP / HNF-4 $\alpha$ association in nuclei of fixed cells: FRET microscopy .....	116
4.5 Mammalian two-hybrid assay of ACBP/ HNF-4 $\alpha$ interaction .....	118
4.6 ACBP and HNF-4 $\alpha$ expression in transfected cells: western blotting.....	119
4.7 ACBP and HNF-4 $\alpha$ expression in transfected cells: LSCM imaging.....	120
4.8 Intracellular distribution of ACBP and HNF-4 $\alpha$ in transfected COS-7: LSCM colocalizations.....	122

FIGURE	Page
4.9 Intracellular distribution of ACBP and HNF-4 $\alpha$ in hepatoma cells: LSCM colocalizations.....	124
4.10 ACBP stimulates HNF-4 $\alpha$ -mediated transactivation.....	126
4.11 LSCM imaging of HNF-4 $\alpha$ -mediated luciferase transactivation in individual hepatoma cells .....	127



## CHAPTER I

### THEORETICAL BACKGROUND ON LIPID BINDING PROTEINS WITH ROLES IN LIPID TRANSFER AND GENE REGULATION

#### 1.1 LIPID BINDING PROTEINS WITH ROLE IN INTRACELLULAR TRAFFIC OF CHOLESTEROL

Cholesterol is an important component of mammalian cellular membranes and the ratio of cholesterol to phospholipid is a primary regulator of membrane structure, fluidity and function (1). Cholesterol concentration is specific for each cellular membrane type (plasma membrane has the highest cholesterol content > endosomes > endoplasmic reticulum > Golgi complex) and the regulation of synthesis, intake and efflux of cholesterol is strictly controlled by the amount of proteins involved in cholesterol transport and metabolism (2).

##### *1.1.1 General Characterization of Cholesterol Binding Proteins that Mediate Intracellular Transport of Cholesterol*

Several proteins involved in pathways of cholesterol uptake, intracellular trafficking and efflux have been characterized and demonstrated to be diverse in their structures and functions. However, several functional categories of cholesterol binding proteins can be distinguished.

First, the best characterized proteins with role in free (nonesterified) cholesterol uptake are: caveolins and scavenger receptor B1 (SR-B1). Caveolin-1 is a membrane protein that binds cholesterol (and fatty acids) and has role in stabilizing microdomains rich in cholesterol and sphingolipids within plasma membranes, i.e. rafts and caveolae. SR-B1 is a receptor for serum, extracellular high density lipoprotein

---

This dissertation follows the style and format of *Journal of Biological Chemistry*.

(HDL), resides in caveolae and mediates a selective transfer of free cholesterol from HDL particle into the cell without HDL internalization, by a mechanism not completely understood (3). Another source of free cholesterol is low density lipoprotein (LDL) which has to be taken inside the cells by clathrin coated vesicles that harbor LDL-receptors (endosome, lysosome pathway) (4).

Second, intracellular cholesterol binding proteins mediate cholesterol transfer among different organelles. Thus, cytoplasmic complexes of caveolin/ cholesterol/ chaperones have been isolated and attributed the role of transferring cholesterol from plasma membrane to ER and Golgi complex (5). Lysosomal cholesterol (from LDL containing clathrin coated vesicles turned into endosomes and fused with lysosomes) can be transited to ER, mitochondria, plasma membrane and lipid droplets by vesicular and non-vesicular protein mediated transport. Sterol carrier protein-2 (SCP-2), a protein that resides mainly in peroxisomes but also in cytoplasm and other organelles, *e.g.* mitochondria and ER, has been found to have important role in the transfer of cholesterol outside lysosomes by both vesicular and non-vesicular mechanisms (1) (6) (7). SCP-2 has also an important contribution to cholesterol concentration in mitochondrial outer membrane (1). The major source of cholesterol for mitochondrial steroidogenesis are plasma membrane and lipid droplets. SCP-2 enhances transfer of cholesterol from isolated lipid droplets to mitochondria in intact cells and stimulate steroidogenesis in transfected cells overexpressing SCP-2 (1). In vitro assays of inter-membrane cholesterol exchange show that SCP-2 enhances the transfer of cholesterol from lysosomes, and also from ER and plasma membranes to mitochondria. Since another protein, steroidogenic acute regulatory protein (StAR) is responsible for the rapid transfer of cholesterol from the outer to inner mitochondrial membrane in steroidogenic cells, it is thought that SCP-2 resupplies the outer membranes of mitochondria with cholesterol.

A protein with function in the exit of cholesterol from lysosomes was discovered in relation to a disease characterized by abnormal accumulation of LDL-derived cholesterol in lysosomes and Golgi due to a mutation in Niemann-Pick type C1 (NPC1)

protein that is believed to have role in recirculating cholesterol-rich late endosomes back to plasma membranes. In NPC1 fibroblasts the turn-over time of late endosomes is about 50% slower than normal (8).

Cells can synthesize their own cholesterol from acetyl-CoA by a long metabolic pathway requiring many enzymes located inside endoplasmic reticulum (ER). Most of the ER biosynthesized cholesterol along with phospholipids and sphingolipids are transported to Golgi complex where a process of sorting and arrangement into specific structures like rafts is carried out. The mechanisms of sorting different membrane structures with various types of vesicles emerging from Golgi complex is poorly understood (2).

Third, until recently it was thought that few proteins other than serum apolipoprotein A (HDL-specific) were involved in cholesterol efflux from cells, since spontaneous transfer of cholesterol from plasma membrane to apolipoproteins occurs continuously. However, in some cell types the transfer of cholesterol from plasma membrane to cholesterol-poor HDL particles is facilitated by the same SR-B1 receptor of HDL that also contributes to cholesterol influx from cholesterol-rich HDL-particles at the caveolae location. During recent years, ATP-binding cassette (ABC) transporters were recognized to be very important in cholesterol efflux (9)(10).

### *1.1.2 Steroidogenic Acute Regulatory Protein (StAR): Structure / Function Relationship*

StAR protein is activated by pituitary tropic hormones and regulates the transport of cholesterol from the outer to inner mitochondrial membrane which constitutes the rate limiting step in steroidogenesis. Cholesterol side chain cleavage enzyme (CYP11A) located on the matrix side of the inner mitochondrial membrane synthesizes pregnenolone, the first metabolite in the pathway of steroid hormone biosynthesis.

StAR protein is synthesized as a 37 kDa precursor which is imported into mitochondria of steroidogenic cells, being subsequently processed to 30 kDa form. Based on the observation that StAR protein is localized at the contact sites between outer and inner mitochondrial membranes, an initial mechanism model suggested that StAR

formed bridges and induced contact sites so that cholesterol would flow down its concentration gradient from the outer to the inner mitochondrial membrane (11) (12). Later studies revealed that StAR mutants lacking the 62 N-terminal amino acids (N-62 StAR) including the mitochondrial targeting signal were also effective in stimulating steroidogenesis (13). A different model emerged explaining the ability of N-62 StAR to transfer cholesterol from the outer to inner mitochondrial membrane even from outside mitochondria. In deed, in vitro experiments showed that StAR stimulated the cholesterol and b-sitosterol from sterol rich liposomes to mitochondria (14). This model also assumes that StAR removal from outer membrane by import inside mitochondria is critical for rapid inhibition of StAR effect , thus accounting for the rapid action and short functional life of StAR and the requirement for continuous StAR synthesis to sustain steroidogenesis.

An alternative model of StAR action was proposed based on the 2.2 Å resolution crystal structure of START domain of MLN64 protein which is very similar to StAR (15). The crystal structure demonstrated that cholesterol could bind to a hydrophobic tunnel with the hydroxyl group interacting with the buried Arg 351 residue of the protein. Thus, in this model, StAR protein binds and exchanges cholesterol between mitochondrial membranes, acting as a shuttle. The issue is still a matter of debate.

StAR has been originally identified as a phosphoprotein and later studies concluded that StAR protein sequences from multiple species had two consensus motifs for protein kinase A phosphorylation at serine 57 and serine 195 residues in human protein (16). The physiological and functional significance of StAR phosphorylation is not fully understood (17).

## 1.2 LIPID BINDING PROTEINS WITH ROLE IN INTRACELLULAR TRAFFIC OF FATTY ACYL-CoAs

Nonesterified long fatty acids (C16-C20, LCFAs) are delivered to tissue cells by albumin, the most prominent extracellular fatty acid carrier. The rate of fatty acid uptake

into cells is stimulated by fatty acyl-CoA syntases as well as by the affluence of intracellular fatty acid binding proteins (FABPs) (18)(19).

### 1.2.1 General Characterization of Intracellular Acyl-CoA Binding Proteins

The ability to bind LCFA-CoA-thioesters was detected and studied in three proteins, i.e. liver-fatty acid binding protein (L-FABP), acyl-CoA binding protein (ACBP) and sterol-carrier protein 2 (SCP-2) which belong to three different families of lipid binding proteins (20).

L-FABP is one of the mammalian cytosolic 14-15 kDa FABP gene family. Unlike ACBP or SCP-2 which do not exhibit tissue-specific isoforms, the FABP family has diverged to express a large number of tissue-specific forms, such as liver-, intestinal-, heart-, adipocyte-, brain-FABP. Most FABPs bind LCFA with high affinities in the nanomolar range at a single binding site. They also bind LCFA-CoAs with lower affinities, in the micromolar range. L-FABP is an exception since it binds LCFAs at two binding sites with similar high affinities and is also able to bind acyl-CoAs and other acyl ligands like lysophospholipids in a molar ratio of 1:1, with low affinities (21) (22) (23). Depending on the techniques used to test ligand binding *i.e.* lipidex binding, titration calorimetry or fluorescence spectroscopy, the affinities reported for FABP/LCFA binding varied from micromolar to low nanomolar respectively, while affinities for FABP/LCFA-CoA binding were reported undetected up to micromolar  $K_d$ s, respectively, the fluorimetric methods showing the highest sensitivity (19)(20).

SCP-2 was first known as an inter-membrane cholesterol and phospholipid exchange protein but in 1996 Frolov *et al.* demonstrated that *in vitro* SCP-2 bound a fluorescent LCFA-CoA, *cis*-parinaroyl-CoA with a  $K_d$  of 80 nM (24). This was an important discovery that prompted Seedorf's group to hypothesize and demonstrate that peroxisomal SCP-x which includes the SCP-2 peptide could bind and stimulate metabolic oxidation of CoA-activated phytanic acid (a long branched fatty acid resulted from chlorophyll digestion) in peroxisomes (25).

### 1.2.2 *Acyl-CoA Binding Protein (ACBP): Functions and Regulation*

ACBP was first isolated from rat brain and described as a diazepam-binding inhibitor (DBI) (26). Independently, a 10 kDa peptide was separated from bovine liver by the virtue of its ability to bind and induce the synthesis of medium chain fatty acyl-CoAs and it was designated ACBP (27). Sequencing has revealed that it was the bovine homologue of rat DBI. Subsequent reports showed that ACBP is highly conserved in a wide variety of species ranging from yeast to mammals. ACBP has been shown to bind acyl-CoAs of 8-22 carbon chain length with high affinities but it exhibits the highest binding activity towards acyl-CoAs with 14-22 carbons (LCFAs) (28) (29).

ACBP is normally expressed in many mammalian tissues but is up-regulated in lipogenic organs like liver, white adipose fat, adrenals and gonads. A significant function of ACBP in adipocyte differentiation was first reported when antisense RNA for ACBP transfected into 3T3-L1 fibroblasts inhibited accumulation of triglyceride in lipid droplets and the overall adipocyte differentiation (30). ACBP was found 30% increased in muscles from obese Zucker rats while LCFA-CoAs and triglycerides were 90% more than in normal controls (31). A 3.5 fold over-expression of ACBP in a rat hepatoma cell line showed that 42% more palmitic acid was incorporated than in control cells and this increase in saturated fatty acid was predominantly found in the triglyceride fraction (32). Thus, high expression of ACBP correlates well with stimulation of fatty acid uptake and storage as triglycerides in hepatocytes, adipocytes and some fiber muscles.

In steroidogenic cells ACBP has a stimulatory effect increasing the rate of mitochondrial steroid synthesis (33). No influence of ACBP on StAR is known. However, a very close association and interaction of acyl-CoA-bound ACBP with the mitochondrial carnitine-palmitoyl transferase I (CPT-I) was reported (28), (34). It has been proposed that CPT-I is not able to bind free acyl-CoA and a physical interaction with ACBP is required to induce conformational changes in CPT-I and ligand channeling into CPT-I binding site. The final outcome of ACBP mitochondrial stimulation is an increased rate of  $\beta$ -oxidation of fatty acids with energy formation. It is not known if this has an impact on steroid biosynthesis.

### 1.3 NUCLEAR RECEPTORS

Nuclear receptors are ligand-binding transcription factors that regulate the expression of target genes involved in cell growth, differentiation and metabolism, providing a direct link between signalling molecules and the transcriptional response (35) (36) (37).

#### *1.3.1 Classification and General Characterization of Nuclear Receptors*

In the mid-1980s, the steroid and thyroid hormone receptors were first cloned and found to exhibit an extensive homology, and this observation led to search for new proteins with similar structure. In 2001, the human genome was reported to contain 48 genes encoding proteins with nuclear receptor-type of structure (38). This superfamily contains not only hormone binding transcription factors like estrogen receptor, progesterone receptor, vitamin D receptor, etc. but also a large number of so-called orphan nuclear receptors whose ligands were initially unknown (39). During recent years, specific ligands and also target genes and physiological functions were elucidated for many orphan nuclear receptors which therefore have been referred to as adopted orphan nuclear receptors (40). Many of these newly found ligands are lipid molecules, metabolites of cholesterol and fatty acids, and their nuclear receptors function as lipid sensors that respond to cellular lipid levels and elicit gene expression changes to maintain metabolic and structural homeostasis.

Even though nuclear receptors are extremely diverse in regard to their ligands and functions in homeostasis, reproduction and development, they have common structural characteristics. Thus, nuclear receptors exhibit a modular structure with different regions corresponding to autonomous functional domains that can be interchanged between related receptors without loss of function. A typical nuclear receptor exhibits a variable NH<sub>2</sub>-terminal region (A/B), a conserved DNA-binding domain (DBD) or region C, a hinge region D, and a conserved E region that contains the ligand binding domain (LBD). The A/B region contains an autonomous transcription activation function, referred to as AF-1 that contributes to constitutive ligand-independent activation of the

receptors. A second transcriptional activation domain, termed AF-2 is strictly ligand dependent. Upon ligand binding, nuclear receptors undergo a conformational change that coordinately dissociates corepressors and facilitates recruitment of coactivator proteins to enable transcriptional activation (41). Some nuclear receptors exhibit a COOH-terminal F region of which function is not fully understood (42). In figure 1.1, the modular structure of HNF-4 $\alpha$  is schematically illustrated. In HNF-4 $\alpha$  region F has been shown to be a prolin-rich repressor domain of 14 residues (amino-acids 428-441) that regulates activation function 2 domain (43).

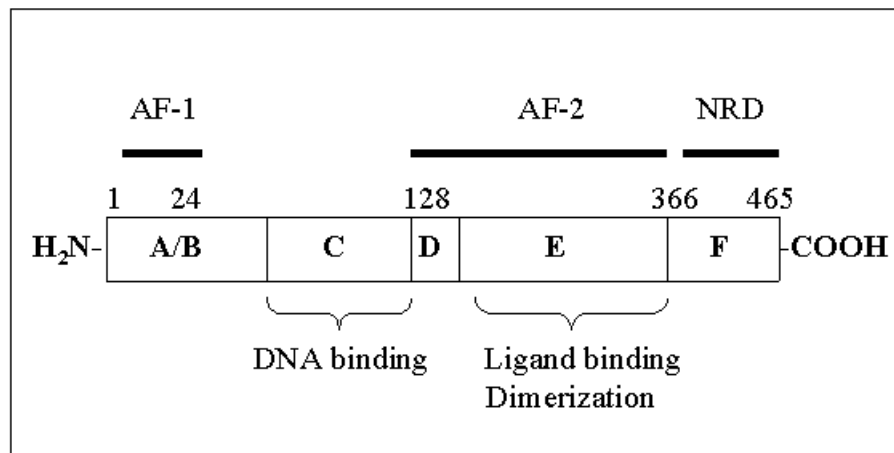


FIG. 1.1. **Schematic presentation of a nuclear receptor modular structure.** HNF-4 $\alpha$  has a modular structure typical for nuclear receptors. -COOH, carboxyl-terminal end; H<sub>2</sub>N, amino-terminal end; AF-1, activation function 1 which is ligand independent; AF-2, ligand-dependent activation function 2; NRD, negative regulatory domain (repressor function).

To perform their extreme diverse functions, nuclear receptors interact directly with the regulatory regions of target genes at specific sequences including the common motif PuGGTCA. This response element is often present in two copies which can be oriented as palindromes (head to head), direct repeats or inverted palindromes (tail to tail) (36). Receptors bind to these sequences as homodimers, heterodimers or monodimers. For



example, steroid receptors (estrogen receptor, progesterone receptor, etc) bind as homodimers, while retinoid X receptors, RXRs, form heterodimers with numerous other members of the superfamily, such as peroxisome proliferator-activated receptors (PPARs), retinoic acid receptors (RARs), thyroid hormone receptor (TR) (37) .

In recent years, nuclear receptors that bind cholesterol, fatty acids or derivatives like oxysterols and fatty acyl-CoAs have been found to be key players in maintaining lipid homeostasis and cellular functions in lipogenic tissues (liver, white adipose fat, adrenals) and also in tissues that use lipids for energy purposes (muscles). In table 1.1 are listed the most extensive characterized nuclear receptors with function in cholesterol and fatty acid metabolism and homeostasis. As Chawla *et al.* (40) pointed out, many nuclear receptors that bind fatty acids (PPARs), fatty acyl-CoAs (hepatocyte nuclear factor 4 $\alpha$ , HNF-4 $\alpha$ ), oxysterols (liver X receptors, LXRs), bile acids (farnesoid X receptor, FXR) and xenobiotics (steroid xenobiotic receptor/pregnane X receptor, SXR/PXR) function as lipid sensors and activate a feed-forward, metabolic cascade by enhancing transcription of genes involved in lipid metabolism, storage, transport and elimination. For example, liver X receptors (LXRs) bind oxysterols when cellular cholesterol is in excess and readily oxidized to 25-, 26- or 27 hydroxycholesterol, and activate several sets of genes through different pathways: I) genes with role in cholesterol-ester formation and storage, i.e. genes of fatty acid synthesis (FAS, stearoyl-CoA desaturase, etc, see Fig. 1.2) ; II) genes of bile acid synthesis (CYP7A); III) genes involved in reverse cholesterol transport (ABCA1, a monomeric transporter that facilitates efflux of cholesterol and phospholipids from cells ). Another example are PPARs, sensors of excess fatty acids in various tissues: PPAR $\alpha$  in liver, PPAR $\gamma$  in adipocytes. Depending on the general tissue-specific function, different isoforms of PPAR induce different genetic changes: in the liver, where lipids can not be stored but rather metabolized and eliminated, activated PPAR $\alpha$  up-regulates genes for fatty acid transport and  $\beta$ -oxidation in mitochondria and peroxisomes (L-FABP, acyl-CoA synthase, acyl-CoA oxidase and others as illustrated in figure 1.3). In adipose tissue which has the function of lipid

TABLE 1.1

*Transcription factors modulated by fatty acids and fatty acyl-CoAs are involved in regulation of lipid transport and metabolism.*

Abbreviations: ACBP, acyl-CoA binding protein; AOX, acyl-CoA oxidase; Apo, apolipoprotein, A-FABP, adipocyte fatty acid binding protein; CYP, cytochrome; FA, fatty acid, saturated (S) or unsaturated (U); -CoAs, CoA-thioesters; HNF-4 $\alpha$ , hepatocyte nuclear factor-4 $\alpha$ ; LACS, long chain acyl-CoA synthase; LCAD, long chain acyl-CoA dehydrogenase; LXR, liver X-receptor; MCAD, medium chain acyl-CoA dehydrogenase; MTP, microsomal transfer protein; PPAR, peroxisome proliferator activated receptor; RXR, retinoid X receptor; TR, thyroid receptor; VLCAD, very long chain acyl-CoA dehydrogenase.

Transcription factor	Modulators	Target gene	Protein function	Regulation (+/-)	Reference
HNF-4 $\alpha$	S-FA-CoAs	Apo CIII	lipid transport	+	(44), (45)
HNF-4 $\alpha$	PUFA-CoAs	Apo CIII	lipid transport	-	(45)
HNF-4 $\alpha$	PUFA-CoAs	GP-6	gluconeogenesis	-	(46)
PPAR $\alpha$	PUFA/-CoAs	ACBP	FA-Coa Transport	+/-	( 47)
PPAR $\alpha$	PUFA/-CoAs	L-FABP	FA transport	+/-	(48) (49)
PPAR $\alpha$	PUFA/-CoAs	VLCAD	FA metabolism	+/-	(50)
PPAR $\alpha$	PUFA/-CoAs	LCAD	FA metabolism	+/-	(50)
PPAR $\alpha$	PUFA/-CoAs	LACS	FA-CoA synthesis	+/-	(50)
PPAR $\alpha$	PUFS/-CoAs	AOX	FA $\beta$ -oxidation	+/-	(50)
PPAR $\gamma$	PUFA/-CoAs	ACBP	FA-CoA transport	+/-	(51)
PPAR $\gamma$	PUFA/-CoAs	A-FABP	lipid transport	+/-	(52)
LXR	PUFA	SREBP-1c	FA synthesis	-	(53) (54)
TR	MCFA	FAS	FA metabolism	-	(55)
TR	MCFA-CoAs	FAS	FA metabolism	-	(56)
RAR	DHA	HNF-4 $\alpha$	FA metabolism	+	(57)

storage, PPAR $\gamma$  activation induces genes responsible for fatty acid and triglyceride synthesis, such as fatty acid synthase, stearoyl-CoA desaturase, glycerophosphate acyl transferase, etc, as shown in figure 1.3.

### 1.3.2. Hepatocyte Nuclear Factor-4 $\alpha$ : Functions, Regulation

Hepatocyte nuclear factor 4 $\alpha$  (HNF-4 $\alpha$ ) had been known as an orphan nuclear receptor until 1998 when it was demonstrated for the first time that fatty acyl-CoA thioesters are the physiological ligands inducing either activation or inhibition of apoCIII, a HNF-4 $\alpha$ -regulated gene, depending on the acyl chain length and saturation (45). Unlike the other nuclear receptors, HNF-4 $\alpha$  does not heterodimerize with RXR, but binds to DR-1 elements RG(G/T)TCA, as homeodimers and for many genes acts as a liver-specific constitutive transcription factor. It has a major function in liver cell differentiation during early stages of embryonic development and its elimination in knock-out mice has been shown to be lethal (58). HNF-4 $\alpha$  is also expressed in kidney, intestine, pancreatic islets and insulinoma cells (59). An increased interest in studying HNF-4 $\alpha$ -dependent regulatory pathways was manifested when several mutations in HNF-4 $\alpha$  gene were correlated with non-insulin-dependent form of diabetes mellitus (NIDDM), i.e. maturity-onset diabetes of the young 1 (MODY 1) (60)(61)(62)(63). MODY1- HNF-4 $\alpha$  mutations result in an autosomal dominant form of NIDDM, characterized by pancreatic  $\beta$ -cell dysfunction and deficient insulin secretion.

Since its first cloning and characterization as a nuclear receptor in 1997 by Sladek *et al.* (64)(65), HNF-4 $\alpha$  was demonstrated to regulate numerous genes most of which are shown in table 1.2.

The regulatory functions of HNF-4 $\alpha$  related to many genes previously studied by gel shift and transactivation assays *in vitro*, were confirmed by recent HNF-4-null mice obtained by Hayhurst *et al.* (66) such as: i) lipoprotein efflux from liver into the blood stream, ii) lipid and glucose synthesis (phosphoenolpyruvate carboxykinase, PEPCK; pyruvate kinase, PK, glucosyl-6-phosphatase); iii) bile acid synthesis (CYP7A1); iv) up-regulation of transcription factors with role in lipid gene regulation (PPAR- $\alpha$  gene has a

TABLE 1.2

*Target genes regulated by HNF-4 $\alpha$  and their functions in cellular physiology.*

Abbreviations: ALDH, aldehyde dehydrogenase; Apo, apolipoprotein; CREB, cellular retinol binding protein; CYP, cytochrome P450; GAPD, glyceraldehyde-phosphate dehydrogenase; I-,L-FABP, intestinal, liver fatty acid binding protein; HNF, hepatocyte nuclear factor; PEPCK, phosphoenolpyruvate carboxykinase;

\*A large number of cytochromes with role in metabolic activation of lipophilic molecules, i.e. CYP2DF6, CYP3A4, CYP3A5, CYP2A6.

Gene	Regulation (+/-)	References
Glucose transport and metabolism		
Glucose transporter 2	+	(71)
Aldolase B	+	(71), (72)
GAPD	+	(71)
Glucose kinase	+	(73)
Pyruvate kinase	+	(71)
PEPCK	+	(74)
Insulin	+	(75)
Lipid transport and metabolism		
I-FABP	+	(71)
L-FABP	+	(71)
CREB-II	+	(71)
ApoB	+	(76)
ApoCIII	+	(77), (55)
ApoAI	-	(78), (79)
CYP7A1	+	(80)
CYP27	+	(81)
Metabolic detoxification		
ALDH 2,3	+	(82), (83)
CYP*	+	(84), (85)
Transcription factors		
HNF-1 $\alpha$	+	(71)
PPAR $\alpha$	+	(86), (87)

binding site for HNF-4 $\alpha$  in its promoter; HNF-1, hepatic nuclear factor-1 is upregulated by HNF-4 $\alpha$  and acts upon many genes responsible for lipid metabolism). An interesting analysis of gene expression profile induced by HNF-4 $\alpha$  in hepatoma cells using an oligonucleotide microarray confirmed that 26 out of 40 induced genes were related to lipid metabolism (67).

HNF-4 $\alpha$  gene regulation has been studied demonstrating that HNF-4 $\alpha$  gene promoter contains fetoprotein transcription factor (FTF) –response elements (68). FTF is an orphan nuclear receptor that activates  $\alpha$ 1-fetoprotein gene along with several other genes during early liver developmental growth. HNF-4 $\alpha$  transcription is activated by FTF carrying important function in early liver differentiation. Direct-repeat 1 elements (DR-1) were identified in promoter of HNF-4 $\alpha$ , suggesting that RAR/RXR heterodimerization can induce HNF-4 $\alpha$  up-regulation (69). An enhancer element has been characterized 6 kb from 5' end of HNF-4 $\alpha$  P1 promoter containing binding sites for the transcription binding sites HNF-1, HNF4, HNF-3 and C/EBP which overlapped with a glucocorticoid consensus site (70).

### *1.3.3 Nuclear Receptors that Regulate Genes in Response to Cholesterol as Signal Molecule*

During recent years numerous studies on gene expression revealed that various lipids and among them cholesterol and unsaturated fatty acids in particular are signaling molecules with important roles in regulation of genes involved in lipid and glucose transport and metabolism (reviews: (88) (89) (91)).

Cholesterol was demonstrated to modulate genes with functions in i) cholesterol homeostasis: LDL receptor, HMG-CoA reductase and synthase, (92) (93) (94) (95); ii) fatty acid synthesis: fatty acid synthase, acyl-CoA carboxylase, stearyl-CoA desaturase (96) (97) (98) (99); iii) fatty acyl-CoA transport and intracellular distribution: acyl-CoA binding protein (99); iv) triglyceride and phospholipid synthesis: glycerol-3-phosphate-acyltransferase gene (100).

A first important breakthrough in understanding how cholesterol can influence gene expression was the discovery of a family of membrane-bound transcription factors, sterol regulatory element-binding proteins or SREBPs, which are synthesized as precursor molecules and reside in endoplasmic reticulum (ER) in association with SREBP cleavage activation protein (SCAP), (93). As illustrated in figure 1.2 the proteolytic activation of precursor SREBPs depends on the cholesterol content in the ER membranes: upon cholesterol depletion of cells, ER membrane becomes fluid and allows SREBP-SCAP complexes to flow into Golgi system where two proteases (S1P and S2P) cleave SREBP precursors and activate them to nuclear forms that act as transcription factors. The most important isoforms of SREBP in mammalian liver in vivo are SREBP-1c and 2 which when activated regulate very different sets of genes: SREBP-1c stimulates fatty acid biosynthesis enzyme genes while SREBP-2 stimulates cholesterol biosynthesis, activating all the enzymes involved in this process (see figure 1.2) (88)(101) (102) (103). Even though SREBPs are not members of nuclear receptor superfamily, they interact closely with nuclear receptors that bind cholesterol derivatives (oxysterols), fatty acids and fatty acyl-CoAs with role in lipid homeostasis .

Liver X receptor, LXR is a nuclear receptor activated by oxysterols, preferentially by 22-hydroxycholesterol, 22HOC (104). In liver, LXR is highly expressed so that an overload with cholesterol results in increased amounts of 22-HOC oxysterols that bind and activate LXRs which further decrease cholesterol biosynthesis and enhance fatty acid synthesis to favor storage of cholesterol as fatty acid esters, by down-regulation of SREBP-2 and up-regulation of SREBP-1c, respectively (105) (106).

An important regulatory pathway initiated by cholesterol overload of steroidogenic tissues such as adrenals and gonads is carried out through oxysterols and a nuclear receptor designated steroidogenic factor-1 (SF-1). SF-1 is a monomer member of the orphan nuclear receptor family with critical role in the expression of cytochrome P450 steroid hydroxylases and steroidogenic acute regulatory protein (StAR) during adrenal and gonads differentiation (107) (108). In steroidogenic tissues, excess of cholesterol uptake results in formation of 25-, 26- and 27-HOC oxysterols that

preferentially bind SF-1 activating StAR protein and CYP27 that favors bioynthesis of steroids (109) (110).

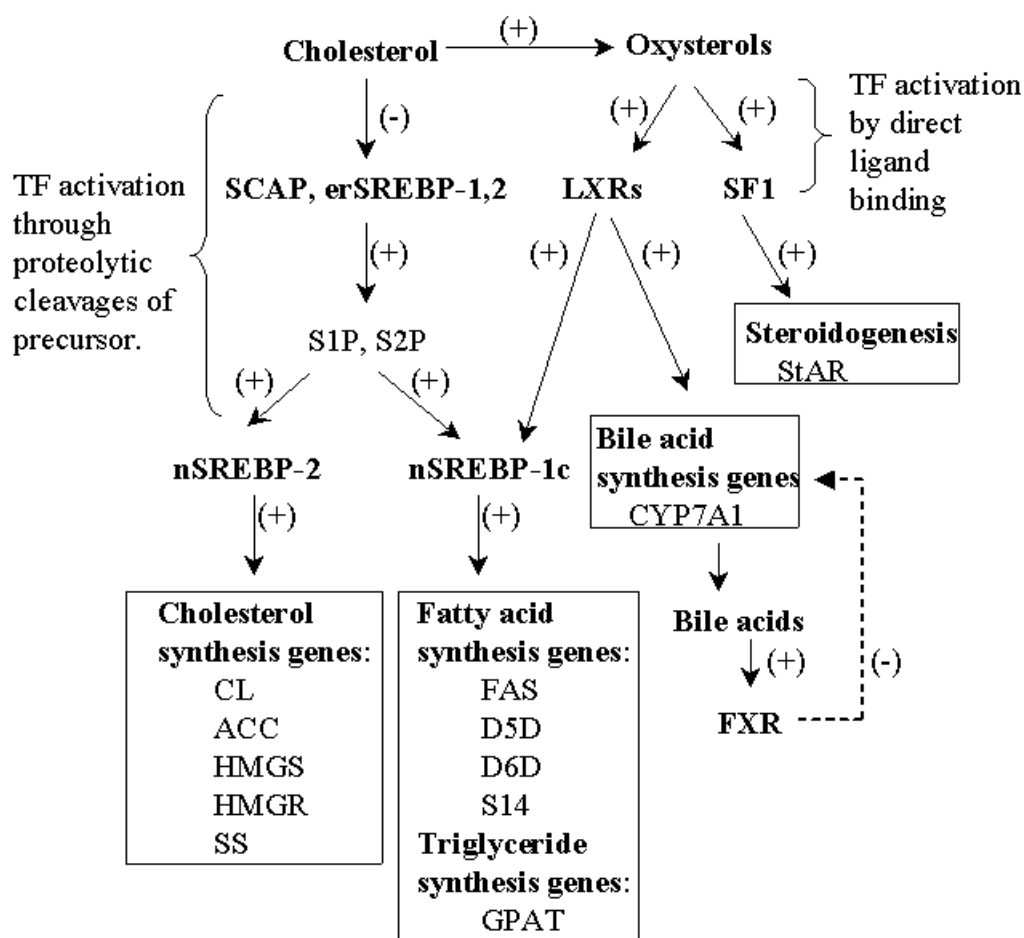


FIG. 1.2. **Cholesterol and oxysterols are transcription factor modulators.**

Cholesterol influences the activity of transcription factor such as SREBPs, sterol regulatory response element binding proteins (er- in ER; n-in nucleus) indirectly through cholesterol sensor protein SCAP, SREBP cleavage-activation protein and S1P, S2P, site-1 and site-2 proteases. Oxysterols formed from excess cholesterol, interact directly with transcription factors: LXR, liver X receptor; SF1, steroidogenic factor. Bile acids bind FXR, farnesyl X nuclear receptor. Genes that are regulated encode for: ACC, acetyl-CoA carboxylase; CL, citrate lyase; CYP, cytochrome; D5D, delta-5 desaturase; D6D, delta-6 desaturase; FAS, fatty acid synthase; GPAT, glycerol-3-phosphate acyltransferase; HMGR, HMG-CoA reductase; HMG-CoAS, synthase; SS, squalene synthase.

#### *1.3.4 Nuclear Receptors that Regulate Genes in Response to Fatty Acids and Acyl-CoAs Signal Molecules*

Fatty acids can influence expression of genes with functions in lipid transport and metabolism in lipogenic tissues like liver and adipose tissue. Four classes of fatty acids are typically encountered in the diet: saturated fatty acids (C12:0-C18:0), n-9 monosaturated fatty acids (C16:1, C18:1) and n-6, n-3 polyunsaturated (PUFAs: C18:2, C18:3, C20:4, C20:5, C22:6 are most common). Saturated and monounsaturated fatty acids affect hepatic gene expression if fed at high levels, for example at more than 40% calories (91). PUFAs on the other hand, even at low feeding levels are able to modulate lipid and glucose metabolism genes in the liver. As illustrated in figure 1.3, nonesterified fatty acids and their CoA-thioesters bind and modulate various transcription factors, many of which are nuclear receptors: peroxisome proliferator-activated receptors (PPAR  $\alpha$ ,  $\beta/\delta$ ,  $\gamma$ ), hepatocyte nuclear receptor-4 $\alpha$  (HNF-4 $\alpha$ ), thyroid hormone (TR), retinoic X receptor (RXR $\alpha$ ) (see table 1.1 for references).

Of the fatty acid-regulated nuclear receptors, PPARs are the most extensively characterized. PPARs bind specific response elements in promoters, enhancers and introns of target genes with role in: i) intracellular traffic and pool distribution of fatty acids (liver, adipocyte and keratinocyte fatty acid binding proteins, FABPs; fatty acyl-CoA binding protein, ACBP); ii) peroxisomal  $\beta$ -oxidation of long (C16-C20) and very long chain fatty acids (C22-C24), (long chain acyl-CoA syntase, LCAS; very long chain acyl-CoA syntase, VLCAS; acyl-CoA oxydase, AOX, etc., see table 1.1); iii) peroxisomal  $\alpha$ -oxidation of branched chain fatty acids; iv) mitochondrial  $\beta$ -oxidation of medium chain fatty acids (C10-C14) (carnitine-palmitoyl transferase I, CTP I). Over-expression of PPAR- $\alpha$  in the liver triggers up-regulation of L-FABP that increases fatty acid transfer rate to oxidative organelles. The overall effect of PPAR- $\alpha$  activation in the liver by nonesterified fatty acids (especially PUFAs) is a large mobilization of fatty acids for peroxisomal and mitochondrial oxidation with energy formation. Interestingly, PUFAs have an opposite effect in adipocytes by activating PPAR $\gamma$  which target genes



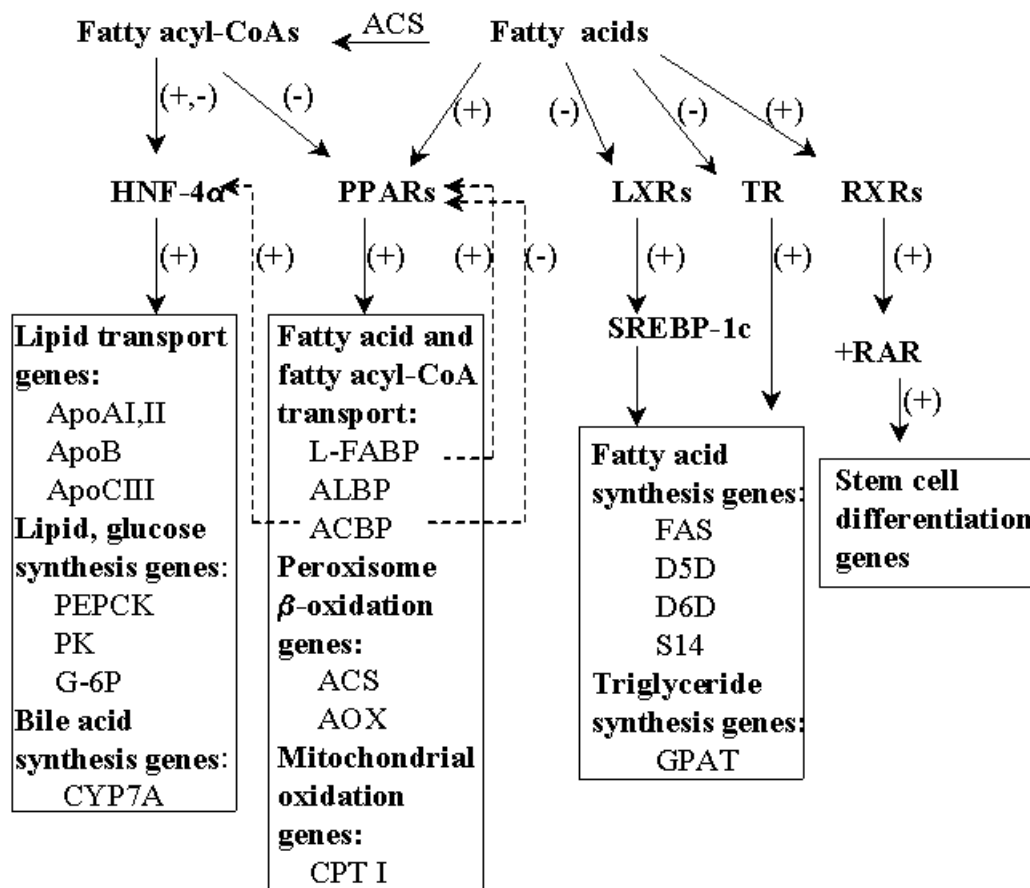


FIG. 1.3. **Fatty acids and acyl-CoAs are transcription factor modulators.**

Transcription factors: HNF-4 $\alpha$ , hepatic nuclear factor-4 $\alpha$ ; LXR, liver X-activated receptor; PPARs, peroxisome proliferator activated receptors; SREBP, sterol regulatory response element binding proteins (er-endoplasmic reticulum precursor, n-nuclear form); RAR, all trans retinoic acid receptor; RXR, retinoid X receptor; TR, thyroid hormone receptor. Genes encoding proteins: ACBP, acyl-CoA binding protein; ACS, acyl-CoA synthase; ALBP, adipocyte lipid binding protein; AOX, acyl-CoA oxidase; Apo, apolipoprotein; CPT1, carnitine-palmitoyl transferase 1; CYP7A, cytochrome 7A; D5D, D6D, delta5- and delta-6 desaturase; D9D, stearoyl-CoA desaturase 1; FAS, fatty acyl synthase; G-6P, glucose-6 phosphatase; GPAT, glyceraldehydephosphate acyl-transferase; L-FABP, liver fatty acid binding protein; PEPCK, phosphoenolphosphate carboxykinase; PK, pyruvate kinase; S14, spot 14.

with role in adipocyte differentiation, determining fatty acid esterification to triglycerides and their massive accumulation in lipid droplets. So, different isoforms of the same fatty acid-dependent nuclear receptor can affect lipid transport and metabolism in very distinct ways depending on the overall function of the tissue where they are expressed.

In the liver, PUFAs act also on LXR transcription factors decreasing their affinity for oxysterols and diminishing SREBP-1c and consequently fatty acid synthesis gene transcription levels (see figure 1.2) (53). In vitro, PUFAs competitively antagonize oxysterol-induced LXR binding to an LXXLL containing peptide derived from a coactivator (53). As it can be seen in figures 1.2 and 1.3, the LXR and SREBP-1c-mediated regulation of fatty acid synthesis genes can be modulated by oxysterols and PUFAs which act in opposite directions. PUFAs inhibit LXR and selectively suppress hepatic levels of the mRNAs encoding for SREBP-1c but not SREBP-2 (111) (112).

Fatty acyl-CoAs can bind and modulate HNF-4 $\alpha$  transactivation function depending on the particular structures of the ligands. Thus, saturated fatty acid thioesters (C14:0-CoA, C16:0-CoA) stimulated HNF-4 $\alpha$ , while PUFA-CoAs (C18:3, n-3-CoA, C20:5, n-3-CoA, C22:6, n-3-CoA) inhibited HNF-4 $\alpha$  mediated transcription of an ApoCIII-promoted reporter gene in COS-7 cells (45). Similar effects of fatty acyl-CoAs on other genes that contain HNF-4 $\alpha$  binding response elements (see table 1.1) in their regulatory sequences remain to be demonstrated. Fatty acids with unusual structures (branched, dicarboxylic fatty acids) known as fibrates were designated peroxisome proliferators (PPs) along with many other chemicals that had a stimulatory effect on the size of peroxisomes in livers of animals fed with these compounds. Fibrates in free acid form as well as their CoA derivatives bind to PPARs but have opposite effects, i.e. fibrate fatty acids induce a high level of oxidation and catabolism of lipids, while fibrate-CoA derivatives inhibit PPAR-activation of gene transcription by diminishing the ability of PPARs to recruit and bind transcription co-activators (47). Fibrates also interfere with HNF-4 $\alpha$  function, leading to a fall in HNF-4 $\alpha$ -mediated transactivation of ApoCIII-

reporter gene (45) (91) (113) (114). There is a degree of variability in direct repeat (DR-1) sequences in different genes, so that some DR-1 sequences are bound by HNF-4 $\alpha$  only, others by PPAR only, and others are promiscuous sequences that can be regulated by multiple transcription factors, like HNF-4 $\alpha$ , PPAR, RXR, COUP-II (115). The DR-1 elements in ApoCIII promoter are regulated by HNF-4 $\alpha$  and PPAR- $\alpha$  which compete for DNA binding depending on the predominance of fibrate-CoAs or fibrate-fatty acids, respectively (114) (116).

Fatty acids and their CoA thioesters have been reported to bind thyroid hormone receptor (TR) antagonizing triiodothyronine (T3) stimulation of lipogenic enzymes (55); (56). As T3-activated TR induces up-regulation of fatty acid synthesis genes, the inhibition prompted by medium chain fatty acids on T3-TR binding to its cognate DNA, functions as a feedback regulatory pathway. Indeed increase in cellular free fatty acid concentration and TR-inhibition were well correlated and much larger in the heart than in the liver, according to Yamamoto *et al.* (117).

A reevaluation of the RXR physiological ligand was recently proposed by deUrquiza *et al.* who purified the RXR-activating factor from various embryonic and adult mouse tissues and found that docosohexaenoic acid (DHA), a long chain polyunsaturated fatty acid highly enriched in adult mouse brain, had the ability to increase RXR- $\alpha$ ,  $\beta$  or  $\gamma$ -mediated transactivation in transfection assays (57). According to de Urquiza *et al.*, 9-*cis* retinoic acid which binds RXRs with very high affinity in vitro, is hardly detected in vivo while DHA constitutes up to 50% of total fatty acids especially in brain, retina and other tissues where RXRs have important roles during differentiation. In these tissues, RXRs can act not only as homeodimer binding retinoic acid response elements within target genes but also as a dimerization partner with other nuclear receptors like PPARs, LXRs, influencing the expression of genes controlled by these transcription factors too.

### 1.3.5 Lipid Binding Proteins Interact with Nuclear Receptors and Coregulate Gene Expression

In 1999, Dong D *et al.* reported for the first time a role of a intracellular lipid binding protein, cellular retinoic-binding protein II (CRABP-II) in retinoic acid receptor (RAR)-mediated gene expression (118). It has been shown that the over-expression of CRABP-II but not CRABP-I markedly enhanced RAR-mediated transcriptional activation of a reporter gene in COS-7 cell. Kinetic studies of retinoic acid (RA) binding to RAR in the presence of CRABP-I suggested that the transfer of RA from CRABP-I to RAR involves two distinctive steps, *i.e.* dissociation of ligand from the binding protein followed by association with the receptor; in contrast, the transfer from CRABP-II to RAR occurs through a ternary complex, with direct interaction between CRABP-II and RAR. In a subsequent article, the same group reported that CRABP-II, a predominantly cytosolic protein, undergoes nuclear localization upon binding of RA, it interacts with RAR in the nucleus in a ligand-dependent fashion and facilitates RAR activation through “channeling” RA to RAR (119). In 1999 Delva *et al.* reported that CRABP-II physically associates with RAR $\alpha$  and RXR $\alpha$  (but contrary to Noy’s group finding) in a ligand independent manner, in various mammalian cells in culture, concluding that CRABP-II is a transcriptional co-regulator involved in RA signaling (120).

In 2001, Wolfrum *et al.* found that another lipid binding protein, liver fatty acid binding protein (L-FABP) colocalized with PPAR- $\alpha$  in nuclei of primary hepatocytes from mice (121). Various approaches like pull-down assays, coimmunoprecipitation and two-hybrid system proved that L-FABP and PPAR- $\alpha$  can associate in a ligand-independent manner and transactivation assays showed that saturated, monounsaturated and polyunsaturated fatty acids as well as fibrates induced a higher rate of PPAR- $\alpha$ -mediated transcription of a reporter gene in the presence of L-FABP (121) (122).

As it has been reported that fatty-acyl-CoA (FA-CoA) thioesters can bind to PPARs preventing coactivators from being recruited and bound to PPARs, Helledie *et al.* studied the influence of lipid binding proteins that bind FA-CoA, such as L-FABP, acyl-CoA binding protein (ACBP), adipocyte lipid binding protein (ALBP), and keratinocyte

lipid binding protein (KLBP) on PPAR  $\alpha$ ,  $\beta/\delta$  and  $\gamma$ -mediated transactivation by peroxisome proliferators - CoA thioesters (123). Over-expression of ALBP and KLBP in CV-1 cells resulted in a significant reduction of ligand dependent transactivation induced by all PPARs, while excess of ACBP inhibited transactivation by PPAR- $\delta$  and  $\gamma$  but not by PPAR- $\alpha$ . A minor reduction in ligand-independent transactivation by PPARs was

TABLE 1.3

*Lipid binding proteins with role in coregulation of nuclear receptors.*

Abbreviations: ACBP, acyl-CoA binding protein; ALBP, adipocyte lipid binding protein; Ch, cholesterol; CRABP-II cellular retinoic binding protein; ER, estrogen receptor; FA, fatty acid; FA-CoA, fatty acyl-CoA; FFA free fatty acid; KLBP, keratinocyte lipid binding protein; PPAR, peroxisome proliferator activated receptor; RAR, all trans retinoic acid receptor; RXR, 9-cis-retinoic acid receptor.

Lipid binding protein	Lipid ligand	Nuclear receptor	Regulation	References
CRABP-II	RA	RAR- $\alpha$ , $\beta$ , $\gamma$	+	(119)
CRABP-II	RA	RXR- $\alpha$ , $\beta$ , $\gamma$	+	(120)
L-FABP	FFA	PPAR- $\alpha$	+	(121)
ACBP	FA-CoA	PPAR- $\delta$ , - $\gamma$	-	(123)
ALBP	FA-CoA	PPAR- $\alpha$ , $\delta$ , $\gamma$	-	(123)
KLBD	FA-CoA	PPAR- $\alpha$ , $\delta$ , $\gamma$	-	(123)
Caveolin	Ch., FAs	ER- $\alpha$	+	(124)

also found indicating that LBPs may interfere with endogenous ligands. The presence of ACBP, ALBP and KLBP in the nuclei of CV-1 cells transfected with expression plasmids for the three proteins suggested that these LBP may have role in transferring

the lipidic ligands to PPARs inside nuclei. No evidence has been reported yet though that any of these LBPs associates with PPARs by protein-protein interactions.

#### 1.4 PRESENT RESEARCH OBJECTIVE

Three different lipid binding proteins, *i.e.* steroidogenic acute regulatory protein (StAR), hepatocyte nuclear factor-4 $\alpha$  (HNF-4 $\alpha$ ) and fatty acyl-CoA binding protein (ACBP) are studied in regard with their ligand binding properties and cellular functions, as follows:

##### *1.4.1. Studies on StAR Protein Ability to Bind Cholesterol and Modulate Sterol Domain Dynamics in Mitochondrial Membranes*

As briefly presented in section 1.1.3, the mechanism of StAR-mediated cholesterol transfer from the outer to inner mitochondrial membrane is largely debated and up to this study no clear evidence has been reported on the ability of StAR to directly bind cholesterol. Using fluorescence spectroscopy and circular dichroism techniques *in vitro* we investigate the ability of StAR protein to bind cholesterol and to induce changes in mitochondrial membrane cholesterol domains.

##### *1.4.2 Ligand Specificity and Conformational Dependence of HNF-4 $\alpha$*

Fatty acyl-CoAs were demonstrated to modulate the HNF-4 $\alpha$ -mediated transactivation of a reporter gene under a promoter regulated by HNF-4 $\alpha$  and hypothesized to be the physiological ligands for this orphan nuclear receptor (45). However, because a radio-labeled ligand assay was used to characterize acyl-CoA/HNF-4 $\alpha$  binding, only low affinities with micromolar  $K_d$ s were determined. Our objective has been to study the acyl-CoA/HNF-4 $\alpha$  binding by fluorescence spectroscopy assays, to measure the intermolecular distance between HNF-4 $\alpha$  and its bound ligand from fluorescence resonance energy transfer (FRET) data, and to characterize possible conformational changes induced upon ligand binding to HNF-4 $\alpha$  by circular dichroism.

### *1.4.3 Physical and Functional Interaction of ACBP and HNF-4 $\alpha$*

We hypothesize that ACBP, as a protein that binds and carries fatty acyl-CoAs not only in cytosol but also in nuclei of cells expressing ACBP, has the ability to modulate the acyl-CoA binding to HNF-4 $\alpha$  and consequently, the HNF-4 $\alpha$ -mediated transactivation function. We have studied a possible physical association of the two proteins at molecular level by circular dichroism, coimmunoprecipitation, confocal microscopy, FRET microscopy. We have also looked for ACBP/HNF-4 $\alpha$  binding in cultured cells by two-hybrid mammalian system. Finally, we tested the influence of ACBP on HNF-4 $\alpha$ -mediated transactivation by functional assays in cells transfected with a reporter gene under HNF-4 $\alpha$ -regulated promoter.

## CHAPTER II

### STEROIDOGENIC ACUTE REGULATORY PROTEIN BINDS CHOLESTEROL AND MODULATES MEMBRANE STEROL DOMAIN DYNAMICS

#### 2.1 INTRODUCTION

Research on the individual pathways for intracellular cholesterol trafficking has dramatically accelerated in recent years (rev. in (1) (6) (17) (125) (126) (127)). Among the more interesting pathways for intracellular cholesterol movement is the mechanism whereby cholesterol is transferred to (rev. in (128) (129) (130) (131)) and within (rev. in (132) (133) (134) (135)) mitochondria wherein the cholesterol side chain is cleaved to synthesize the first steroid of the steroidogenic pathway (136). Cholesterol delivery to mitochondria may be considered in two parts:

The first step is the transfer of cholesterol to the mitochondrial outer membrane from other intracellular sites, primarily lipid droplets and plasma membrane. This transfer of cholesterol to the mitochondria may be mediated by proteins such as sterol carrier protein-2 (SCP-2) (rev. in (128) (129) (130) (131)). The observation of normal phenotype and normal serum steroid (testosterone, progesterone, corticosteroids) levels in SCP-2 gene ablated mice suggests that SCP-2 is not essential for gonadal and adrenal steroidogenesis (137) (138) and that additional/compensatory mechanism(s) must exist for cholesterol transfer to the mitochondria (135) (139).

The rate-limiting step in gonadal and adrenal steroidogenesis is the transfer of cholesterol from the relatively cholesterol-rich outer mitochondrial membrane to the cholesterol-poor inner mitochondrial membrane (rev. in (133) (134) (135) (139)). This regulated step in steroid production is catalyzed by the steroidogenic acute regulatory protein (StAR) (rev. in (133) (135) (139)). The importance of StAR in steroidogenesis is underscored by studies of mutations in humans and StAR gene ablation in mice. Humans carrying mutations that inactivate StAR exhibit markedly reduced gonadal and



adrenal steroidogenesis, a condition that leads to accumulation of cholesterol in lipid droplets and a disease named congenital lipid adrenal hyperplasia (107) (140). Ablation of StAR gene in mice also results in a phenotype of impaired steroidogenesis and adrenal lipid accumulation (141).

The mechanism whereby StAR mediates cholesterol transfer from the outer to the inner mitochondrial membrane remains elusive. An early hypothesis favored stimulation of cholesterol movement as a result of StAR being physically transported through the outer to the inner mitochondrial membranes (rev. in (139)). In this model the StAR translocation process was envisioned to promote formation of contact sites between outer and inner mitochondrial membranes, thereby allowing cholesterol to flow down a chemical gradient from the outer to the inner membranes. Consistent with this hypothesis, immunoelectron microscopy localized StAR in the intermembranous space and the intermembranous face of the inner mitochondrial membrane (142), while immunoblotting of isolated mitochondrial membrane contact sites revealed the presence of StAR (12). However, recent studies from our laboratories favor another mechanism whereby StAR acts like most other typical lipid transfer proteins (14) (143). This model is based on observations that StAR is a cholesterol transfer protein (14) and acts on the outside of mitochondria (143). StAR molecules lacking a mitochondrial targeting sequence that were shown to be incapable of mitochondrial importation were able to stimulate conversion of cholesterol into steroid hormones in intact cells and isolated mitochondria (143). A third hypothesis has emerged from the characterization of a StAR-related lipid-transfer (START) domain found in a related protein, MLN64 (35% identity with the StAR START domain) (15) (144) (145). X-Ray crystallography and molecular modeling revealed a hydrophobic tunnel in the MLN64 START domain capable of accommodating a cholesterol molecule (15). These data suggested that StAR could be a cholesterol carrier from the outer to the inner mitochondrial membrane.

To explore the properties of StAR and its action on mitochondria predicted by the existing models of StAR function, we performed experiments to address the following questions: Does StAR bind cholesterol? Do interactions with sterol affect

StAR structure? Does StAR enhance mitochondrial sterol transfer by altering mitochondrial cholesterol domain dynamics? The data presented herein yielded the following new insights: (i) Fluorescence resonance energy transfer demonstrated the close molecular interaction between StAR and bound sterol. (ii) A fluorescent sterol binding assay established that StAR has two sterol binding sites with high affinity (nM  $K_{ds}$ ). A functionally inactive StAR mutant had much lower affinity for cholesterol. (iii) By application of a fluorescent sterol transfer assay, it was shown that StAR dramatically enhanced mitochondrial sterol transfer and altered the sterol domain structure of the mitochondrial membranes.

## 2.2 EXPERIMENTAL PROCEDURES

### 2.2.1 *Materials*

NBD-cholesterol, [22-(N-(7-nitrobenz-2-oxa-1,3-diazol-4-yl)amino)-23,24-bisnor-5-cholen-3b-ol], was obtained from Molecular Probes Inc. (Eugene, OR). Dehydroergosterol (DHE) was prepared as reported previously (146) (147). GTP, isocitrate, cholesterol, N-acetyl-L-tryptophan-amide (NATA), and guanidine-HCl were obtained from Sigma Chemical Co., St. Louis, MO.

### 2.2.2 *Recombinant Proteins*

N-62 StAR containing a C-terminal 6-histidine tag (His<sub>6</sub> tag) and C-terminal His<sub>6</sub> tag N-62 StAR mutant with an A218V amino acid replacement were expressed in *E. coli* and purified as described previously (14) (142). N-62 StAR concentration was 0.13 mg/ml phosphate buffered saline (50 mM Na phosphate, 75 mM NaCl, pH 7.4) containing 0.01% Tween-20. Since similar NBD-cholesterol binding and sterol transfer data were obtained with N-62 StAR in 50 mM Na phosphate, 300 nM NaCl, pH 8.0, the presence of a small amount of Tween (diluted several orders of magnitude in the binding assay and sterol transfer assays) in the stock protein solution did not affect the results. The A218V mutant N-62 StAR was 4.58 mg/ml in 50 mM Na phosphate, 300 nM NaCl, pH 8.0. Both proteins were stored at 4°C for immediate use or stored frozen at -80°C.

The A218V mutation was chosen because it functionally inactivates the protein and causes congenital lipoid adrenal hyperplasia in humans (140). The A218V mutation did not result in global destabilization of the StAR molecule, but did induce a modest change in StAR secondary structure as indicated by analysis of circular dichroic spectra. N-62 StAR had  $24\pm 1.4\%$   $\alpha$ -helix,  $20\pm 1.4\%$   $\beta$ -sheet,  $23\pm 1.4\%$  turn, and a  $T_m$  (mid-point of thermal denaturation) of  $45\pm 0$  °C (n=2). A218V N-62 StAR had  $23\pm 6.1\%$   $\alpha$ -helix,  $27\pm 9\%$   $\beta$ -sheet,  $19\pm 2.1\%$  turn, and a  $T_m$  of  $50\pm 4.7$ °C (n=3). Human recombinant SCP-2, isolated as described previously (30), was stored at 1 mg/ml in 10 mM K phosphate, pH 6.8, 2.5 mM dithiothreitol at  $-80$ °C. Both proteins were stable stored at  $-80$ °C under these conditions (143) (148).

### 2.2.3 Cell Culture

MA-10 mouse Leydig tumor cells were generously provided by Dr. M. Ascoli (Dept. of Pharmacology, U. of Iowa College of Medicine, Iowa City). Cells were cultured as described by Clark et al (149). Normal human skin fibroblasts (CWN), generously provided by Drs. Edward Neufeld and Peter Pentchev (National Institutes of Health, Bethesda, MD), were cultured as described previously (8). For isolation of mitochondria to be used in fluorescent sterol transfer assays (see below), MA-10 cells or CWN fibroblasts were cultured as above with the following modifications: The cells were grown and incubated on 20 cm x 20 cm trays (Nalge-Nunc, Milwaukee, WI). To obtain mitochondrial sterol acceptor membranes, the cells were cultured in serum containing medium supplement with cholesterol (15  $\mu$ g/ml) for a total of four days. To obtain mitochondrial sterol donor and acceptor membranes, cells were cultured in serum containing medium supplemented with 15  $\mu$ g/ml cholesterol (for acceptor mitochondria) or dehydroergosterol (for donor mitochondria) for a total of four days. Cells were then washed with phosphate buffered saline, followed by isolation of mitochondria.

#### 2.2.4 Isolation of Mitochondria for Sterol Transfer Assay

MA-10 and CWN cell mitochondria were isolated as described earlier for fibroblasts (131). Purification of mitochondria was estimated by Western blotting (131). Isolated mitochondria were suspended in 0.25 M sucrose, 10 mM TRIS-HCl, pH 7.4 buffer. The stock mitochondrial membrane donor and acceptor protein concentrations were 0.18-0.25 mg/ml and 0.3-0.5 mg/ml, respectively. Mitochondria stored at 4<sup>0</sup> were used immediately for sterol transfer assay or stored frozen at -80°C. Freezing the mitochondria did not adversely affect StAR (143) or SCP-2 (131) activity in sterol transfer. Protein concentration was by the method of Lowry (150).

#### 2.2.5 Fluorescence Assay for Sterol Binding to StAR

NBD-cholesterol or dehydroergosterol binding to StAR was monitored by steady-state fluorescence intensity using an ISS Photon Counting Fluorimeter (ISS, Champaign, IL) in the L-format and ratio mode to correct for wavelength and lamp intensity variations in the excitation system. The light source was a 300 Watt Xenon arc lamp. Temperature was maintained with a Isotemp Model 1016S cooling system (Fisher Scientific, Pittsburgh, PA). NBD-cholesterol was excited at 473 nm; emission was scanned from 500-600 nm; excitation and emission bandpasses were 4 and 4 nm, respectively. Dehydroergosterol excitation was at 324 nm and fluorescence emission was scanned from 200-500 nm using excitation and emission bandpasses of 4 and 4 nm, respectively. The sample absorbance for NBD-cholesterol at 473 nm and dehydroergosterol at 324 nm was kept below 0.15 in order to avoid the inner filter effect. Light scatter was reduced by the use of dilute samples and appropriate low fluorescence cutoff filters in the emission paths.

StAR binding affinity for NBD-cholesterol was determined at 37<sup>0</sup>C as previously described for SCP-2 binding of NBD-cholesterol (151), with the following modifications. A 40 µl aliquot of N-62 StAR protein stock solution (0.13 mg/ml in 50 mM Na phosphate, 75 mM NaCl, 0.01% Tween-20, pH 7.4) was diluted to 2 ml with 25 mM K phosphate buffer, pH7.4. At the final dilutions used for the NBD-cholesterol

binding assay, the concentration of Tween-20 ( $1.5 \times 10^{-6}\%$ ) had no effect on NBD-cholesterol fluorescence in the presence or absence of StAR and did not affect NBD-cholesterol binding to StAR. In contrast, 0.1% Tween-20 ( $10^5$ - fold higher than normally used in the binding assay) significantly altered NBD-cholesterol fluorescence and binding to StAR. The integrated NBD-cholesterol emission was measured after each addition of the ligand. Each emission spectrum, corrected for the background and blank, was used to construct the binding isotherm.

Sigmoid ligand binding curves were analyzed by Lineweaver-Burke plot for allosteric enzymes (152) where enzyme activity,  $v$ , was substituted with binding,  $b$ , defined in equation 2.1,

$$b = (F_i/F_{max})B_{max} \quad (\text{Eq.2.1})$$

in which  $F_i$  = fluorescence of bound NBD-cholesterol at concentration  $i$  of ligand,  $F_{max}$  = fluorescence of NBD-cholesterol bound at maximal binding (i.e. binding site saturation),  $B_{max}$  = maximum binding site concentration for the given amount of protein is given by equation 2.2,

$$B_{max} = nE_o \quad (\text{Eq.2.2})$$

where  $n$  is the number of binding sites on the protein and  $E_o$  is the protein concentration in the assay.

$$F_{max}/F_i = K(1/[NBD\text{-cholesterol}]^n) + 1 \quad (\text{Eq.2.3})$$

$K$  in equation 2.3 is defined as  $K = (k_d)^n$  with  $k_d$  as the dissociation constant for protein-ligand complex. Hyperbolic binding curves were analyzed as described earlier (153).

### 2.2.6 Fluorescence Resonance Energy Transfer

Fluorescence resonance energy transfer (FRET) is used as a molecular ruler to examine the relative distance between two molecules (154). Since FRET efficiency varies as  $r^{-1/6}$  (where  $r$  = the distance between the molecules), the fluorescence donor and acceptor must be in very close proximity, i.e a few angstroms (154). FRET efficiency is high if there is significant spectral overlap of donor emission with acceptor excitation/absorbance. Finally, if the acceptor molecule is fluorescent, then FRET can be

readily detected as sensitized emission of the acceptor. FRET from StAR Trp to NBD-cholesterol was determined basically as described earlier for SCP-2 Trp to cis-parinaric acid (155) except as follows: The N-62 StAR protein stock solution (0.13 mg/ml in 50 mM Na phosphate, 75 mM NaCl, 0.01% Tween-20, pH 7.4) was diluted to 2 ml with 25  $\mu$ M K phosphate buffer, pH7.4. The final concentration of Tween-20 (0.0002%) had no effect on NBD-cholesterol fluorescence (with or without StAR), did not affect NBD-cholesterol binding to StAR, and did not affect StAR Trp/Tyr FRET to bound NBD-cholesterol. The donor and acceptor molecules were StAR Trp and NBD-cholesterol, respectively. StAR Trp was excited at 295 nm. StAR trp emission was monitored near 340 nm while sensitized NBD-cholesterol emission was monitored at 530 nm.

The intermolecular distances between StAR Trp (donor) and bound NBD-cholesterol (acceptor) was determined as described earlier (155) and modified as follows. According to Forster's theory on energy transfer (154) (155) (156) , the intermolecular distance for a donor-acceptor pair can be calculated from:

$$E = R_0^6 / (R_0^6 + R_{2/3}^6) \quad (\text{Eq. 2.4})$$

where E is the fluorescence energy transfer efficiency,  $R_0$  is the critical distance for 50% efficiency and  $R_{2/3}$  is the actual distance between donor and acceptor. The energy transfer efficiency was calculated from StAR-Trp quenching as well as from sensitized emission of NBD-cholesterol, by using the following equations:

$$E = 1 - F_{DA}/F_D \quad (\text{Eq. 2.5})$$

$$E = (F_{AD}/F_A - 1)(\epsilon_A/\epsilon_D) \quad (\text{Eq. 2.6})$$

where  $F_{DA}$  and  $F_D$  are the fluorescence intensities of StAR at 340nm in the presence and in the absence of NBD-cholesterol, respectively;  $F_{AD}$  and  $F_A$  are fluorescence intensities of acceptor (NBD-cholesterol) at 530nm, in the presence and in the absence of donor (StAR) respectively;  $\epsilon_A$  and  $\epsilon_D$  are the molar extinction coefficients of acceptor and donor, respectively, at the wavelength of excitation (280nm), (157).  $R_0$  was calculated from equation 2.7:

$$R_0 = 0.211[k^2 n^4 Q_D J(\lambda)]^{1/6} \quad (\text{Eq. 2.7})$$

in angstroms (Å), wavelength being expressed in nm and  $J(\lambda)$ , the overlap integral, in  $M^{-1} \text{ cm}^{-1}$ .  $Q_D$  for StAR protein and  $J(\lambda)$  were calculated as previously described (157) (158). The orientation factor  $k^2$ , and the refractive index  $n$  were assumed to be 2/3 and 1.4 respectively, as for protein solutions(156).

### 2.2.7 Stern-Volmer Fluorescence Quenching

To examine the surface exposure of StAR trp, increasing acrylamide (5 M stock solution) was added as 20  $\mu\text{l}$  aliquots to StAR (40  $\mu\text{M}$  in 2 ml of PBS). StAR trp was excited at 295 nm and decreasing emission with increasing acrylamide was measured at 333 nm. Parallel experiments were performed with N-acetyl-L-tryptophan-amide (NATA) to assess quenching of trp when acrylamide was completely accessible to the quencher in aqueous solution. The exposure of StAR bound NBD-cholesterol to the aqueous was examined with KI as a quencher. Successive 10  $\mu\text{l}$  aliquots of 5 M KI (made freshly with 0.1 mM sodium hydrosulfite) were added to 2 ml PBS containing 80  $\mu\text{M}$  StAR preincubated with or without 50 nM NBD-cholesterol (from a 2 mM stock solution in dimethylformamide). Fluorescence emission of NBD-cholesterol was measured at 530 nm with excitation at 470 nm. Parallel experiments were performed with free NBD-cholesterol (from a 2 mM stock solution in dimethylformamide). Fluorescence intensities were corrected for dilution, scattering, and ionic strength. Quenching data were analyzed by the Stern-Volmer equation 2.8 (159):

$$F_0/F = 1 + K_{SV} [Q] \quad (\text{Eq. 2.8})$$

where  $F_0$  and  $F$  are the fluorescence intensities in the absence and the presence of quencher respectively.  $Q$  and  $K_{SV}$  are the quencher concentration and Stern-Volmer quenching constant, respectively.

### 2.2.8 Circular Dichroism of StAR with and without Cholesterol

Circular dichroic spectra of StAR (2.9  $\mu\text{M}$ ) in the presence of cholesterol (1  $\mu\text{M}$ ) were obtained basically as described earlier for SCP-2 (160) except that the buffer used was phosphate buffered saline (147  $\mu\text{M}$ , pH 7.4) containing 0.01% Tween. For

guanidine-HCl induced denaturation studies, StAR (2  $\mu$ M) was preincubated with or without cholesterol (30  $\mu$ M) for 15 min followed by denaturation in the presence of increasing (up to 4M) guanidine-HCl in PBS/0.01% Tween. After denaturation for 12 h at room temperature, the circular dichroic spectra were measured with a J-710 Spectropolarimeter (JASCO, Baltimore, MD) using a 0.1 mm cuvette. Spectra were recorded from 250-210 nm at 50 nm/min with a time constant of 1 sec and a band width of 2 nm. For each circular dichroic profile an average of 4 scans was obtained. Stability parameters of guanidine-HCl induced unfolding of StAR with or without cholesterol were calculated as described earlier (161). Briefly,  $Y_N$  and  $Y_D$  were graphically calculated from the intercepts of pre- and post-unfolding baselines in the plot of guanidine-HCl concentration vs molar ellipticity at 222 nm. The observed equilibrium constant  $K_{obs}$  was calculated according to equation 2.9:

$$K_{obs} = (\theta_{222} - Y_N)/(Y_D - \theta_{222}) \quad (\text{Eq. 2.9})$$

The corresponding observed  $\Delta G^\circ$  ( $\Delta G^\circ_{obs}$ ) were calculated with equation 2.10:

$$\Delta G^\circ_{obs} = -RT \ln(K_{obs}) \quad (\text{Eq.2.10})$$

From the plot of guanidine-HCl vs  $\Delta G^\circ_{obs}$  the  $\Delta G^\circ$  was calculated according to equation 2.11:

$$\Delta G^\circ_{obs} = \Delta G^\circ + m_G [\text{Guanidine-HCl}] \quad (\text{Eq.2.11})$$

$C^{50\%}$ , the concentration of guanidine-HCl for which  $\Delta G^\circ$  was equal to zero, was obtained from the plot.

### 2.2.9 Fluorescence Sterol Transfer Assays

Sterol transfer between donor mitochondrial membranes and 10-fold excess acceptor mitochondrial membranes was determined exactly as described earlier for L-cell mitochondrial membranes (131) (162) (163). For all sterol transfer assays, the donor and acceptor mitochondrial membrane final concentrations were 7 and 70  $\mu$ g/ml, respectively, in 10 mM PIPES, pH 7.4, buffer. Performing the sterol transfer assays in a buffer (123 mM KCl, 5 mM  $Mg_2Cl_2$ , 10 mM  $KH_2PO_4$ , 25 mM HEPES, 100  $\mu$ M GTP, 10 mM isocitrate, pH 7.4) previously used to determine StAR mediated cholesterol transfer



and steroidogenesis in mitochondria (143) did not significantly affect the sterol transfer assay. The following control experiments were performed: (i) Stability of the mitochondrial membrane donor was determined by measuring dehydroergosterol polarization in donor mitochondrial membranes in the absence of acceptor mitochondrial membranes for 4 hours at a temperature of 37<sup>0</sup>C. The dehydroergosterol fluorescence polarization was not significantly altered in donor mitochondria isolated from either normal (CWN) human fibroblasts or MA-10 cells. (ii) StAR or SCP-2 were added to donor (CWN or MA-10 cell) mitochondria and dehydroergosterol polarization in the mitochondrial membranes was measured. Neither StAR nor SCP-2 significantly altered the dehydroergosterol polarization in donor mitochondrial membranes in the absence of acceptor mitochondrial membranes. These observations were consistent with those previously determined with L-cell fibroblasts mitochondria (131), (162), (163).

Spontaneous sterol transfer from mitochondrial membrane donors was determined by measuring dehydroergosterol polarization in mitochondrial membrane donors for 10 minute to obtain a baseline, followed by addition of 10-fold excess mitochondrial membrane acceptor, and measurement of dehydroergosterol fluorescence polarization for 4 hours.

The effect of StAR or SCP-2 (1.5  $\mu$ M) on sterol transfer from mitochondrial donor membranes (contain dehydroergosterol) to mitochondrial acceptor membranes (initially containing only cholesterol, but no dehydroergosterol) was determined by measuring dehydroergosterol polarization in mitochondrial membrane donors for 10 minute to obtain a baseline, followed by addition of 10-fold excess mitochondrial membrane acceptor plus 1.5  $\mu$ M StAR or SCP-2.

Steady-state fluorescence polarization of dehydroergosterol was measured with an ISS Photon Counting Fluorimeter (ISS, Champaign, IL), motorized polarizers in the L format, and a 300 Watt Xenon arc lamp as a light source. Sample temperature was maintained at 37<sup>0</sup>C with a Isotemp Model 1016S cooling system (Fisher Scientific, Pittsburgh, PA). Total sample absorbance at the wavelength of excitation, 324 nm, was

<0.15 in order to avoid the inner filter effect. Light scatter was minimized by the use of dilute samples and KV 389 low fluorescence cutoff filters in the emission paths.

### *2.2.10 Calculation of Molecular Sterol Transfer*

Molecular sterol transfer was calculated from measurements of dehydroergosterol polarization change during the dehydroergosterol transfer between mitochondrial membrane donor/acceptor pairs exactly as described earlier (131) (162) (163). Establishment of standard curves and the mathematical basis for the calculation of molecular sterol transfer were detailed therein. The initial rate (pmol/min) of sterol transfer between mitochondrial donor and mitochondrial acceptor membranes was determined also as described earlier (131) (162).

## 2.3 RESULTS

### *2.3.1 The Sterol Binding Site of StAR; NBD-Cholesterol Spectral Shifts and KI Quenching*

The recombinant N-62 StAR protein employed herein contained the START, but not mitochondrial targeting, domain (143). As noted above, X-ray crystallography and molecular modeling of the MLN64 START domain revealed a hydrophobic tunnel capable of accommodating a cholesterol molecule (15). These data indicated that StAR might also had a relatively hydrophobic ligand binding site. To test this possibility, the spectral properties of NBD-cholesterol were examined in the absence and presence of StAR. NBD-cholesterol exhibited much lower fluorescence emission in the absence of StAR. NBD-cholesterol emission was tested in aqueous buffer 10 nM (Fig. 2.1A, spectrum 1) and 100 nM (Fig. 2.1B, spectrum 1). In both cases, NBD-cholesterol emission was at least 10-fold lower than in the presence of StAR. Further, NBD-cholesterol in buffer had a maximal emission near 562 nm (Fig. 2.1B, spectrum 1), consistent with exposure of the NBD-group of NBD-cholesterol to the aqueous. In contrast, in the presence of StAR (Fig. 2.1A, spectra 2-8, Fig. 2.1B, spectrum 3), the

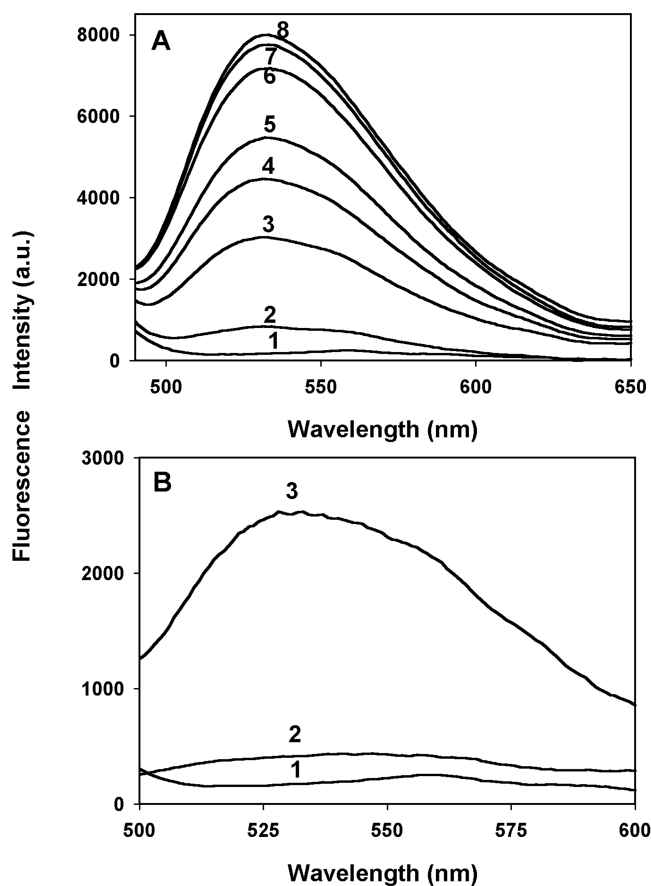


FIG. 2.1. **Fluorescence emission spectra of NBD-cholesterol in the absence and presence of N-62 StAR or A218V N-62 StAR.** *Panel A.* NBD-cholesterol emission spectra (excitation at 473nm) in absence (spectrum 1) and presence of 6.35nM StAR protein (spectra 2-8). NBD-cholesterol concentration were as follows: spectrum 1, 10 nM; spectrum 2, 10nM; 3, 15nM; 4, 30nM; 5, 40nM; 6, 60nM; 7, 80nM; 8, 100nM. *Panel B.* Shows the emission spectra of NBD-cholesterol (100 nM) in buffer alone (spectrum 1), in the presence of 6.35nM mutant StAR (spectrum 2), and in the presence of 6.35nM StAR (spectrum 3). The maximum emission wavelengths of the three spectra were 562 nm, 545 nm, and 530nm, respectively.

NBD-cholesterol fluorescence intensity increased >10-fold. This increase was much smaller, <2-fold, for NBD-cholesterol in the presence of the A218V mutant N-62 StAR. Concomitant with increased NBD-cholesterol fluorescence emission on binding to StAR, the NBD-cholesterol emission maximum wavelength was significantly blue-shifted by 32 nm to 530 nm (Fig. 2.1A, spectrum 8 vs 1; Fig. 2.1B, spectrum 3 vs 1).

To determine if binding to StAR protected NBD-cholesterol from an aqueous quenching agent, KI, quenching of NBD-cholesterol by KI was examined. StAR significantly reduced the KI quenching of NBD-cholesterol fluorescence (Fig. 2.2A). The Stern-Volmer quenching constant,  $K_{SV}$ , for NBD-cholesterol in the absence and presence of StAR was  $5.7 \text{ M}^{-1}$  and  $2.4 \text{ M}^{-1}$ , respectively. Thus, the NBD-group of NBD-cholesterol was 2.4-fold less accessible to the water soluble quencher KI when the NBD-cholesterol was bound to StAR as compared to NBD-cholesterol in aqueous solution.

### 2.3.2 *StAR Binding of NBD-Cholesterol: Affinity and Stoichiometry*

Because of the low solubility of cholesterol in aqueous buffer, critical micellar concentration (CMC) of 25-40  $\mu\text{M}$  (164), radioligand binding assays requiring the separation of bound from free radiolabeled cholesterol are complicated by the presence of micelles, aggregates, and/or protein/cholesterol coaggregates that preclude accurate determination of StAR binding parameters (15). To circumvent these problems, a fluorescent sterol (NBD-cholesterol) binding assay was used to determine the binding parameters of StAR. NBD-cholesterol was chosen because: (i) The CMC of NBD-cholesterol is higher than that of cholesterol (165). This suggested that concentrations <CMC of NBD-cholesterol could be used to determine sterol binding affinity and stoichiometry of StAR. (ii) NBD-cholesterol emission maximum shifted in the presence of StAR, indicating close molecular interaction rather than coaggregation. (iii) NBD-cholesterol fluorescence intensity increased in the presence of StAR.

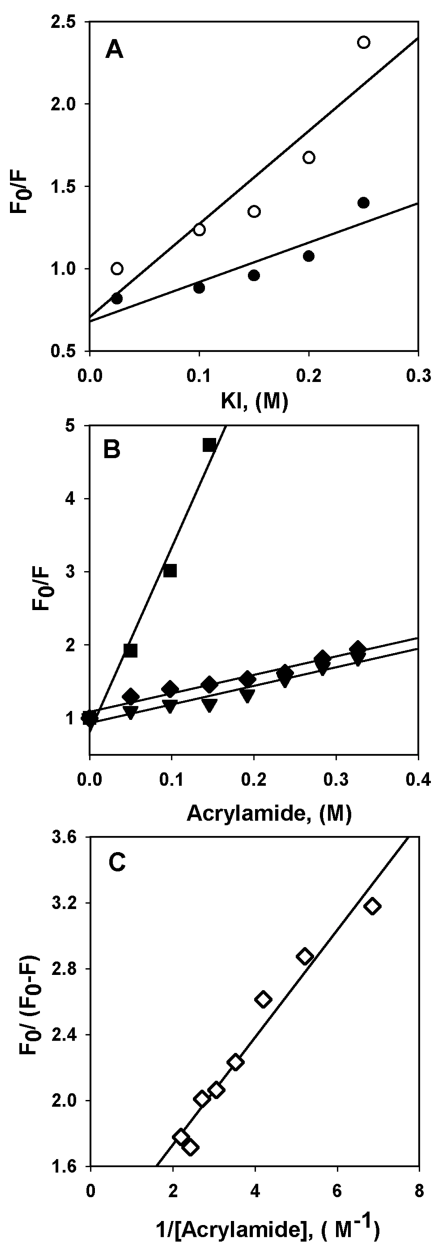


FIG. 2.2. **Stern-Volmer quenching of N-62 StAR bound NBD-cholesterol and of N-62 StAR Trp residues.** All conditions were as described in Methods. *Panel A*, KI quenching of NBD-cholesterol in the absence (open circles) and presence (solid circles) of StAR. *Panel B*, acrylamide quenching of N-acetyl tryptophanamide (solid squares) as well as StAR Trp in the absence (filled diamonds) and presence (filled triangles) of cholesterol. *Panel C*, the inaccessible fraction was determined from extrapolation to high acrylamide for data from Panel A plotted as  $F_0/(F_0-F)$ .

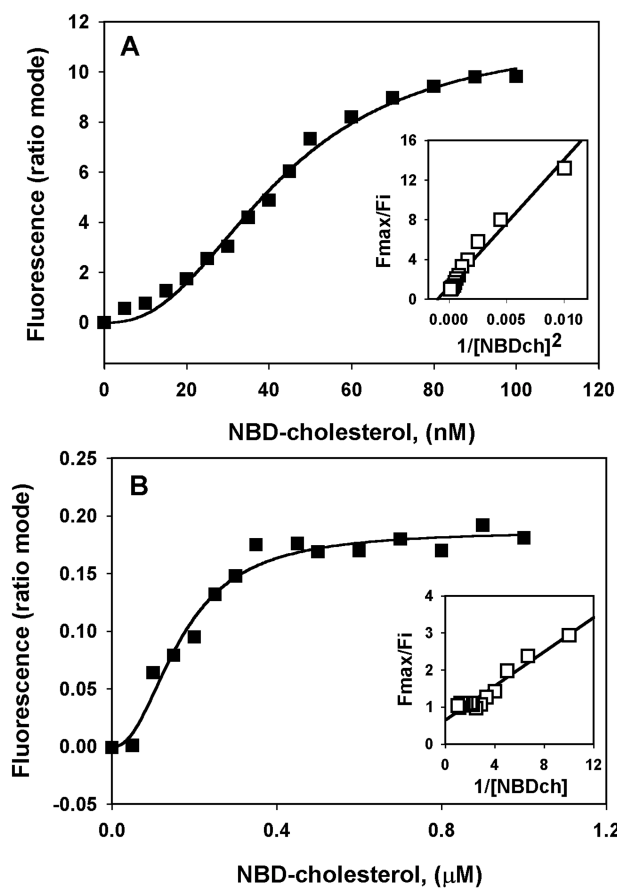


FIG. 2.3. **Fluorescence ligand binding assay for N-62 StAR (panel A) and the A218V mutant StAR (panel B).** *Panel A.* StAR (4.2nM) was titrated with 5 to 100nM NBD-cholesterol in phosphate buffered saline, pH 7.4, at 37C. The inset represents a linear plot of the sigmoid curve as  $F_{max}/F_i$  versus  $1/[NBD\text{-cholesterol}]^2$ . Best linear regression plots for the binding curve in panel A yielded  $n=2$  and an average  $k_d$  of  $32.4 \pm 4.1$  nM for the two sites. *Panel B.* The mutant StAR (126nM) was titrated with 0.01 to 1  $\mu$ M NBD-cholesterol under the same conditions as for the native StAR. The inset represents a linear plot of the hyperbolic curve as  $F_{max}/F_i$  versus  $1/[NBD\text{cholesterol}]$ . Best linear regression plots of the binding curve in panel B yielded  $n=1$  and a  $K_d$  of 231.2 nM.

As shown in Fig. 2.3A, increasing the concentration of NBD-cholesterol (over the range 5-100 nM) while maintaining the concentration of StAR constant (4.2 nM) resulted in increased fluorescence emission of NBD-cholesterol. Analysis of the sigmoidal shaped binding curve (Fig. 2.3A) as described in Methods, revealed that StAR contained two binding sites for NBD-cholesterol. A plot of the data as  $F_{max}/F_i$  vs  $1/[NBD\text{-cholesterol}]^2$  was nearly linear (Fig. 2.3A, inset) indicating that the affinities of the two binding sites for NBD-cholesterol were very similar. Fitting the data in Fig. 2.3A to a single exponential yielded an average  $K_d = 35.8$  nM, while fitting the data to two exponentials yielded two very similar  $K_d$ s of 32.5 and 47.4, respectively. When multiple binding curves were analyzed, the single exponential fit was better and yielded an average  $K_d = 32.4 \pm 4.1$  nM ( $n=3$ ). It should be noted that the high affinity of StAR for NBD-cholesterol was not due to the fact that NBD-cholesterol is a synthetic fluorescent sterol. Similar binding curves (not shown) yielded a  $K_d=76\pm 10$  nM for StAR binding dehydroergosterol, a naturally occurring fluorescent sterol with similar CMC as cholesterol (147) (166). However, because of its higher quantum yield, NBD-cholesterol was chosen for use in StAR sterol binding studies and determination of fluorescence resonance energy transfer from StAR Trp (see below).

### 2.3.3 Binding of NBD-Cholesterol to the A218V Mutant Recombinant StAR

The A218V mutation in StAR causes congenital lipoid adrenal hyperplasia in humans. Likewise, the N-62 StAR mutant A218V has negligible steroidogenic activity in transfected COS-1 cells (143) and only weakly transferred cholesterol from liposomes to liver mitochondria (14). To determine if these differences in A218V StAR from StAR might also be associated with altered ligand binding ability, the interaction of A218V StAR with NBD-cholesterol was examined. The interaction of equivalent amounts of NBD-cholesterol interaction with A218V StAR differed significantly from that with native StAR in several respects:

First, A218V StAR only weakly shifted the emission maximum of NBD-cholesterol from 562 nm to 545 nm (Fig, 2.1B, spectrum 1 vs spectrum 2), as compared to the shift

from 562 nm to 530 nm (Fig. 2.1B, spectrum 1 vs spectrum 3) exhibited by NBD-cholesterol binding to StAR. Thus, the A218V StAR mutation altered the polarity of the ligand binding site to make it less hydrophobic in the region sensed by the NBD-fluorophore of NBD-cholesterol.

Second, the maximal fluorescence intensity of NBD-cholesterol in A218V StAR was markedly reduced (Fig. 1B) as compared to NBD-cholesterol bound to StAR (Fig. 2.1 A and B). When this difference was evaluated over the concentration range from 5-100 nM NBD-cholesterol, the maximal fluorescence intensity of A218V StAR bound NBD-cholesterol was up to 50-fold lower than that of NBD-cholesterol bound to StAR (Fig. 2.3B vs 2.3A).

Third, A218V StAR exhibited much lower affinity for NBD-cholesterol than StAR. Analysis of the NBD-cholesterol binding data in Fig. 2.3B as described in Methods yielded a  $k_d = 232$  nM for A218V StAR binding NBD-cholesterol. This  $k_d$  was 7.2-fold lower than that obtained for StAR.

Fourth, the shape of the A218V StAR binding curve for NBD-cholesterol (Fig. 2.3B) was much less sigmoidal than that of StAR (Fig. 3A). Best linear regression analysis of the binding data as described in Methods showed that A218V StAR bound NBD-cholesterol only at a single binding site.

In summary, the A218V mutant StAR maximally bound only half as much sterol as StAR and at 7.2-fold lower affinity than StAR. The observation that A218V StAR binds NBD-cholesterol less and more weakly may be rationalized on the basis of the structural information available. It is possible that the more bulky valine side chain provides steric hindrance to the cholesterol binding site in StAR based on comparison with the X-ray crystal structure of MLN64 (15).

#### 2.3.4 *StAR Trp: Aqueous Accessible or Buried*

The N-62 StAR portion of complete StAR protein has 4 Trp and 3 Tyr residues(149). The fluorescence emission of StAR Trp can be selectively resolved from that of Tyr residues by excitation at 295 nm, at which wavelength Trp is preferentially



excited. The localization of the StAR Trp residues as being buried or aqueous accessible was determined by Stern-Volmer quenching (see Methods). StAR Trp residues were poorly accessible to acrylamide, an aqueous quenching molecule (Fig. 2.2B). Acrylamide quenching constants,  $K_{SV}$ , calculated from these data were  $25.2 \text{ M}^{-1}$  for N-acetyl tryptophanamide, consistent with earlier data (167), and  $2.8 \text{ M}^{-1}$  for StAR Trp.

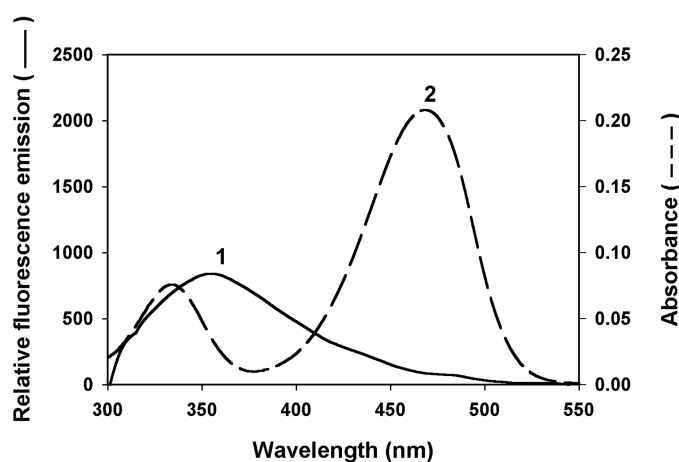


FIG. 2.4. **Spectral overlap of N-62 StAR Trp fluorescence emission with NBD-cholesterol absorption (excitation).** All conditions were as described in Methods and excitation was at 295 nm. Spectrum 1 represents the emission spectrum of StAR (42 nM in PBS). Spectrum 2 demonstrates the absorbance spectrum of NBD-cholesterol (10  $\mu\text{M}$  in ethanol).

Since the StAR Trp was nearly 10-fold less accessible to acrylamide quenching than N-acetyl tryptophanamide, these data suggest that StAR Trp residues were buried in the protein and not much accessible to the aqueous environment. Extrapolation of a plot of  $F_0/(F_0-F)$  vs  $[\text{acrylamide}]^{-1}$  to high acrylamide concentration yields an intercept that reflects the inaccessible fraction (159). For StAR Trp quenching by acrylamide such a plot yielded an intercept near 1 (Fig. 2.2C), consistent with all the StAR trp residues being inaccessible to the aqueous. Thus, these data showed that StAR Trp residues were buried in the protein and not aqueous accessible.

### *2.3.5 Fluorescence Resonance Energy Transfer of StAR Trp to Bound NBD-Cholesterol; Quenching of StAR Trp Fluorescence Emission*

As indicated in the Methods section, efficient fluorescence resonance energy transfer (FRET) is possible when the donor and acceptor exhibit significant spectral overlap between the emission of the donor and the excitation/absorbance of the acceptor. When the donor is excited, FRET is observed as (i) reduced emission of the donor, and (ii) appearance of sensitized emission of the acceptor. Sensitized emission refers to emission of the FRET acceptor (NBD-cholesterol) due to energy transfer rather than direct excitation of the acceptor. The spectral properties of NBD-cholesterol and StAR Trp are well suited for Forster energy transfer. StAR Trp excitation at 295 results in maximal emission near 352 nm (Fig. 2.4, spectrum 1) which overlaps well with the NBD-cholesterol absorbance maximum centered near 340 nm (Fig. 2.4, spectrum 2). These data suggest that the StAR Trp and NBD-group of NBD-cholesterol may be an excellent donor/acceptor pair for FRET.

The extent of FRET from StAR Trp to bound NBD-cholesterol was examined by incubating NBD-cholesterol in the presence of StAR, exciting StAR Trp at 295 nm, and measuring emission over the range from 300-600 nm (Fig. 2.5A). The reduced StAR Trp emission near 352 nm and the appearance of sensitized NBD-cholesterol emission at 530 nm clearly demonstrated efficient FRET. The lack of complete StAR quenching by

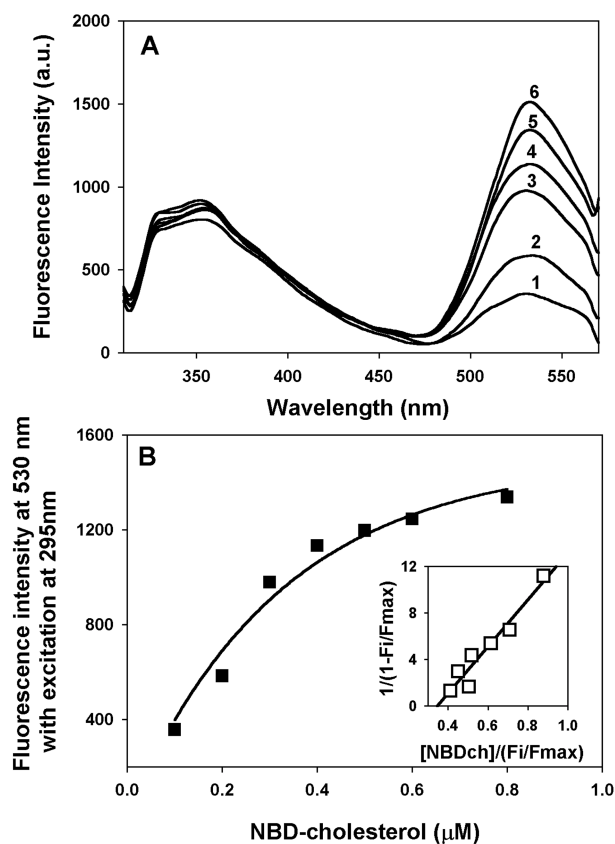


FIG. 2.5. **Effect of FRET between N-62 StAR Trp and bound NBD-cholesterol.** *Panel A.* StAR (42nM) was incubated with increasing concentrations of NBD-cholesterol over the range 100-1000 nM as indicated in Methods. The StAR Trp was excited at 295nm and fluorescence emission spectra were obtained from 300-600 nm. NBD-cholesterol concentrations were: spectrum 1, 100nM; spectrum 2, 200nM; spectrum 3, 300nM; spectrum 4, 400nM; spectrum 5, 600nM; spectrum 6, 1 $\mu\text{M}$ . *Panel B.* NBD-cholesterol binding curve obtained by plotting the increase in NBD-cholesterol sensitized emission at 530 nm (panel A) as a function of increasing NBD-cholesterol concentration. The inset in Panel B shows a linear transformation of the data consistent with a single binding site with  $k_d$  of 49 nM.

NBD-cholesterol suggested that not all four of the Trp residues in StAR are located near and/or correctly oriented to the NBD-cholesterol for efficient quenching. Of the four Trp residues in StAR, three are conserved in StAR and MLN64 and one in beta strand 9 (Trp241) on MLN64 was shown to directly contribute to the hydrophobic tunnel (15). Because of the structural similarity between StAR and MLN64 (15), these data suggest that the NBD-cholesterol energy transfer occurs to one StAR Trp located in a ligand binding tunnel (analogous to that for MLN64) wherein at one Trp residue was in close proximity to the NBD-group.

To further refine the above qualitative observations, the above tryptophan fluorescence quenching data were used to determine the intermolecular distance between StAR Trp and bound NBD-cholesterol as described in Methods. The overlap integral  $J$  was determined experimentally to be  $5.68 \pm 0.45 \times 10^{-14} \text{ M}^{-1} \text{ cm}^{-1}$  (Table 2.1), basically similar to that obtained for other proteins (rev. in (158)). The transfer efficiency was calculated from Trp quenching (Equation 2.5, see Methods) to be 64% and the  $R_{2/3}$  value obtained thereby (Equation 2.4, see Methods) was  $32.6 \pm 1.3 \text{ \AA}$  (Table 2.1). Based on comparisons with MLN64 (15), this distance was consistent with the putative location of the energy donor (NBD-cholesterol) located in StAR.

### *2.3.6 Sterol Binding Parameters of StAR Determined by FRET and Sensitized Emission of Bound NBD-Cholesterol*

Excitation of StAR Trp at 295 nm resulted in sensitized fluorescence emission at 530 nm from StAR bound NBD-cholesterol. This sensitized emission increased with increasing NBD-cholesterol concentration (Fig. 2.5A) and was plotted as a binding curve (Fig. 2.5B). Analysis of the latter binding curve as described in Methods showed that StAR bound NBD-cholesterol with  $K_d = 49 \text{ nM}$ . A plot of the hyperbolic increase in sensitized NBD-cholesterol emission as  $1/(1-F_i/F_{\text{max}})$  vs  $[\text{NBD-cholesterol}]/(F_i/F_{\text{max}})$  as described earlier (153) was linear (Fig. 2.5B, inset), consistent with a single binding site containing a Trp interacting with cholesterol.

TABLE 2.1  
*Forster energy transfer from N-62 StAR Trp to bound NBD-cholesterol.*

$R_{2/3}$  is the distance between the N-62 StAR Trp and bound NBD-cholesterol was calculated from the quenching of N-62 StAR Trp emission as described in Methods.  $J$  is the overlap integral.  $R_0$  is the critical distance at which 50% energy transfer occurs.  $R_0$  is calculated from the quantum yield of N-62 StAR Trp (0.24), the refractive index (1.4), and the orientation factor (2/3) as described in Methods.  $E$  is the energy transfer efficiency.

Energy donor	Energy acceptor	$J$	$R_0$	$E$	$R_{2/3}$
		$M^{-1} cm^{-1}$	$\text{\AA}$	%	$\text{\AA}$
N-62 StAR	NBD-cholesterol	$5.68 \pm 0.45$	$36.0 \pm 1.1$	64	$32.6 \pm 1.3$

In addition to the above described Trp residues, N-62 StAR has 3 Tyr residues (149) concomitant excitation of StAR Trp as well as Tyr residues at 280 nm resulted in maximal emission near 350 nm that exhibited slightly, about 8%, higher intensity (Fig. 2.6A vs Fig. 2.5A). In the presence of NBD-cholesterol, excitation of StAR Trp as well as Tyr residues at 280 nm also resulted in the appearance of sensitized NBD-cholesterol emission due to energy transfer from StAR bound NBD-cholesterol (Fig. 2.6A).

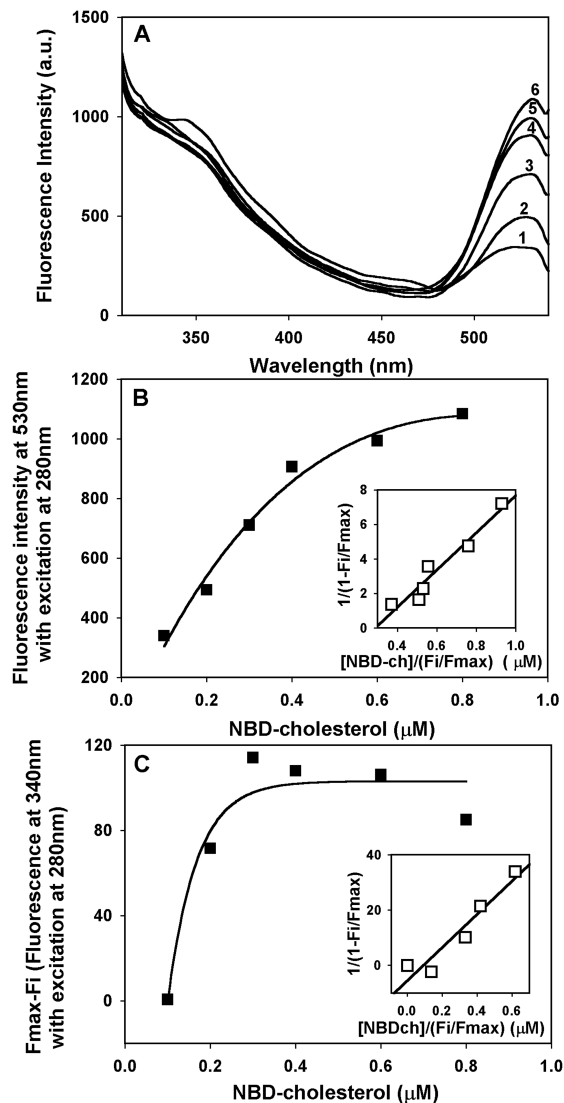


FIG. 2.6. **Effect of FRET between N-62 StAR Trp/Tyr and bound NBD-cholesterol.** All conditions were the same as in Fig. 5 except that StAR Trp and Tyr residues were excited at 280 nm. *Panel A*, emission spectra; protein and ligand concentrations as in Fig. 5A. *Panel B*, binding curve plotted as NBD-cholesterol concentration versus its emission at 530 nm. Inset in Panel B shows the linear plot of data in panel B. *Panel C*, NBD-cholesterol binding plotted as NBD-cholesterol concentration versus decrease in StAR Trp/Tyr emission at 340 nm. The inset in Panel C shows a linear transformation of the data.

The sensitized emission increased with increasing NBD-cholesterol concentration (Fig. 2.6A). These data were plotted as a binding curve (Fig. 2.6B) which showed that StAR bound NBD-cholesterol with  $K_d = 93$  nM. Again, the plot of the hyperbolic increase in sensitized NBD-cholesterol emission as  $1/(1-F_i/F_{max})$  vs  $[NBD-cholesterol]/(F_i/F_{max})$  (Fig. 2.6B, inset) was linear, consistent with a single binding site.

When the StAR Trp and Tyr were excited at 280 and emission was monitored at 350 nm in the presence of increasing NBD-cholesterol, a decrease in StAR aromatic amino acid residue emission was observed (Fig. 2.6A). This decrease was plotted as a function of increasing NBD-cholesterol (Fig. 2.6C). These data, plotted as a binding curve (Fig. 2.6C), were analyzed as described in Methods and yielded a  $K_d = 17$  nM for StAR binding NBD-cholesterol. The plot of the hyperbolic increase in sensitized NBD-cholesterol emission as  $1/(1-F_i/F_{max})$  vs  $[NBD-cholesterol]/(F_i/F_{max})$  (Fig. 2.6C, inset) was linear, again consistent with a single binding site.

The NBD-cholesterol sensitized fluorescence emission data were used to determine the intermolecular distance between StAR Tyr/Trp (excitation at 280 nm) and bound NBD-cholesterol (see Methods). The transfer efficiency was calculated from the sensitized emission of StAR-bound NBD-cholesterol (see Methods) to be 61% and the  $R_{2/3}$  value obtained therefrom was 33.4 Å, essentially the same as that obtained from quenching of StAR Trp (excitation at 295 nm) (Table 2.1)

Together these data suggested that FRET from StAR to bound NBD-cholesterol occurred at a single binding site from the same Trp excited either at 295 or 280 nm. Interestingly, the mean  $K_d = 53 \pm 22$  nM determined by FRET (Figs. 2.5 and 2.6) was very similar to the  $K_d = 32 \pm 4$  nM determined from exciting NBD-cholesterol at 473 and plotting the increase in NBD-cholesterol fluorescence emission at 562 nm (Fig. 2.3). Since FRET did not reveal the presence of the second binding site noted by plots of fluorescence emission of NBD from StAR bound NBD-cholesterol (Fig. 2.3), the second bound NBD-cholesterol was probably not located closely enough and/or oriented such for FRET to occur in StAR.

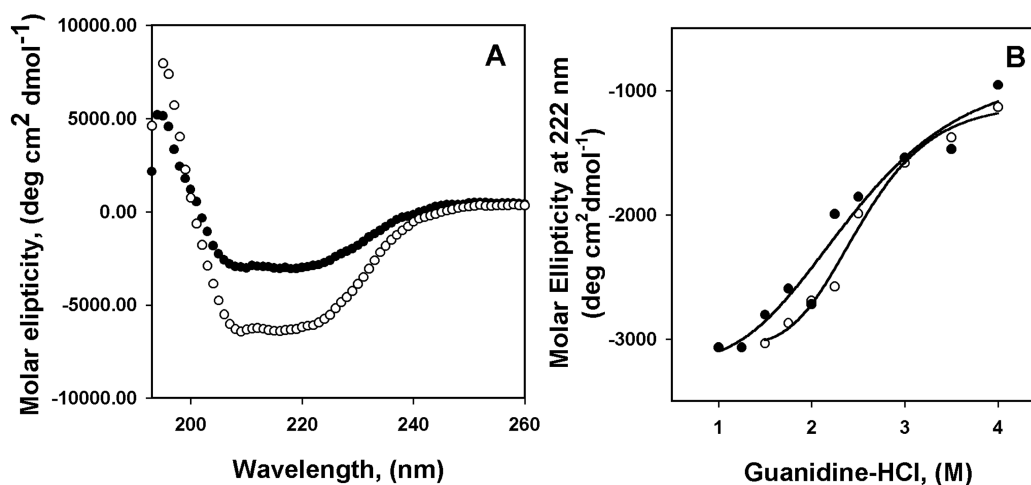


FIG. 2.7. **Effect of cholesterol binding on circular dichroic spectra of N-62 StAR protein.** *Panel A*, circular dichroic spectra of StAR (2.59 μM) in the absence (open circles) and in the presence (black circles) of cholesterol (1 μM) were obtained as described in Methods. *Panel B*, guanidine-HCl unfolding curves of StAR in the absence (filled circles) and presence (open circles) of cholesterol. Guanidine-HCl unfolding was conducted as described in Methods.

### 2.3.7 Effect of Sterol Binding on StAR Conformation

The effect of cholesterol binding on StAR conformation was examined by acrylamide quenching and by circular dichroism, a technique sensitive to alterations in protein secondary structure, as follows:

First, Stern-Volmer quenching studies with acrylamide showed that cholesterol binding did not alter structure of StAR to make Trp residues more aqueous accessible. Examination of the effect of sterol binding on the emission maxima of StAR aromatic amino acids upon excitation of StAR Trp at 295 (Fig. 2.5A) or StAR Trp/Tyr at 280 nm (Fig. 2.6A) showed in neither case was the wavelength of StAR maximal emission



near 350 nm shifted. In addition, binding of cholesterol to StAR did not significantly alter the StAR Trp quenching by acrylamide (Fig. 2.2B). The acrylamide Stern-Volmer quenching constant,  $K_{SV}$ , of StAR Trp was  $2.7 \text{ M}^{-1}$  and  $2.5 \text{ M}^{-1}$  in the absence and presence of cholesterol.

Second, circular dichroic spectra of StAR were significantly altered in the presence of cholesterol. Circular dichroic spectra of StAR exhibited minima at 208 and 222 nm (Fig. 2.7A, open circles), consistent with the presence of substantial  $\alpha$ -helical structure (168). In the presence of cholesterol, the minima at 208 and 222 nm were both significantly reduced (Fig. 2.7A, closed circles). The effects of cholesterol (Fig. 2.7A) and NBD-cholesterol (not shown) on StAR spectra were similar.

Third, the cholesterol induced conformational change in StAR secondary structure observed by circular dichroism involved polar group(s) in StAR, since circular dichroism spectral changes were absent in the presence of high salt (50 mM  $\text{NaH}_2\text{PO}_4$ , 300 mM NaCl, pH 8). Nevertheless, StAR binding curves for NBD-cholesterol were the same in the absence (Fig. 2.3) or presence (not shown) of high salt.

Fourth, since lower molar ellipticity of StAR containing bound cholesterol (Fig. 2.7A) indicated less structured StAR in the presence of ligand, the stability of the unliganded and liganded StAR were examined by guanidine-HCl induced unfolding. Guanidine-HCl induced unfolding curves of StAR in the presence and absence of cholesterol were very similar (Fig. 2.7B). The concentrations for 50% unfolding,  $C^{50\%}$ , calculated from these curves were  $2.4$  and  $2.5 \text{ M}^{-1}$ , respectively.

In summary, these data showed that cholesterol binding significantly altered the relative proportion of  $\alpha$ -helical structure, this did not alter the exposure of StAR Trp residues to the aqueous.

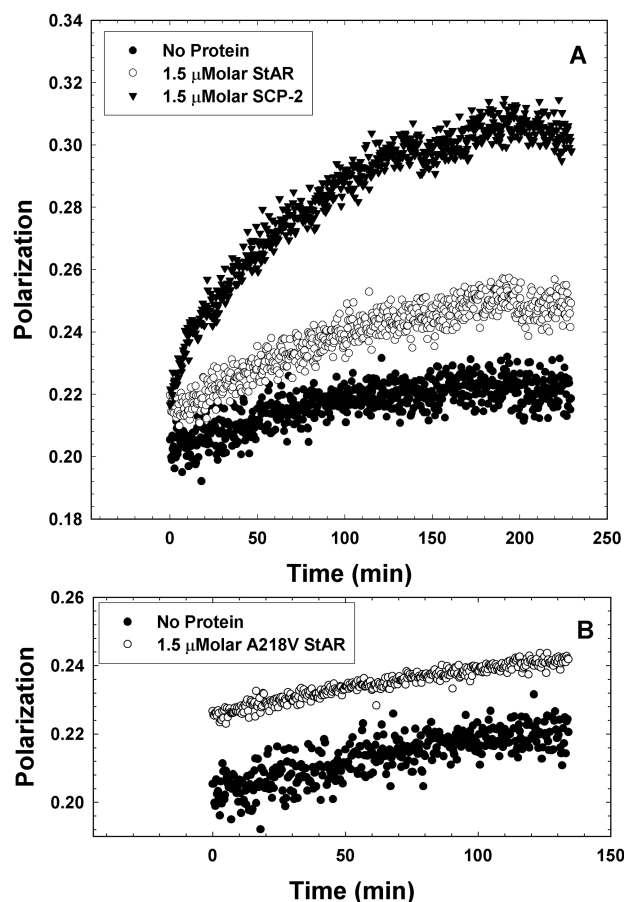


FIG. 2.8. **Effect of N-62 StAR, A218V N-62 StAR, and SCP-2 on sterol transfer from mitochondrial membranes isolated from normal (CWN) human fibroblasts.** Sterol transfer was measured as described in Methods. *Panel A:* The curves show the change in fluorescence polarization as a function of time after addition of a 10-fold excess of acceptor (dehydroergosterol deficient) membranes to donor (dehydroergosterol rich) membranes. Closed circles, donor + acceptor only; open circles, donor + acceptor + 1.5  $\mu\text{M}$  StAR; closed triangles, donor + acceptor + 1.5  $\mu\text{M}$  SCP-2. *Panel B:* The curves show the change in fluorescence polarization as a function of time after addition of a 10-fold excess of acceptor (dehydroergosterol deficient) membranes to donor (dehydroergosterol rich) membranes. Closed circles, donor + acceptor only; open circles, donor + acceptor + 1.5  $\mu\text{M}$  mutant StAR.

### 2.3.8 *Spontaneous Sterol Transfer from Mitochondrial Membranes*

The basic characteristics of spontaneous sterol transfer between mitochondrial membrane donors and mitochondrial acceptors were obtained for normal (CWN) human fibroblast mitochondria (Fig. 2.8A, bottom curve) and MA-10 mitochondria (Fig. 2.9, bottom curve). In the absence of mitochondrial membrane acceptors, dehydroergosterol polarization in mitochondrial membrane donors was unaltered over the time period examined (not shown). However, addition of 10-fold excess acceptor mitochondrial membranes elicited a slow spontaneous sterol transfer. The initial rates of molecular sterol transfer from CWN fibroblast and MA-10 cell mitochondria were  $0.40 \pm 0.03$  and  $0.04 \pm 0.01$  pmol/min (Table 2.2). Thus, spontaneous sterol transfer from mitochondria isolated from steroidogenic cells (MA-10 cells) was 10-fold slower than that from mitochondria isolated from normal (CWN) human fibroblasts.

### 2.3.9 *StAR Preferentially Enhanced the Initial Rate of Molecular Sterol Transfer from Mitochondrial Membranes of Steroidogenic MA-10 Cells versus Fibroblasts*

StAR significantly enhanced sterol transfer from mitochondrial membranes isolated from normal (CWN) human fibroblasts (Fig. 2.8A, middle curve), while the A218V mutant StAR did not enhance sterol transfer (Fig. 2.8B). StAR also significantly enhanced sterol transfer from mitochondrial membranes isolated from MA-10 cells (Fig. 2.9, top curve). Comparison of the magnitude of StAR induced polarization changes showed that StAR was much more effective in enhancing sterol transfer from mitochondria isolated from the steroidogenic MA-10 cells. The initial rate of StAR-mediated molecular sterol transfer from normal (CWN) fibroblast mitochondria,  $0.60 \pm 0.04$  pmol/min, was only 1.5-fold faster than spontaneous sterol transfer from

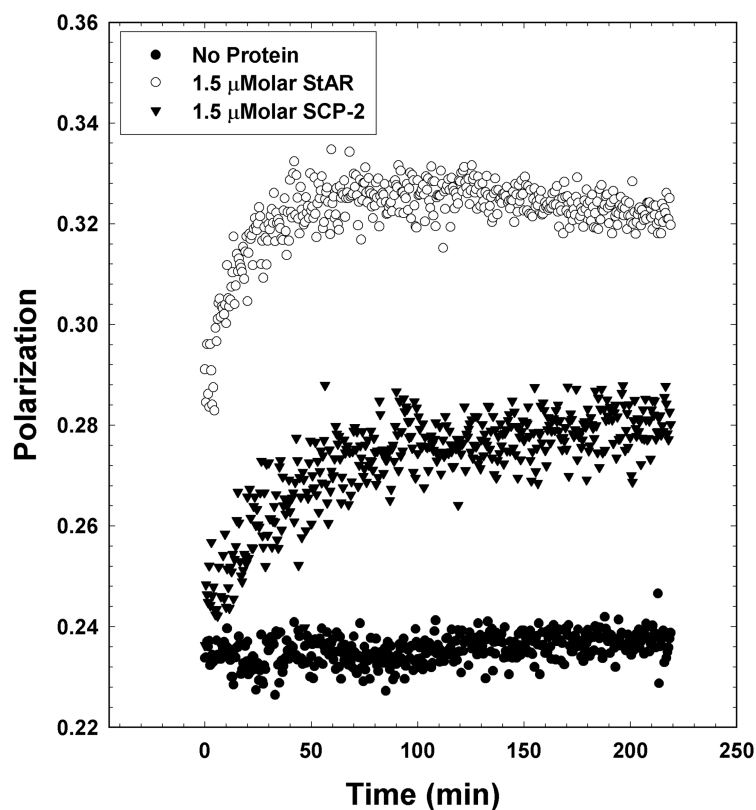


FIG.2.9. **Effect of N-62 StAR and SCP-2 on sterol transfer from mitochondrial membranes isolated from steroidogenic MA-10 Leydig cells.** Sterol transfer was measured as described in Methods. The curves show the change in fluorescence polarization as a function of time after addition of a 10-fold excess of acceptor (dehydroergosterol deficient) membranes to donor (dehydroergosterol rich) membranes. Closed circles, donor + acceptor only; open circles, donor + acceptor + 1.5  $\mu$ M StAR; closed triangles, donor + acceptor + 1.5  $\mu$ M SCP-2.

these mitochondria (Table 2.2). In contrast, the initial rate of StAR-mediated molecular sterol transfer from the steroidogenic MA-10 cell mitochondria,  $3.97 \pm 0.36$  pmol/min, was enhanced 100-fold when compared to spontaneous sterol transfer from these mitochondria (Table 2.2). Even when the absolute initial rates of StAR-mediated

molecular sterol transfer of the two types of mitochondria was compared, the StAR-mediated molecular sterol transfer from MA-10 cell mitochondria was 6.6-fold faster than the StAR-mediated molecular sterol transfer from normal (CWN) human fibroblast mitochondria (Table 2.2).

*2.3.10 Effect of SCP-2 on Initial Rate of Molecular Sterol Transfer from Mitochondrial Membranes of Steroidogenic MA-10 Cells and Normal CWN Human Fibroblasts*

SCP-2 significantly enhanced sterol transfer from normal (CWN) human fibroblast (Fig. 2.8, top curve) and MA-10 cells (Fig. 2.9, middle curve) mitochondrial membranes. Comparison of the magnitude of SCP-2 induced increase in dehydroergosterol polarization showed that SCP-2 was more effective in enhancing sterol transfer from mitochondria isolated from steroidogenic MA-10 cells, but the effect was not as large as that observed with StAR. The initial rate of SCP-2-mediated molecular sterol transfer from normal (CWN) fibroblast mitochondria,  $4.10 \pm 0.15$  pmol/min, was 10-fold faster than spontaneous sterol transfer from these mitochondria (Table 2.2). In contrast, the initial rate of SCP-2-mediated molecular sterol transfer from the steroidogenic MA-10 cell mitochondria,  $1.58 \pm 0.19$  pmol/min, was enhanced 45-fold when compared to spontaneous sterol transfer from these mitochondria (Table 2.2). Even when the absolute initial rates of SCP-2-mediated molecular sterol transfer of the two types of mitochondria were compared, the SCP-2-mediated molecular sterol transfer from normal (CWN) fibroblast mitochondria was 2.5-fold faster than the SCP-2-mediated molecular sterol transfer from steroidogenic MA-10 cell mitochondria (Table 2.2).

In summary, SCP-2 was nearly 7-fold more effective than StAR in enhancing the initial rate of molecular sterol transfer from mitochondrial membranes isolated from normal (CWN) human fibroblasts. In contrast, both StAR and SCP-2 (2.2-fold less so) effectively enhanced the initial rate of molecular sterol transfer from steroidogenic MA-10 cell mitochondria.

TABLE 2.2  
*Initial rates of molecular sterol transfer from mitochondrial membranes isolated from normal CWN human fibroblasts and steroidogenic MA-10 Leydig cells.*

Mitochondrial membrane Source	Protein <sup>a</sup>	Initial rate <sup>b</sup>
		<i>pmol/min</i>
CWN fibroblasts	None	0.40 ± 0.03
	N-62 StAR	0.60 ± 0.04
	SCP-2	4.10 ± 0.15
MA-10 cells	None	0.04 ± 0.01
	N-62 StAR	3.97 ± 0.36
	SCP-2	1.58 ± 0.19

<sup>a</sup> Protein concentration was 1.5 μM N-62 StAR or 1.5 μM SCP-2

<sup>b</sup> Values indicate mean ± S.D. (n=3 or 4).

<sup>c</sup> p < 0.05 and p < 0.01, respectively, as compared to no protein added.

<sup>d</sup> p < 0.01 versus SCP-2.

### 2.3.11 Dynamic Analysis of Spontaneous Sterol Transfer from Mitochondrial Membranes

In order to determine if mitochondrial membrane cholesterol may be present in multiple kinetic pools, the dehydroergosterol polarization data in Figs. 2.8 and 2.9 were fit to one- and two-exponential equations and kinetic parameters of the sterol transfer process were resolved as described in Methods. Spontaneous transfer of sterol from mitochondrial membranes isolated from normal (CWN) human fibroblasts displayed two kinetic pools of cholesterol, a slowly exchangeable sterol pool with a  $t_{1/2}$  of 564±80 min, comprising 11% of the total sterol, and an essentially non-exchangeable sterol pool ( $t_{1/2}$  was too slow to be measured), comprising 89% of the total sterol (Table 2.3). In contrast, spontaneous transfer of sterol from mitochondrial membranes isolated from steroidogenic MA-10 cells displayed only a single kinetic pool of cholesterol that was

essentially non-exchangeable sterol pool ( $t_{1/2}$  was too slow to be measured) (Table 2.3). Thus, the mitochondrial membrane sterols of steroidogenic MA-10 cells were significantly different from those of the fibroblast mitochondria. In contrast to the fibroblast mitochondria, the MA-10 cell mitochondria exhibited only a single domain of essentially non-transferable sterol.

TABLE 2.3

*Mitochondrial membrane cholesterol domain dynamics.*

Half-times are in minutes while fractions refer to  $f_1$  = transferable fraction,  $f_2$  = nontransferable fraction. Values represent the mean  $\pm$  S.D. (n=3).

Mitochondrial membranes Source	Protein	$t_{1/2}$	$f_1$	$F_2$
		<i>min.</i>		
CWN fibroblasts	None	564 $\pm$ 80	0.11 $\pm$ 0.01	0.89 $\pm$ 0.02
	N-62 StAR	462 $\pm$ 70	0.22 $\pm$ 0.01	0.78 $\pm$ 0.01
	SCP2	65 $\pm$ 10	0.67 $\pm$ 0.03	0.33 $\pm$ 0.02
MA-10 cells	None			1.00
	N-62 StAR	10 $\pm$ 1	0.64 $\pm$ 0.02	0.36 $\pm$ 0.01
	SCP-2	35 $\pm$ 2	0.31 $\pm$ 0.01	0.70 $\pm$ 0.01

### 2.3.12 *StAR Preferentially Altered the Sterol Kinetic Pools of Mitochondrial Membranes Isolated from Steroidogenic MA-10 Cells versus Fibroblasts*

StAR significantly altered mitochondrial membrane sterol domains resolved by kinetic analysis. StAR-mediated transfer of sterol from mitochondrial membranes isolated from normal (CWN) human fibroblasts best fit two kinetic pools of cholesterol. While the  $t_{1/2}$  of the slowly exchangeable sterol pool, 462 $\pm$ 70 min, was not significantly different from that of spontaneous sterol transfer, its fractional contribution was increased 2-fold (Table 2.3). Thus, StAR did not induce formation of additional kinetically resolvable sterol domains in mitochondria of normal human fibroblasts.

Instead, StAR increased the size of a slowly exchangeable sterol domain. StAR-mediated transfer of sterol from mitochondrial membranes isolated from steroidogenic MA-10 cells also fit two kinetic pools of cholesterol. The transferable sterol pool exhibited a very rapid  $t_{1/2} = 10 \pm 1$  min and accounted for  $64 \pm 3\%$  of MA-10 mitochondrial membrane sterol (Table 2.3). These data indicated that StAR induced the formation of a large, rapidly transferable sterol domain in mitochondria from steroidogenic MA-10 cells. The size of the StAR-induced, transferable sterol domain was 3-fold larger than that of StAR-mediated sterol transfer from normal CWN human fibroblast mitochondria. Finally, the  $t_{1/2}$  of the transferable sterol domain induced by StAR in MA-10 cell mitochondria was 56-fold faster than that of StAR-mediated sterol transfer in normal CWN human fibroblast mitochondria (Table 2.3).

### *2.3.13 Effect of SCP-2 on Sterol Kinetic Pools of Mitochondrial Membranes Isolated from Steroidogenic MA-10 Cells versus Fibroblasts*

SCP-2 qualitatively exhibited the same effects on mitochondrial sterol domains as noted above for StAR. However, the effects of SCP-2 were quantitatively very different from those of StAR. SCP-2-mediated sterol transfer of sterol from mitochondrial membranes isolated from normal (CWN) human fibroblasts best fit two kinetic pools of cholesterol. SCP-2 accelerated the  $t_{1/2}$  of the slowly exchangeable sterol pool,  $65 \pm 10$  min, nearly 9-fold as compared to spontaneous sterol transfer (Table 2.3). Furthermore, SCP-2 increased the size of the transferable sterol domain,  $f_1 = 0.67 \pm 0.03$ , nearly 6-fold as compared to spontaneous sterol transfer from normal CWN human fibroblast mitochondrial membranes (Table 2.3). Therefore, although SCP-2 did not induce formation of additional kinetically-resolvable sterol domains in mitochondria of normal human fibroblasts, SCP-2 dramatically increased the size and decreased the half-time of the slowly transferable sterol domain.

In contrast to spontaneous sterol transfer from MA-10 cell mitochondria, which fit only a single non-transferable sterol pool, SCP-2-mediated transfer of sterol from mitochondrial membranes isolated from steroidogenic MA-10 cells fit two kinetic pools



of cholesterol. The transferable sterol pool had a very rapid  $t_{1/2} = 35 \pm 2$  min and accounted for  $31 \pm 1\%$  of MA-10 mitochondrial membrane sterol (Table 2.3). Thus, SCP-2 induced the formation of a large, rapidly transferable sterol domain in mitochondria from steroidogenic MA-10 cells. The size of the SCP-2-induced, transferable sterol domain was 2-fold smaller than that of SCP-2-mediated sterol transfer from normal CWN human fibroblast mitochondria. Finally, the  $t_{1/2}$  of the transferable sterol domain induced by SCP-2 in MA-10 cell mitochondria was  $<2$ -fold faster than that of SCP-2-mediated sterol transfer from normal CWN human fibroblast mitochondria (Table 2.3).

Taken together with the data in the previous section, these findings suggested that StAR was much less promiscuous than SCP-2 and preferentially induced the formation of rapidly transferable sterol domains in mitochondria isolated from the steroidogenic MA-10 cells.

## 2.4 DISCUSSION

Significant advances in the molecular biology of StAR have greatly contributed to our understanding of the role that this protein plays in acute regulation of gonadal and adrenal steroidogenesis. In contrast, much less is known regarding the nature of putative ligand binding sites and the mechanism(s) of action of this intriguing protein. The full-length StAR protein is comprised of at least two functional regions: an N-terminal mitochondrial targeting sequence encompassed within the 62 N-terminal amino acid portion of the protein; an N-62 portion of StAR comprising the cholesterol transfer component. The data presented herein provide several novel insights concerning the ligand binding site of StAR and mechanism whereby StAR enhances sterol transfer from mitochondrial membranes.

First, the results showed for the first time the close molecular interaction of StAR with a fluorescent cholesterol derivative. This represents a major advance over the use of cholesterol for ligand binding assays. Cholesterol has a very low CMC, near 20-45 nM

(164). This extremely poor aqueous solubility makes it difficult to use standard radioligand binding assays (requiring separation of bound from free cholesterol) to distinguish true cholesterol binding to a protein from cholesterol aggregation/coaggregation with the protein. In contrast, the NBD-cholesterol based fluorescence binding assays used herein did not require separation of bound from free sterol and, because of the much greater sensitivity of the photon-counting based fluorescence assay, were performed at very low concentrations of NBD-cholesterol (below the CMC). Two types of experiments demonstrated a close molecular interaction between StAR and NBD-cholesterol. (i) The emission maximum of NBD-cholesterol was 32 nm blue-shifted in the presence of StAR, but not in the presence of the inactive A218V mutant StAR. When compared to a standard curve of NBD-group emission wavelength vs solvent dielectric constant (169), the blue-shifted NBD-spectrum in the presence of active StAR was consistent with a shift of the NBD-group from an aqueous to a more hydrophobic environment with a dielectric constant near 2. Consistent with the relatively hydrophobic nature of the StAR ligand binding pocket, computer models of the x-ray crystal structure of the MLN64 START domain showed the presence of a hydrophobic tunnel thought to be the cholesterol binding site (15). Taken together, these data suggested that the NBD-group of NBD-cholesterol was buried deep in a putative “hydrophobic tunnel”, assuming a similar structure of StAR as for MLN64. It should be noted that the proposed orientation of NBD-cholesterol or cholesterol in StAR or MLN64, respectively, differs significantly from that of sterol in the binding pocket of SCP-2, a totally unrelated cholesterol binding/transfer protein. NBD-cholesterol binding to SCP-2 did not result in significant shift of the NBD-emission spectrum, thereby suggesting that the NBD-group of NBD-cholesterol bound to SCP-2 was localized near the surface opening of the SCP-2 protein binding pocket (165). NMR data confirmed that SCP-2-bound 3- $^{13}\text{C}$ -cholesterol was oriented with the polar  $3\beta\text{-OH}$  of the sterol being oriented near the surface opening of the SCP-2 binding pocket (151). (ii) FRET from StAR Trp to bound NBD-cholesterol was detected as decreased StAR Trp emission and appearance of sensitized NBD-cholesterol emission. Calculation of the energy

transfer distances from either the decrease in StAR Trp emission or the appearance of sensitized NBD-cholesterol emission revealed that the StAR Trp and NBD-cholesterol were within 33 Å. This distance was in the range of those reported for other lipid binding proteins (155) (22). These data could not be accounted for by coaggregation of NBD-cholesterol with StAR.

Second, the cholesterol binding affinity of StAR was calculated for the first time, establishing that StAR binds sterol with high affinity,  $K_d$  near 32 nM. This conclusion was based on data obtained from direct binding of fluorescent sterols (NBD-cholesterol with  $K_d$  near 32 nM; dehydroergosterol with  $K_d$  near 76 nM), FRET from StAR Trp to bound NBD-cholesterol (decreased StAR Trp emission), and FRET induced sensitized emission from StAR bound NBD-cholesterol. Native N-62 StAR bound sterol with 7.3-fold higher affinity than did the functionally inactive A218V N-62 StAR mutant. It should be noted that earlier preliminary data from this laboratory suggested that the full-length StAR protein binds NBD-cholesterol, but solubility problems with this protein preparation precluded accurate determination of binding parameters (170). Likewise, the use of  $\mu\text{M}$  concentrations of radiolabeled cholesterol resulted in cholesterol aggregates that precluded determination of  $k_d$  of StAR for cholesterol (15).

Third, it was shown for the first time that StAR has two ligand binding sites for cholesterol with similar low nM  $K_d$ s. A direct NBD-cholesterol binding assay determined both cholesterol binding sites, while FRET based binding assays detected only one of these sites. The basis for the latter observation was probably due to only one of these sites containing a Trp residue. The structure of the MLN64 START domain (15) suggests that this site is likely to be adjacent to Trp241 which directly contributes to the hydrophobic tunnel and is in close proximity/orientation within the binding site for efficient FRET to bound NBD-cholesterol. Computer modeling of the MLN64 START domain (analogous to N-62 StAR) revealed a hydrophobic tunnel whose volume was estimated near  $1900 \text{ \AA}^3$  (15). This tunnel was postulated to be the ligand binding site. Because the volume occupied by cholesterol is about  $741 \text{ \AA}^3$  (170), the  $1900 \text{ \AA}^3$  hydrophobic tunnel in the MLN64 START domain (15) is sufficient to accommodate at

least one, or easily two, cholesterol molecules. In addition, the MLN64 START hydrophobic tunnel contains two buried polar residues, Asp and Arg, each of which could provide an interaction site for a  $3\beta$ -OH of each of two bound cholesterol molecules. The close sequence homology (35% identity) of N-62 StAR to the START domain of MLN64, as well as similar function in mediating cholesterol transfer for steroidogenesis (albeit in different types of tissues) (15), suggests that N-62 StAR may structurally adopt a similar hydrophobic tunnel/ligand binding cavity that may accommodate up to two cholesterol molecules. It should be noted that these observations showing two sterol binding sites in N-62 StAR were at variance with an earlier report wherein StAR bound radiolabeled cholesterol at a single sterol binding site(15). It may be that problems with cholesterol solubility experienced in the latter work precluded accurate measurements of the number of binding sites therein.

What is the functional significance of high affinity, low affinity sterol binding to StAR? High affinity, low capacity sterol binding is a general property of proteins that are capable of transferring sterols: SCP-2 (6) (151) (171) ; liver fatty acid binding protein (L-FABP), (6) (147) (172). This binding activity appears to be critical for StAR's action on mitochondrial membranes because a point mutation (A218V) that dramatically reduces affinity and capacity for sterol binding ablates the steroidogenic activity of StAR. Likewise, abolition of ligand binding to SCP-2 and L-FABP also inhibits their ability to enhance membrane sterol transfer (173)(174). Our findings indicate that the hydrophobic tunnel of the START domain can accommodate two cholesterol molecules and possibly other hydrophobic molecules in addition to sterols. This high affinity hydrophobic ligand binding domain may well be the catalyst for membrane perturbation (see below) forcing sterol ejection from the outer mitochondrial membrane.

Fourth, cholesterol binding elicits a structural change in StAR. This observation was supported by circular dichroism and by the sigmoidal shape of the NBD-cholesterol binding curve (Fig. 2.3A). Circular dichroic data showed for the first time that cholesterol binding to StAR altered the secondary structure of StAR to reduce the proportion of  $\alpha$ -helix. Furthermore, the sigmoidal shape of the NBD-cholesterol binding

curve and the presence of two binding sites was consistent with a conformational/allosteric effect wherein binding of the first sterol altered the conformation of StAR to allow binding of a second sterol. The functional significance of these ligand-induced alterations in StAR secondary structure and conformation is not yet clear, but may be related to the fact that sensitized emission of StAR bound NBD-cholesterol occurred from only one ligand binding site. In addition, the ligand induced change in StAR structure may play a role in altering the cholesterol domain structure of the mitochondrial membrane, thereby induce formation of rapidly transferable sterol domains as observed with mitochondria isolated from steroidogenic MA-10 cells.

Fifth, StAR dramatically enhanced the initial rate of sterol transfer from the outer mitochondrial membrane. Our assay for sterol transfer detects the movement of probe (dehydroergosterol) from donor mitochondria to acceptor mitochondria, presumably the transfer of dehydroergosterol from the outer membrane of the donor to the outer membrane of the acceptor mitochondria. This assumption is predicated upon the fact that StAR did not cause a change in dehydroergosterol polarization when added to donor mitochondria in the absence of acceptor mitochondria. A change in polarization under these circumstances might be anticipated if StAR enhanced dehydroergosterol transfer from the outer to the inner mitochondrial membrane. Because the mitochondria were not incubated under conditions (i.e. incubation with an energy source for generation of required reducing equivalents) that support steroidogenesis (MA-10 cell mitochondria) or cholesterol side chain 27-hydroxylation (human fibroblast mitochondria), it is likely that the inner membrane substrate pool of cholesterol was occupied, limiting flux of dehydroergosterol to the inner membrane. This would be expected given the observation that a “back-up” of cholesterol resulting in cholesterol loading of the endoplasmic reticulum and subsequently conversion of free cholesterol into cholesteryl esters occurs when steroidogenic cells are incubated with an inhibitor of the mitochondrial side-chain cleavage enzyme, aminoglutethimide (175).

Our findings using a recombinant protein lacking a mitochondrial targeting sequence are consistent with the hypothesis that StAR acts on the outer mitochondrial

membrane to cause a selective perturbation resulting in transfer of sterol to closely opposed inner membranes, as long as cholesterol metabolism is taking place. Our findings are inconsistent with a model that requires mitochondrial importation of StAR to effect sterol translocation. With a stoichiometry of two sterols bound per StAR molecule, it is also difficult to imagine StAR acting as a carrier protein with respect to cholesterol transfer to the inner mitochondrial membrane in steroidogenic cells because it is a low abundance protein. For example, the 2 gm (wet weight) human corpus luteum produces 80-160  $\mu$ moles of progesterone per 24 h. This requires the movement of an equivalent amount of cholesterol to the inner mitochondrial membrane. Approximately 1.3 to 2.6 g of StAR protein would be needed per 24 h to move this amount of substrate to the inner mitochondrial membrane cholesterol side-chain cleavage enzyme, assuming StAR makes a one way (i.e. non-recycling) trip with its charge of cholesterol. The fact that import-incompetent StAR is capable of stimulating mitochondrial steroidogenesis (143) argues against any model based on an intermembranous shuttle (15).

Sixth, StAR differentially stimulated the initial rate of sterol transfer from mitochondrial membranes of steroidogenic MA-10 cells as compared to normal CWN human fibroblasts. In contrast, SCP-2 appeared nearly equally effective regardless of mitochondrial source. It is interesting to speculate that the StAR-mediated preferential transfer of sterol from MA-10 mitochondria might be due to a StAR-receptor (protein or lipid) in the donor and/or possibly the acceptor mitochondrial membrane. Consistent with a requirement for a StAR "receptor" in the donor membrane to reveal differential effects of StAR and SCP-2, earlier data from our laboratory showed that StAR and SCP-2 were equally effective in mediating cholesterol transfer from liposomal model membrane donors (comprised of phospholipid and cholesterol, but no protein) to rat liver mitochondria (14). Furthermore, since trypsin treatment of the acceptor mitochondria did not significantly affect StAR mediated cholesterol transfer from the donor liposomes, this suggested that a StAR receptor in the acceptor membrane was not essential. Putative StAR receptors have been proposed, including the peripheral benzodiazepine

receptor (176) among others (143). It should be noted, however, that since StAR overexpressed in COS-1 cells enhances steroidogenesis (143) there cannot be an absolute specificity of mitochondrial responsiveness to StAR (i.e. non-steroidogenic cell mitochondria can respond to high levels of StAR). These findings do not rule out differences in relative sensitivity of mitochondria of steroidogenic cells that could be critical, however, under physiological conditions where StAR is present in low levels.

Seventh, StAR is not only a cholesterol binding protein, but equally important dramatically altered the cholesterol domain structure of mitochondrial membranes. Spontaneous sterol transfer from mitochondrial membranes was very slow ( $t_{1/2} > \text{days}$ ). StAR induced formation of a rapidly ( $t_{1/2}$  near 10 min) sterol pool that accounted for 64% of mitochondrial membrane sterol. This effect of StAR was relatively specific for mitochondrial membranes isolated from steroidogenic MA-10 cells as opposed to mitochondria isolated from normal (CWN) human fibroblasts. This specificity of StAR was not shared by another sterol carrier protein (SCP-2) which promiscuously enhanced sterol transfer from mitochondrial membranes of steroidogenic MA-10 cells as well as normal (CWN) human fibroblasts. The significance of the StAR induced alteration in mitochondrial membrane cholesterol domain structure is three-fold: (i) StAR elicits sterol transfer by acting on the outer mitochondrial membrane (14)(143) ; (ii) A StAR mediated membrane fusion mechanism has been ruled out(14); (iii) StAR is not present in large enough quantities in steroidogenic cells to transfer large quantities of cholesterol to the inner mitochondrial membrane solely by a cholesterol-carrier mechanism(14). However, by altering the domain structure of the outer mitochondrial membrane, the effect of low quantities of StAR may be magnified to induce a much larger flux of cholesterol to the inner mitochondrial membrane than could be accounted for by a simple carrier mechanism. A similar mechanism not requiring an aqueous carrier has been established for SCP-2 (171) and L-FABP (174) mediated sterol transfer between membranes.

In summary, the data presented herein provided several new insights into the mechanism of action of StAR. The finding that StAR binds cholesterol is consistent with

the proposal that StAR may act as a cholesterol binding/transfer protein, an activity separate from mitochondrial import of StAR (14) (143) . Likewise, the finding that StAR alters mitochondrial cholesterol domain structure to induce formation of a rapidly transferable sterol pool is also consistent with this hypothesis. However, the latter observation may also support the view that localization of StAR in mitochondrial intermembrane (outer-inner membrane) contact sites (142) (12) may disrupt cholesterol domain structure therein to allow the flow of cholesterol from the outer to the inner mitochondrial membrane wherein the first committed step of cholesterol oxidation for steroidogenesis occurs. The fact that the inactive A218V mutant N-62 StAR has only a single, 7-fold lower affinity site for sterol binding, suggests that either mechanism must take into account the requirement for high affinity binding of at least two cholesterol molecules/StAR.



### CHAPTER III

## LIGAND SPECIFICITY AND CONFORMATIONAL DEPENDENCE OF THE HEPATOCTE NUCLEAR FACTOR-4 $\alpha$ (HNF-4 $\alpha$ )

### 3.1 INTRODUCTION

Hepatocyte nuclear factor 4 (HNF-4) is a member of the superfamily of nuclear receptors which includes steroid hormone receptors and nonsteroid ligand dependent transcription factors, e.g. thyroid hormone receptor, RXR, RAR, peroxisome proliferator activated receptors (PPARs) (rev.in (36)(177)). HNF-4 $\alpha$  isoforms ( $\alpha_1$ - $\alpha_3$ ) have been cloned and characterized and are expressed in mammals in liver, kidney, intestine and pancreas (rev. in (178)(179)(180). Unlike RXR $\alpha$ , with which it has 40% amino acid sequence homology, HNF-4 does not form heterodimers with any other nuclear receptor, but binds to direct repeat-1 (DR-1) DNA sequences as homeodimer (178). DR-1 motifs are promiscuous binding sites for HNF-4, PPAR, RAR, RXR, COUP-TFI and COUP-TFII homeo or heterodimers(115).

HNF-4 $\alpha$  responsive genes encode transcription factors (HNF-1 $\alpha$ , PXR), proteins involved in fatty acid, lipoprotein and lipid metabolism (apo A-I, A-II, B, C-II, C-III, Lp(a), microsomal triglyceride transfer protein, mitochondrial fatty acyl-CoA dehydrogenases, fatty acid binding protein), carbohydrate metabolism (insulin, glut2, glucose-6-phosphatase, PEPCK, pyruvate kinase, aldolase B, glyceraldehyde-3-phosphate dehydrogenase), amino acid and protein metabolism (ornithine transcarbamylase, tyrosine amino transferase, phenylalanine hydroxylase, antitrypsin  $\alpha$ 1), P450 enzymes (steroid 15 $\alpha$ -hydroxylase, fatty acyl  $\omega$ -hydroxylase, cholesterol-7 $\alpha$ -hydroxylase, drug metabolizing P450 enzymes (cyp3 $\alpha$ ), hematopoiesis (erythropoietin, transferrin), blood coagulation (factors VII, IX and X, fibrinogen) and others (e.g., cellular retinol binding protein, transthyretin) (reviewed in (65) (66) (71) (85)(116)(177)(180)(181)(182)(183)(184). Since HNF-4 $\alpha$  activates the transcription of some nuclear receptors (HNF-1 $\alpha$ ) and may further directly interact with other

transcription factors (HNF-1 $\alpha$ ), the above list of HNF-4 $\alpha$  responsive genes may include some which are transcriptionally affected by HNF-4 $\alpha$  indirectly.

The first demonstration of putative HNF-4 ligands showed that long chain fatty acyl-CoA (LCFA-CoAs) thioesters (45) as well as CoA-thioesters of hypolipidemic peroxisome proliferators (*e.g.*, fibrate drugs, Medica homologues) (116) bind to HNF-4 $\alpha$  and, depending on their chain length, degree of saturation, and respective substitutions are able to activate or inhibit transcription of a reporter gene enhanced by the C3P element of the apo CIII promoter (116), (45). However, the radioligand competition assay used to demonstrate acyl-CoA binding in these previous studies yielded  $K_d$ s in the  $\mu$ M range (116) (45). Although total tissue levels of LCFA-CoAs (free + bound) are in the range 0.4–164  $\mu$ M, depending on tissue, cell, nutrition, and pathology (reviewed in (20)(185)), free (unbound) LCFA-CoA are estimated to be 5–200 nM in cytosol (185) and only 1–10 nM in the nucleus (186). Based on these considerations as well as computer modeling of HNF-4 $\alpha$  structure, it has been suggested that HNF-4 $\alpha$  does not significantly bind LCFA-CoAs (187). However, it must be considered that radioligand competition assays for lipidic ligand binding proteins typically yield  $K_d$ s that are 2–3 orders of magnitude higher (*i.e.* lower affinity) than  $K_d$ s determined by direct fluorescence or microcalorimetry binding assays (reviewed in (18)). Thus, it seems possible that the radioligand acyl-CoA competition binding results significantly underestimated the affinity of HNF-4 $\alpha$  for its endogenous ligands.

The objective of the present investigation was to resolve these issues through (i) direct fluorescent ligand binding assays based on quenching of tryptophan emission by putative HNF-4 $\alpha$  ligands using a recombinant HNF-4 $\alpha$  ligand binding domain (HNF-4 $\alpha$ LBD), (ii) fluorescence resonance energy transfer (FRET) between HNF-4 $\alpha$ LBD aromatic amino acids and bound *cis*-parinaroyl CoA (naturally occurring fluorescent LCFA-CoA) to calculate the intermolecular distance between ligand and its binding site, and (iii) circular dichroism to characterize the secondary structure of HNF-4 $\alpha$ LBD as well as potential changes induced therein by LCFA-CoA binding.

## 3.2 EXPERIMENTAL PROCEDURES

### 3.2.1 Chemicals

*Cis*-Parinaric acid and NBD-stearic acid were purchased from Molecular Probes (Eugene, OR). Coenzyme A, palmitoyl-CoA, stearoyl-CoA, linoleoyl-CoA, arachidonoyl-CoA, arachidonic acid, and bezafibrate were from Sigma Chemical Co. (St. Louis, MO). Medica 16 as well as the coenzyme A thioesters of Medica 16 and bezafibrate were chemically synthesized as described (188) (189) .

### 3.2.2 Expression of Recombinant Rat HNF-4 $\alpha$ LBD

Rat HNF-4 $\alpha$ 1 cDNA encoding the sequence from amino acid 132 to 455 was synthesized by PCR with the following primers: 5'-CCGGCTCGAGGATGGCTTCCTGCTT-3' and 5'-GCGCCATATGAGG TCAAGCTACGAG-3'. This DNA fragment was cloned into the NdeI/XhoI site of pET21b plasmid (Novagen, Milwaukee, WI) and sequenced. The recombinant protein was expressed in BL21(DE3)plyS strain of *E. coli*.

### 3.2.3 Purification, SDS-PAGE and Western Blotting of Recombinant HNF-4 $\alpha$ LBD

His-tagged HNF-4 $\alpha$ LBD was purified by affinity chromatography on a nickel-NTA resin (Quiagen, Chatsworth, CA), desalted, lyophilized and stored at  $-70^{\circ}\text{C}$ . Prior to use, the protein was solubilized in 20 mM Tris-HCl buffer, pH 8.0, containing 0.3 M NaCl, 10% glycerol and 1 mM 2-mercaptoethanol or dithiothreitol (binding buffer). Protein was determined by BCA Protein Assay (Pierce, Rockford, IL). Purity of recombinant rat His-HNF-4 $\alpha$ LBD (amino acids 132–455 of the wild type rat HNF-4 $\alpha$ 1 with 6 His residues attached at the C-terminus) was assessed by SDS-PAGE and western blotting (Fig. 3.1). SDS-PAGE separated a single protein band of 36 kD as detected by staining with Coomassie Blue and indicated 97% purity (Fig. 3.1, panel A). Western blotting with rabbit anti-rat HNF-4 $\alpha$ LBD polyclonal antibody followed by goat

anti-rabbit-IgG-alkaline phosphatase conjugate was performed as described (3) . A single reacting band at the same molecular weight was detected by western blot analysis (Fig. 3.1, panel B).

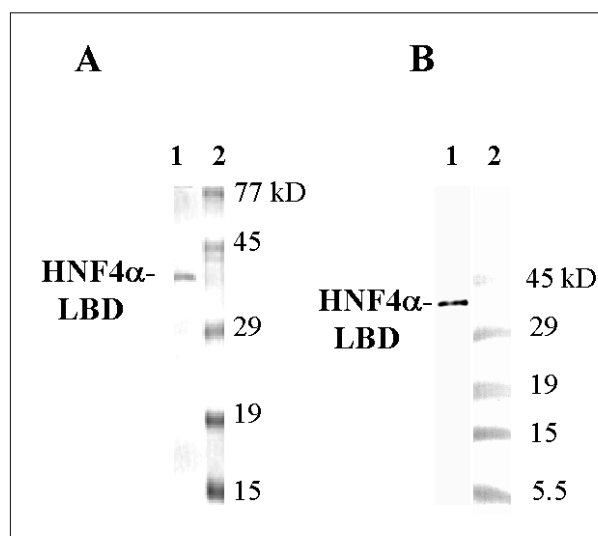


FIG. 3.1. **Purity of recombinant rat HNF-4 $\alpha$ LBD.** *Panel A:* Ni-column purified His-HNF-4 $\alpha$ LBD (lane 1) and molecular weight standards (lane 2) were run in SDS-PAGE and stained with Coomassie-Blue as described in Experimental Procedures. *Panel B:* Western blot of the recombinant His-HNF-4 $\alpha$ LBD with rabbit polyclonal anti-HNF-4 $\alpha$ LBD and alkaline phosphatase-labeled goat anti-rabbit IgG; lane 1, 5 ng purified recombinant HNF-4 $\alpha$ LBD; lane 2, prestained molecular weight standards.

#### 3.2.4 Synthesis and Purification of Fluorescent *cis*-Parinaroyl-CoA (cPNA-CoA)

Fluorescent cPNA-CoA was chemically synthesized (189) utilizing a naturally occurring fluorescent fatty acid, *cis*-parinaric acid (Molecular Probes, Eugene, OR). Unreacted, free *cis*-parinaric acid was retained into the organic phase of a chloroform:methanol:water mix (190). Further removal of free CoA from cPNA-CoA in

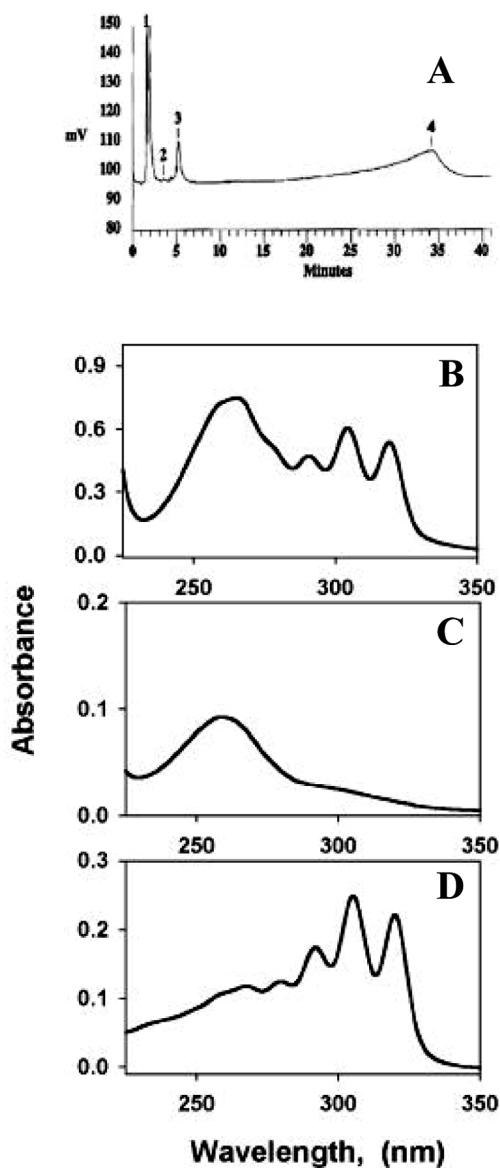


FIG.3.2. **HPLC purification of *cis*-parinaroyl-CoA.** *Panel A:* HPLC chromatogram indicating early exclusion of polar components in peaks 1, 2 and 3, and late exclusion of a hydrophobic component in peak 4 with retention time at 34 min. *Panel B:* Absorbance spectrum of a sample of partially purified *cis*-parinaroyl-CoA, before HPLC run. *Panel C:* the absorbance spectrum of a sample of peak 1, identical to free CoA (not shown). *Panel D:* The absorbance spectrum of HPLC purified peak 4 (from panel A) containing *cis*-parinaroyl-CoA.

the aqueous phase was performed by HPLC, as described (21). The purity level of the HPLC fraction containing cPNA-CoA was checked by assessing the absorption spectrum with a UV/VIS spectrometer, model Lambda 2 (Perkin Elmer, Norwalk, CT). HPLC of the aqueous extract showed two major peaks, 1 and 4 separated by over 32 min, as well as two minor peaks 2 and 3 with retention times between 3-6 min (Fig. 3.2A). The absorbance spectrum of the partially purified cPNA-CoA (Fig. 3.2B) exhibited a 260 nm maximum characteristic for CoA as well as three maxima within 280-324 nm, characteristic for the conjugated double bonds of cPNA-CoA. The absorbance spectrum of HPLC-peak 1 (Fig. 3.2C) did not reveal the presence of a conjugated tetraene (peaks between 280-324 nm) of cPNA-CoA, but instead showed absorbance maximum near 260 nm, typical of free CoA (not shown). In contrast, the absorbance spectrum of peak 4 taken from the HPLC chromatogram in Fig. 3.2A exhibited absorbance characteristics of both the conjugated tetraene and thioester linkage present in cPNA-CoA (Fig. 3.2D). Absorbance spectra of oleoyl CoA demonstrated only the presence of the thioester linkage but not the conjugated tetraene present only in cPNA-CoA (not shown).

### 3.2.5 *Direct Ligand Binding Assays*

#### 3.2.5.1 *Fluorescent Ligands*

Direct binding assays not requiring separation of bound from free ligand were performed using *cis*-parinaroyl CoA as described (6) (21) (24) (153) (191) (192). To establish specificity for LCFA-CoA, this assay was repeated using fluorescent fatty acids: *cis*-parinaric acid and NBD-stearic acid. Briefly, HNF-4 $\alpha$ LBD was added to phosphate buffer saline, pH 7.4 or binding buffer described above to yield final concentration of 170nM HNF-4 $\alpha$ LBD. Increasing fluorescent ligand was then added to yield final concentrations of 10-4000 nM *cis*-parinaroyl CoA. Fluorescence emission spectra were obtained using a PC1 photon counting fluorimeter (ISS Inc., Urbana, IL) and maximal intensities measured. The  $K_d$  and number of binding sites ( $n$ ) were

calculated as previously described (153) (192). Where it was possible (e.g. NBD-stearic acid) the number of binding sites was determined with a higher degree of accuracy from the reverse titration binding curve in which a constant amount of ligand was titrated with increasing concentration of HNF-4 $\alpha$ LBD.

### 3.2.5.2 Quenching of Intrinsic Fluorescence of HNF-4 $\alpha$ LBD Aromatic Amino Acids Tyr/Trp or Trp

To investigate direct binding of nonfluorescent LCFA-CoAs to HNF-4 $\alpha$ LBD, the effect of LCFA-CoA binding on intrinsic fluorescence of HNF-4 $\alpha$ LBD aromatic amino acids was examined. Briefly, 170 nM HNF-4 $\alpha$ LBD were titrated with increasing ligand (5-4000 nM). Two types of fluorescence measurements were obtained. First, both Tyr and Trp residues were excited at 280 nm. Second, the contribution of Trp from Tyr residues was resolved by selective excitation of Trp at 295 nm. Since fluorescence emission was maximal at 333 nm in both cases, Trp was the main contributor to HNF-4 $\alpha$ LBD fluorescence emission. All steady state fluorescence measurements were performed using a PC1 photon counting fluorimeter (ISS, Champaign, IL) in the L-format with 300 watt xenon arc lamp light source and 4 nm band-passes in both excitation and emission monochromators. In ligand-induced HNF-4 $\alpha$ LBD fluorescence quenching experiments the number of binding sites ( $n$ ) was estimated by fitting the binding curve to a Hill plot according to the equation

$$y = ax^b / (c^b + x^b) \quad (\text{Eq.3.1})$$

where  $a$  is  $F_{\text{max}}$  corresponding to  $B_{\text{max}} = nE_0$ ,  $b$  is the number of binding sites ( $n$ ) and  $c$  is  $K_d$ .

### 3.2.6 FRET Determination of Intermolecular Distance between the HNF-4 $\alpha$ LBD Trp and Bound *cis*-Parinaroyl-CoA

Examination of the excitation and emission spectra of HNF4 $\alpha$ -LBD revealed that the emission of Trp overlapped significantly with excitation of *cis*-parinaroyl CoA, a condition ideal for Forster FRET (154). Since FRET varies as (intermolecular

distance)<sup>1/6</sup>, the donor (HNF-4 $\alpha$ LBD Trp) and acceptor (*cis*-parinaroyl CoA) residues must be in very close proximity, generally a few Å, for efficient FRET to occur. To determine the average intermolecular distance between HNF-4 $\alpha$ LBD Trp residues and bound *cis*-parinaroyl CoA, HNF-4 $\alpha$ LBD (170 nM) was titrated with increasing *cis*-parinaroyl-CoA (5-4000 nM final concentration). The HNF-4 $\alpha$ LBD Tyr/Trp or Trp only, were excited at 280 and 295 nm, respectively. Maximal fluorescence emission intensities of HNF-4 $\alpha$ LBD Tyr/Trp or Trp were obtained at 333 nm while maximal emission of *cis*-parinaroyl-CoA was measured at 430 nm. If bound *cis*-parinaroyl CoA acceptor was located within the optimal FRET distance from the HNF-4 $\alpha$ LBD Trp, then efficient energy transfer occurred such that HNF-4 $\alpha$ LBD Tyr/Trp or Trp fluorescence emission was quenched while, concomitantly, sensitized fluorescence emission of *cis*-parinaroyl-CoA was at 430 nm. The intermolecular distance between HNF-4 $\alpha$ LBD Trp and bound *cis*-parinaroyl-CoA was calculated from:

$$E = R_0^6 / (R_0^6 + R_{2/3}^6) \quad (\text{Eq.3.2})$$

where E is the FRET efficiency,  $R_0$  is the critical distance for 50% efficiency, and  $R_{2/3}$  is the actual distance between donor and acceptor (154), (155), (159). The energy transfer efficiency was calculated from quenching of HNF-4 $\alpha$ LBD Trp according to:

$$E = 1 - F_{DA} / F_D \quad (\text{Eq.3.3})$$

where  $F_{DA}$  and  $F_D$  are the fluorescence intensities of HNF-4 $\alpha$ LBD Trp (energy donor) at 333 nm in the presence and absence of *cis*-parinaroyl-CoA (energy acceptor) upon excitation of HNF-4 $\alpha$ LBD Trp at 295 nm. The transfer efficiency (E) was also calculated from the excitation spectrum of the energy acceptor (i.e. *cis*-parinaroyl-CoA) as previously described by Stryer (193) according to:

$$E = [G(\lambda_2) / G(\lambda_1) - \epsilon_A(\lambda_2) / \epsilon_A(\lambda_1)] \times [\epsilon_A(\lambda_1) / \epsilon_D(\lambda_2)] \quad (\text{Eq.3.4})$$

where  $G(\lambda)$  is the magnitude of the corrected excitation spectrum of the energy acceptor excited at wavelength  $\lambda_1$ ;  $\epsilon_D(\lambda)$  and  $\epsilon_A(\lambda)$  are the extinction coefficients of the donor and acceptor at wavelength  $\lambda$ . G is measured at two wavelengths: at  $\lambda_1$ , where the donor has low absorption (320 nm), and at  $\lambda_2$ , where the extinction coefficient of the donor is large



compared to that of the acceptor (280 nm). This second method is especially useful when the local environment of the donor is different in the presence of the acceptor, provided that the absorption spectra of the donor and acceptor moieties are known (193). The critical distance for 50% efficiency ( $R_0$  in Å) was calculated as described (157), (158) using:

$$R_0 = 0.211[k^2 n^{-4} Q_D J(\lambda)]^{1/6} \quad (\text{Eq.3.5})$$

with wavelength expressed in nm and  $J(\lambda)$ , the overlap integral, expressed as  $M^{-1} \text{cm}^{-1} \text{nm}^4$ .  $Q_D$ , the quantum yield for HNF-4 $\alpha$ LBD Trp and  $J(\lambda)$  were calculated as described earlier (157) (158). The orientation factor  $k^2$  and the refractive index  $n$  were assumed to be 2/3 and 1.4, respectively, as for proteins in solution.

### 3.2.7 Circular Dichroism (CD) of HNF-4 $\alpha$ LBD

Far UV CD spectra of HNF-4 $\alpha$ LBD (2  $\mu$ M) were taken in the absence and presence of ligands as described (194) except that 2mM Tris-HCl, pH 8 containing 30 mM NaCl, 1% glycerol and 0.1 mM DTT was used as buffer. The CD measurements were performed with a J-710 Spectropolarimeter (Jasco, Baltimore, MD) using a 1 mm cuvette. Spectra were recorded from 250 to 195 nm at 50 nm/min with a time constant of 1 s and a bandwidth of 2 nm. For each CD profile an average of ten scans was obtained. Percentages of various secondary structures in HNF-4 $\alpha$ LBD were calculated from the CD spectra by using the CDSstr program (195).

## 3.3 RESULTS

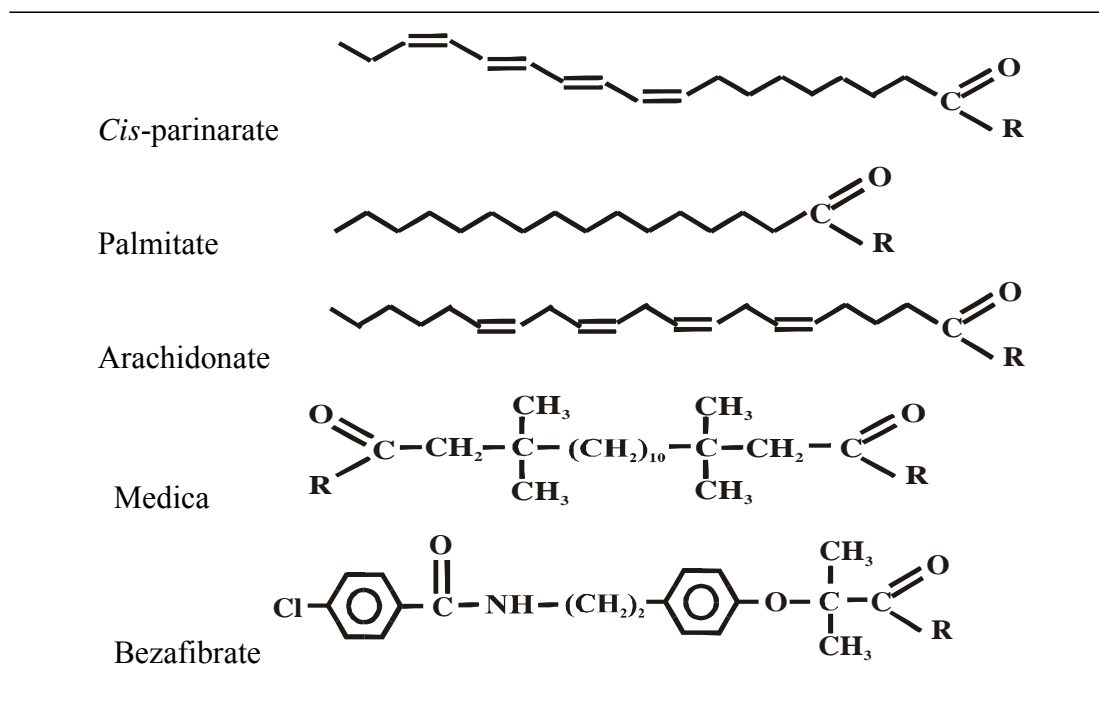
### 3.3.1 Determination of the Binding Parameters of HNF-4 $\alpha$ LBD for a Naturally Occurring Fluorescent Fatty Acyl-CoA: *cis*-Parinaroyl-CoA Quenching of HNF-4 $\alpha$ LBD Trp

*Cis*-parinaroyl CoA was chosen as a fluorescent ligand to examine the fatty acyl CoA binding properties ( $K_d$  and  $B_{\text{max}}$ ) of HNF-4 $\alpha$ LBD because: (i) *cis*-parinaroyl CoA is a naturally occurring fluorescent fatty acyl CoA with structure similar to other fatty acyl CoAs (Table 3.1); (ii) *cis*-parinaroyl CoA absorbance overlaps with aromatic amino

acid fluorescence emission, thereby allowing fluorescence resonance energy transfer; (iii) *cis*-parinaroyl CoA has been extensively used in fatty acyl CoA fluorescence binding assays (6) (21) (24) (153) (191). Furthermore, *cis*-parinaroyl CoA binding fluorescence assay does not underestimate fatty acyl CoA binding as do radioligand binding assays (rev. in (18) (22)). Thus, quenching of HNF-4 $\alpha$ LBD Trp emission at 333 nm was examined upon titration with increasing concentration of *cis*-parinaroyl-CoA. HNF-4 $\alpha$ LBD was excited either at 280 nm to excite both Trp/Tyr (Fig. 3A) or at 295 nm to selectively excite HNF-4 $\alpha$ LBD Trp (Fig. 3C). In both cases, the fluorescence emission of HNF-4 $\alpha$ LBD was quenched by increasing concentrations of *cis*-parinaroyl-CoA. Upon excitation of both Trp/Tyr (at 280 nM), the binding curve of *cis*-parinaroyl-CoA to HNF-4 $\alpha$ LBD demonstrated saturation binding (Fig. 3.3B).

TABLE 3.1

*Chemical structures of fatty acids and peroxisome proliferators whose CoA thioesters as well as free fatty acid forms were tested for HNF-4 $\alpha$ LBD binding.*



R = OH, free fatty acid form; R = CoA, thioester form.

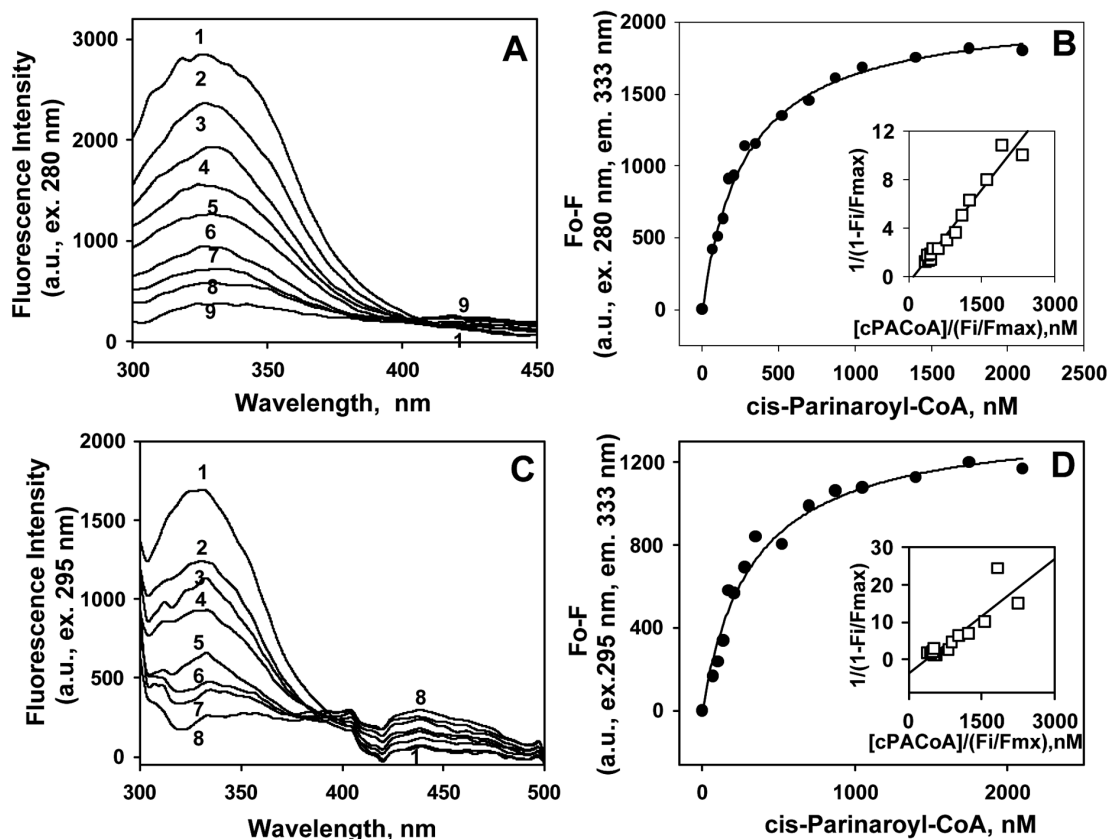


FIG. 3.3. **Titration of HNF-4 $\alpha$ LBD with *cis*-parinaroyl-CoA: binding curves derived from quenching in HNF-4 $\alpha$ LBD fluorescence.** *Panel A:* Emission spectra of HNF-4 $\alpha$ LBD upon excitation of Tyr/Trp at 280 nm; spectrum 1, 170 nM HNF-4 $\alpha$ LBD with no ligand added; spectra 2-9, HNF-4 $\alpha$ LBD in the presence of 105 nM, 175 nM, 280 nM, 525 nM, 875 nM, 1400 nM, 2100 nM and 3500 nM *cis*-parinaroyl-CoA. *Panel B:* Plot of fluorescence emission maxima at 333 nm upon excitation at 280 nm, over the *cis*-parinaroyl-CoA concentrations. Inset: linear plot of the binding curve in panel B. *Panel C:* Emission spectra of HNF-4 $\alpha$ LBD upon excitation of Trp only, at 295 nm; spectrum 1, 170 nM HNF-4 $\alpha$ LBD in the absence of ligand; spectra 2-8, HNF-4 $\alpha$ LBD in the presence of 105 nM, 280 nM, 525 nM, 875 nM, 1400 nM, 2100 nM and 3500 nM *cis*-parinaroyl-CoA. *Panel D:* Plot of fluorescence emission intensity maxima at 333 nm with excitation at 295 nm over increasing concentrations of *cis*-parinaroyl-CoA. Inset: linearization of the binding curve fits one exponential.

A reciprocal plot of the binding curve (Fig. 3.3B, inset) was linear, suggesting either a single binding site or two binding sites with the same  $K_d$ . The number of binding sites was resolved by fitting the binding curve to a Hill plot, as described in Methods. The Hill plot yielded  $n=1.08$ , i.e. one binding site with a  $K_d$  of 248.5 nM (Table 3.2). The number of binding sites calculated from direct titration, considering the molecular weight of HNF-4 $\alpha$ LBD monomer (36 kD), was 0.73. On selective excitation of Trp at 295 nm, a saturation binding curve was again obtained (Fig. 3.3D) with linear reciprocal plot of the binding curve (Fig. 3.3D, inset). Fitting to Hill plot resulted in  $n=1.42$  and  $K_d$  of 238.2 nM (Table 3.2). Taken together, measurement of the direct quenching of HNF-4 $\alpha$ LBD aromatic amino acid fluorescence by *cis*-parinaroyl-CoA indicated that HNF-4 $\alpha$ LBD bound *cis*-parinaroyl-CoA with nanomolar affinity at one binding site per monomer.

### 3.3.2 Molecular Interaction of *cis*-Parinaroyl-CoA with HNF-4 $\alpha$ LBD: Fluorescence Resonance Energy Transfer (FRET)

To investigate in more detail the close molecular interaction of HNF4 $\alpha$  with *cis*-parinaroyl CoA, advantage was taken of the spectral properties of *cis*-parinaroyl CoA absorbance and HNF4 $\alpha$ LBD Trp emission. FRET provided a sensitive technique for determining if interaction between *cis*-parinaroyl CoA and HNF-4 $\alpha$ LBD represented close molecular binding rather than coaggregation. Comparison of a portion of the absorbance characteristics of *cis*-parinaroyl-CoA (Fig. 3.4, dashed line) with the emission of HNF-4 $\alpha$ LBD Trp, selectively excited at 295 nm (Fig. 3.4, solid line), demonstrated partial but significant overlap. This overlap of the energy acceptor absorbance with the donor fluorescence emission is a required condition for efficient FRET. To determine if FRET occurred between HNF4- $\alpha$ LBD and bound *cis*-parinaroyl-CoA, HNF-4 $\alpha$ LBD was titrated with increasing concentrations of *cis*-parinaroyl-CoA followed by determination of fluorescence emission spectra from 300 to 450 nm upon excitation of Tyr/Trp at 280 nm or of Trp only at 295 nm (Figs. 3.3). When HNF-4 $\alpha$ LBD Tyr/Trp were excited at 280 nm, Trp emission at 333 nm was highly

quenched with increasing *cis*-parinaroyl-CoA (Fig. 3.3A). While this suggested that efficient FRET occurred between HNF-4 $\alpha$ LBD and *cis*-parinaroyl-CoA, a conformational change in HNF-4 $\alpha$ LBD upon ligand binding may also cause Trp fluorescence quenching. This possibility was resolved by the appearance of *cis*-parinaroyl-CoA sensitized emission near 430 nm upon increasing *cis*-parinaroyl-CoA concentration.

TABLE 3.2  
*Binding affinity of HNF-4 $\alpha$ LBD for cis-parinaroyl-CoA, CoA and cis-parinaric acid.*

Cis-parinaroyl-CoA (cPNA-CoA); cis-parinaric acid (cPNA)<sup>a</sup>.

Ligand	Ex. <sup>b</sup> (nm)	Em <sup>c</sup> (nm)	Fluorophore	Kd (nM)	n
cPNA-CoA	280	333	Tyr/Trp	248.5	1.08
cPNA-CoA	295	333	Trp	238.2	1.42
cPNA-CoA	280	430	cPNA-CoA *	250.4	0.71
cPNA-CoA	295	430	cPNA-CoA *	758.9	1.02
CoA	280	333	Tyr/Trp	429.1	1.35
CoA	295	333	Trp	680.4	0.98
cPNA	280	333	Tyr/Trp	421.3	1.09
cPNA	295	333	Trp	588.9	0.82

<sup>a</sup>Binding parameters were obtained by Hill plot as described in Experimental Procedures; <sup>b</sup>excitation wavelength; <sup>c</sup>emission wavelength; \* sensitized emission.

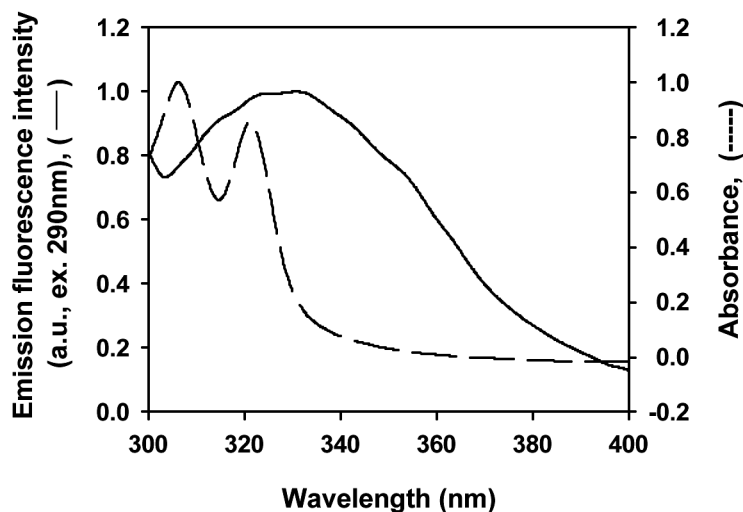


FIG. 3.4. **Spectral overlap of HNF-4 $\alpha$ LBD Trp fluorescence emission with *cis*-parinaroyl-CoA absorption (excitation).** *Spectrum 1*, the emission spectrum of HNF-4 $\alpha$ LBD (170 nM in PBS); *spectrum 2*, the absorbance spectrum of *cis*-parinaroyl-CoA (10  $\mu$ M in PBS).

The increase in the acceptor *cis*-parinaroyl-CoA sensitized fluorescence emission was even more apparent when HNF-4 $\alpha$ LBD Trp was selectively excited at 295 nm (Fig. 3.5C). Since a conformational change in HNF-4 $\alpha$ LBD cannot elicit sensitized emission of *cis*-parinaroyl-CoA, these data indicated the close molecular interaction between HNF-4 $\alpha$ LBD and bound *cis*-parinaroyl-CoA.

### 3.3.3 Calculation of the Intermolecular Distance between HNF-4 $\alpha$ LBD and Bound *cis*-Parinaroyl-CoA by FRET

To determine the intermolecular distance between HNF-4 $\alpha$ LBD and bound *cis*-parinaroyl-CoA it was essential to remove complicating HNF-4 $\alpha$ LBD internal energy transfer from Tyr to Trp residues. This process occurred upon excitation of HNF-4 $\alpha$ LBD at 280 nm (excites both Trp and Tyr residues) since fluorescence emission was

detected only from Trp near 333 nm (Fig. 3.3A). In contrast, preferential excitation of HNF-4 $\alpha$ LBD Trp at 295 nM resulted in maximal emission near 333 nm as expected (Fig. 3.3C). Since separate emission of Tyr (typically near 308 nm) was not observed upon excitation at 280 nm (Fig. 3.3A), this was consistent with efficient internal nonradiative transfer of energy from Tyr to Trp within HNF-4 $\alpha$ LBD.

Based on the significant overlap between the absorbance of *cis*-parinaroyl-CoA (Fig. 3.4, dashed line) with the emission of HNF-4 $\alpha$ LBD Trp (Fig. 3.4, solid line), it was possible to calculate  $R_0$ , the critical distance for 50% energy transfer, as described in Experimental Procedures. The calculated  $R_0$  for the HNF-4 $\alpha$ LBD Trp/*cis*-parinaroyl-CoA donor/acceptor pair was 30 Å (Table 3.3). Since FRET decreases with (intermolecular distance)<sup>1/6</sup>, efficient FRET will only occur between HNF-4 $\alpha$ LBD Trp and *cis*-parinaroyl-CoA if these donors/acceptors are close to 30 Å apart.

To determine  $R_{2/3}$ , the actual intermolecular distance between HNF-4 $\alpha$ LBD and *cis*-parinaroyl-CoA, HNF-4 $\alpha$ LBD was titrated with increasing concentrations of *cis*-parinaroyl-CoA followed by selective excitation of HNF-4 $\alpha$ LBD Trp at 295 and determination of fluorescence emission between 300 to 450 nm, so that changes in both HNF-4 $\alpha$ LBD Trp fluorescence at 333 nm and of *cis*-parinaroyl-CoA emission at 430 nm were observed (Figs 3.3C, 3.5C). The energy transfer efficiency was calculated from these data as described in Experimental Procedures. Based on the equation that determines energy transfer efficiency with the assumption that no protein conformational change is induced upon ligand binding, a value of 85% energy transfer efficiency between HNF-4 $\alpha$ LBD Trp and *cis*-parinaroyl-CoA was obtained (Table 3.3). Thus, in the absence of a ligand induced conformational change in HNF-4 $\alpha$ LBD, an intermolecular distance between HNF-4 $\alpha$ LBD and *cis*-parinaroyl-CoA, i.e.  $R_{2/3} = 22.6$  Å was determined. However, if fatty acyl-CoA binding elicits a conformational change in HNF-4 $\alpha$ LBD then this value may overestimate how close the *cis*-parinaroyl-CoA approaches HNF-4 $\alpha$ LBD. Stryer's equation in Experimental Procedures allows calculation of energy transfer efficiency when both FRET and protein conformational

TABLE 3.3  
*Forster energy transfer from HNF-4 $\alpha$ LBD Trp to bound cis-parinaroyl-CoA.*

J is the overlap integral.  $R_0$  is the critical distance that allows 50% energy transfer efficiency and was calculated as described under Experimental Procedures. E is the energy transfer efficiency.  $R_{2/3}$  is the actual distance between HNF-4 $\alpha$ LBD Trp and bound cis-parinaroyl-CoA.

Energy donor	Energy acceptor	J ( $M^{-1}cm^{-1}nm^4$ )	$R_0$ ( $\text{\AA}$ )	E (%)	$R_{2/3}$ ( $\text{\AA}$ )
HNF-4 $\alpha$ LBD <sup>a</sup>	<i>cis</i> -parinaroyl-CoA <sup>a</sup>	$2.718 \times 10^{14}$	30.1	12	42.0
HNF-4 $\alpha$ LBD <sup>b</sup>	<i>cis</i> -parinaroyl-CoA <sup>b</sup>	$2.718 \times 10^{14}$	30.1	85	22.6

<sup>a</sup> Both FRET and conformational change are induced by ligand binding to the protein.

<sup>b</sup> FRET but no conformational change is induced by ligand binding to the protein.

changes upon ligand binding contribute to the sensitized emission of the bound ligand (193). For this case a much lower energy transfer efficiency, i.e. 12% was found and the resultant intermolecular distance between HNF-4 $\alpha$ LBD and *cis*-parinaroyl-CoA,  $R_{2/3}$ , was 42  $\text{\AA}$  (Table 3.3). Thus, depending on whether fatty acyl-CoA binding elicits a conformational change in HNF-4 $\alpha$ LBD structure, the intermolecular distance between HNF-4 $\alpha$ LBD Trp and bound *cis*-parinaroyl-CoA was in the range of 23-42  $\text{\AA}$ . In either case, these data were consistent with fatty acyl-CoA binding to HNF-4 $\alpha$ LBD being due to close molecular interaction between these molecules. Whether 23  $\text{\AA}$  or 42  $\text{\AA}$  is the correct intermolecular distance was resolved by circular dichroism (see below).



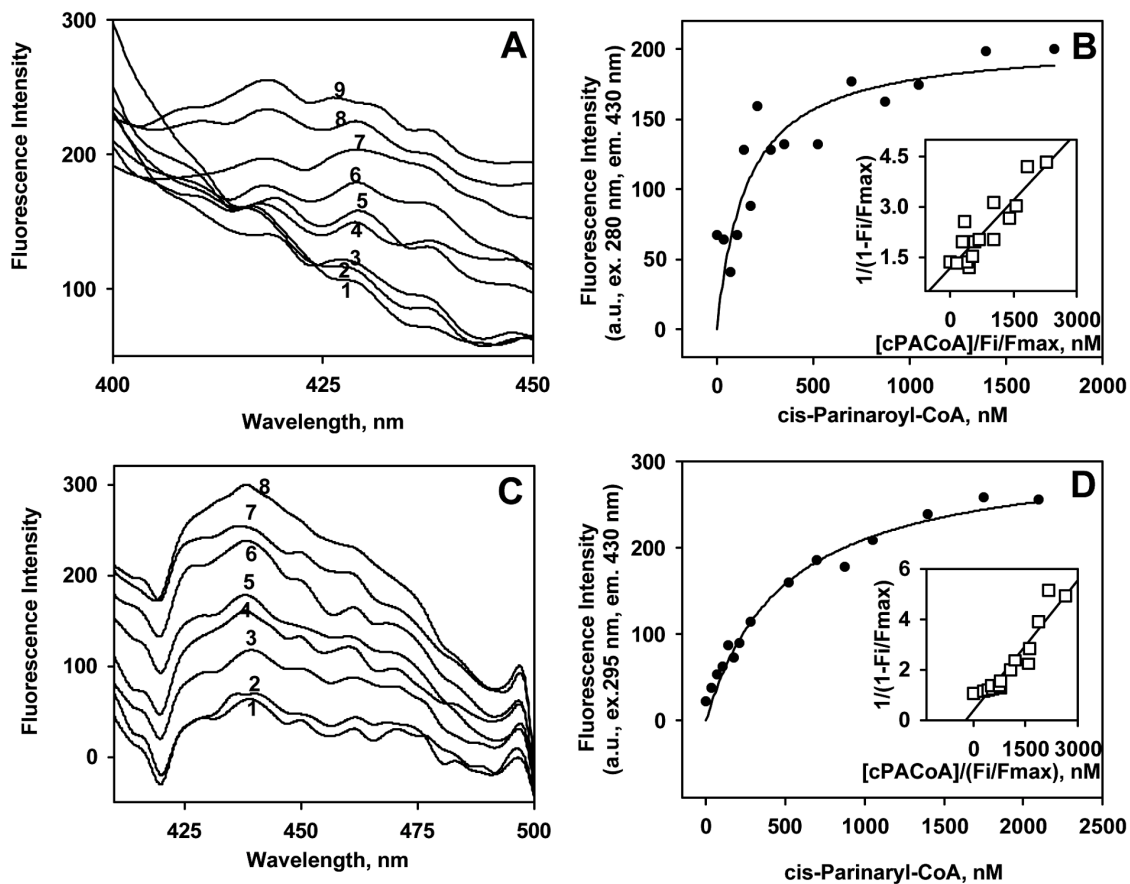


FIG. 3.5. Sensitized emission of HNF-4 $\alpha$ LBD-bound *cis*-parinaroyl-CoA and binding curves as resulted from FRET data. *Panel A*: Emission spectra between 400 and 450 nm, showing increase in *cis*-parinaroyl-CoA fluorescence intensity with excitation of Tyr/Trp at 280 nm; spectra 1 to 9, as described in Fig.3 A. *Panel B*: Plot of fluorescence emission maxima of *cis*-parinaroyl-CoA at 430 nm upon excitation at 280 nm, over the *cis*-parinaroyl-CoA concentrations. Inset: linear plot of the binding curve in panel B. *Panel C*: Spectra portion from 400 to 500 nm showing increase in *cis*-parinaroyl-CoA fluorescence intensity from spectrum 1 to 8, with excitation of Trp at 295 nm; spectra 1-8, as described in Fig. 2 C. *Panel D*: Plot of fluorescence intensity maxima at 430 nm upon excitation of HNF-4 $\alpha$ LBD Trp at 295 nm, over increasing concentrations of *cis*-parinaroyl-CoA. Inset: linearization of the binding curve fits one exponential.

### 3.3.4 Determination of the Binding Parameters of HNF-4 $\alpha$ LBD for *cis* Parinaroyl-CoA from FRET Data

The appearance of sensitized *cis*-parinaroyl-CoA fluorescence emission upon FRET between HNF-4 $\alpha$ LBD and bound *cis*-parinaroyl CoA was used to obtain binding parameters. Plotting the increase in sensitized emission of HNF-4 $\alpha$ LBD-bound ligand (excited at 280 nm) as a function of increasing *cis*-parinaroyl- CoA yielded a saturation binding curve (Fig. 3.5B). A double reciprocal plot of the binding curve was linear (Fig. 3.5B, inset), consistent with a binding site or two binding sites with the same affinity. A Hill plot of the binding data resolved this issue by demonstrating  $n = 0.71$ , i.e. consistent with a single binding site, with a  $K_d$  of 250.4 nM (Table 3.2). Upon selective excitation of HNF-4 $\alpha$ LBD Trp at 295 nm (Fig. 3.5C), the binding curve based on *cis*-parinaroyl-CoA sensitized emission again demonstrated binding to saturation (Fig. 3.5D). A double reciprocal plot of the binding data was linear again, consistent with one binding site or two binding sites of similar affinity (Fig. 3.5D, inset). A Hill plot yielded  $n = 1.02$ , consistent with a single binding site, and a  $K_d$  of 758.9 nM (Table 3.2).

In summary, the binding curves constructed from the FRET induced sensitized emission of HNF-4 $\alpha$ LBD bound *cis*-parinaroyl-CoA indicated that HNF-4 $\alpha$ LBD bound *cis*-parinaroyl-CoA to one site which, in general, showed a similar affinity for *cis*-parinaroyl-CoA as based on HNF-4 $\alpha$ LBD Trp emission quenching at 333 nm (Table 3.2).

### 3.3.5 Binding Specificity of HNF-4 $\alpha$ LBD for *cis*-Parinaroyl-CoA: Interaction with *cis*-Parinaric Acid and CoA

The ligand binding specificity of HNF-4 $\alpha$ LBD was determined by titration with increasing amounts CoA or *cis*-parinaric acid. Upon HNF-4 $\alpha$ LBD Trp/Tyr excitation at 280 nm, CoA slightly quenched HNF-4 $\alpha$ LBD fluorescence emission at 330 nm (Fig. 3.6A). The CoA concentration plot was hyperbolic, indicating saturation binding (Fig. 3.6B). The double reciprocal plot of this curve was linear (Fig. 3.6B, inset) and a Hill plot resolved one binding site ( $n = 1.53$ ) with  $K_d$  of 429.1 nM (Table 3.2). Similarly,

excitation of HNF-4 $\alpha$ LBD Trp and determination of fluorescence resulted in quenching of fluorescence upon the presence of increasing concentrations of CoA

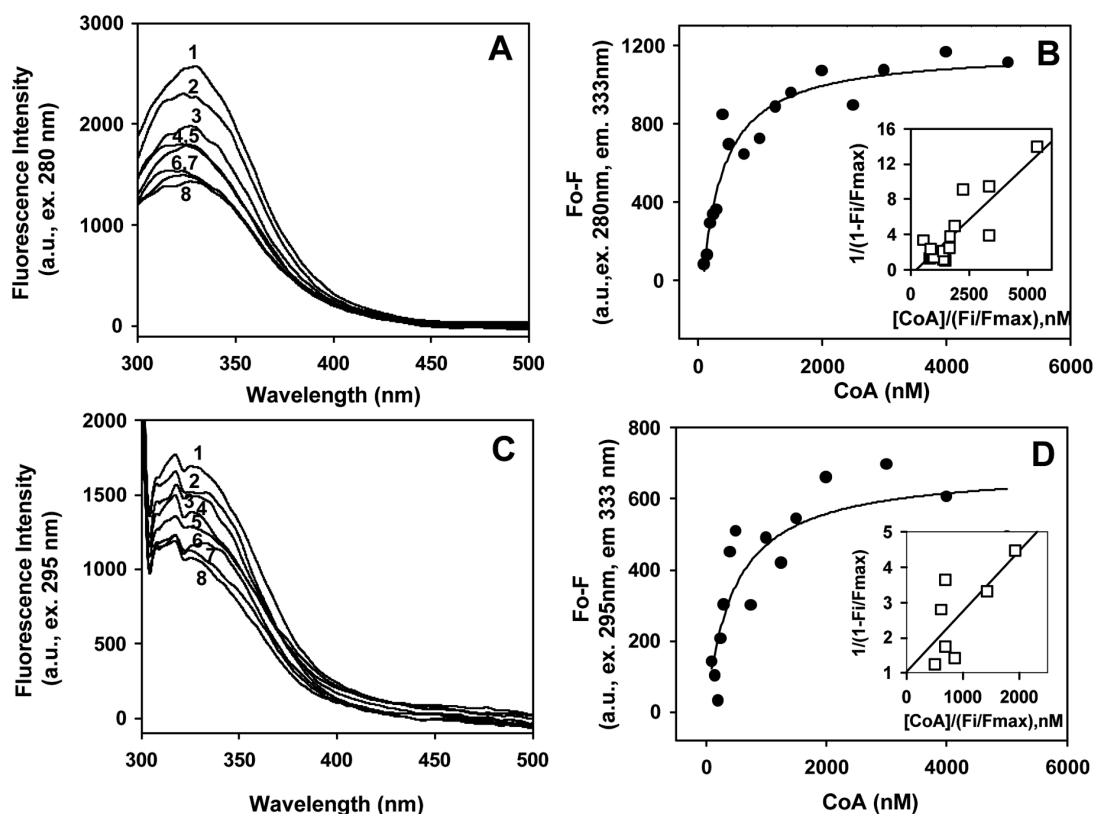


FIG. 3.6. **Titration of HNF-4 $\alpha$ LBD with CoA.** *Panel A:* Fluorescence emission spectra of HNF-4 $\alpha$ LBD (170 nM) upon excitation at 280 nm, in the absence (spectrum 1) and presence of increasing concentrations of CoA (spectra 2-8); 2, 250 nM; 3, 400 nM; 4, 750 nM; 5, 1250 nM; 6, 2  $\mu$ M; 7, 3  $\mu$ M; 8, 5  $\mu$ M CoA. *Panel B:* The binding curve plotted with data in panel A. Inset: linearization of the binding curve fits to a single exponential. *Panel C:* Fluorescence emission spectra of HNF-4 $\alpha$ LBD upon excitation at 295 nm, over increasing concentrations of CoA; spectrum 1, 170 nM HNF-4 $\alpha$ LBD with no CoA added; spectra 2-8, CoA was added in concentrations from 250 nM to 5  $\mu$ M. *Panel D:* The plot of fluorescence intensity maxima at 333 nm with excitation at 295 nm, over increasing concentrations of CoA. Inset: linear plot of the binding curve fits to a single exponential.

(Fig. 3.6C). The binding curve constructed from these data was hyperbolic (Fig.3.6D) indicating saturation binding. Both the double reciprocal plot (Fig. 3.6D, inset) and Hill plot ( $n=0.98$ ) indicated a single binding site for CoA. The binding affinity of HNF-4 $\alpha$ LBD to CoA was low, i.e.  $K_d$  of 680.4 nM (Table 3.2). Thus, quenching of HNF-4 $\alpha$ LBD Trp (regardless of whether both Trp/Tyr or only Trp were excited) fluorescence suggested that: (i) HNF-4 $\alpha$ LBD binds CoA at one binding site, and (ii) HNF-4 $\alpha$ LBD has 2-fold lower affinity for CoA at that site as compared to *cis*-parinaroyl-CoA.

Binding of free *cis*-parinaric acid to HNF-4 $\alpha$ LBD was assayed similarly as for CoA binding above, except that increasing concentrations of *cis*-parinaric acid were used. When HNF-4 $\alpha$ LBD Trp/Tyr were excited at 280 nm, increasing *cis*-parinaric acid also quenched HNF-4 $\alpha$ LBD Trp emission (Fig. 3.7A). However, this binding of *cis*-parinaric acid did not result in FRET as indicated by the absence of sensitized emission of at 430 nm (Fig. 3.7A, inset). The latter was in contrast to titration with *cis*-parinaroyl-CoA binding which induced sensitized emission at 430 nm (Fig. 3.5A). The plot of *cis*-parinaric acid concentration versus HNF-4 $\alpha$ LBD Trp fluorescence quenching indicated weak binding (Fig. 3.7B). The double reciprocal plot of the binding curve showed a single binding site (Fig. 3.7B, inset); this was confirmed by Hill plot which yielded  $n=1.09$  and a  $K_d$  of 421.3 nM (Table 3.2). When only HNF-4 $\alpha$ LBD Trp was selectively excited at 295 nm, quenching of HNF-4 $\alpha$ LBD fluorescence was observed (Fig. 3.7C) but, again, there was no appearance of *cis*-parinaric acid sensitized emission at 430 (Fig. 3.7C, inset). Construction of the *cis*-parinaric acid binding curve showed a hyperbolic shape (Fig. 3.7D). The double reciprocal plot again was linear, consistent with a single binding site (Fig. 3.7D, inset). This was confirmed by Hill plot which yielded  $n=0.82$  and  $K_d$  of 588.9 nM (Table 3.2). Thus, quenching of HNF-4 $\alpha$ LBD Trp (regardless of whether both Trp/Tyr or only Trp were excited) fluorescence suggested that (i) HNF-4 $\alpha$ LBD binds *cis*-parinaric acid at one binding site, and (ii) HNF-4 $\alpha$ LBD has about 2-fold lower affinity for *cis*-parinaric acid at that site then for *cis*-parinaroyl-CoA.

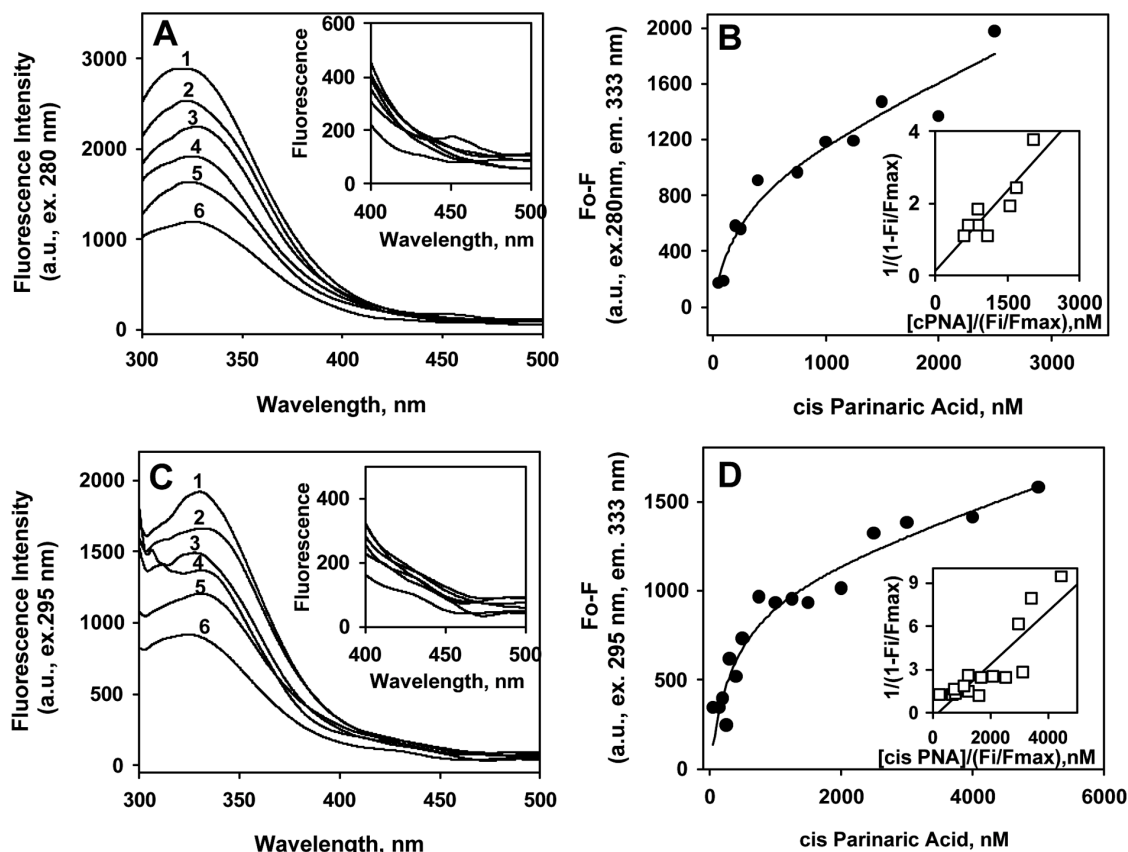


FIG. 3.7. Titration of HNF-4 $\alpha$ LBD with *cis*-parinaric acid. *Panel A*: Emission fluorescence spectra of 170 nM HNF-4 $\alpha$ LBD in the absence (spectrum 1) and in the presence of 0.15-2.5  $\mu$ M of *cis*-parinaric acid (spectra 2-6), with excitation at 280 nm. Inset: blow up of the emission spectra from 400 to 500 nm, showing no consistent increase in the fluorescence intensity at 440 nm. *Panel B*: The binding curve plotted as *cis*-parinaric acid concentration versus quenching in Tyr/Trp fluorescence of HNF-4 $\alpha$ LBD protein with excitation at 280 nm. Inset: linear plot of the binding curve fits to a single exponential. *Panel C*: Emission fluorescence spectra of 400 nM HNF-4 $\alpha$ LBD in the absence (spectrum 1) and in the presence of 0.25-2.5  $\mu$ M *cis*-parinaric acid (spectra 2-6), with excitation of Trp only, at 295nm. Inset: close up of the spectra from 400 to 500 nm, demonstrating no significant increase of the bound *cis*-parinaric acid, at 440 nm; *Panel D*: The binding curve plotted as *cis*-parinaric acid concentration versus In summary, these data based on quenching of HNF-4 $\alpha$ LBD aromatic amino acid fluorescence emission indicated that HNF-4 $\alpha$ LBD has a single binding site with  $K_d$  near 250 nM for *cis*-parinaroyl-CoA. The individual residues, i.e. CoA and *cis*-parinaric acid, constituting *cis*-parinaroyl-CoA, interact with HNF-4 $\alpha$ LBD at lower-affinities (i.e.  $K_d$ s in the range of 420-680 nM), thus indicating that both portions of the *cis*-parinaroyl CoA molecule apparently contributed to binding.

quenching of Trp of HNF-4 $\alpha$ LBD with excitation at 295 nm. Inset: linear plot of the binding curve fits to one exponential.

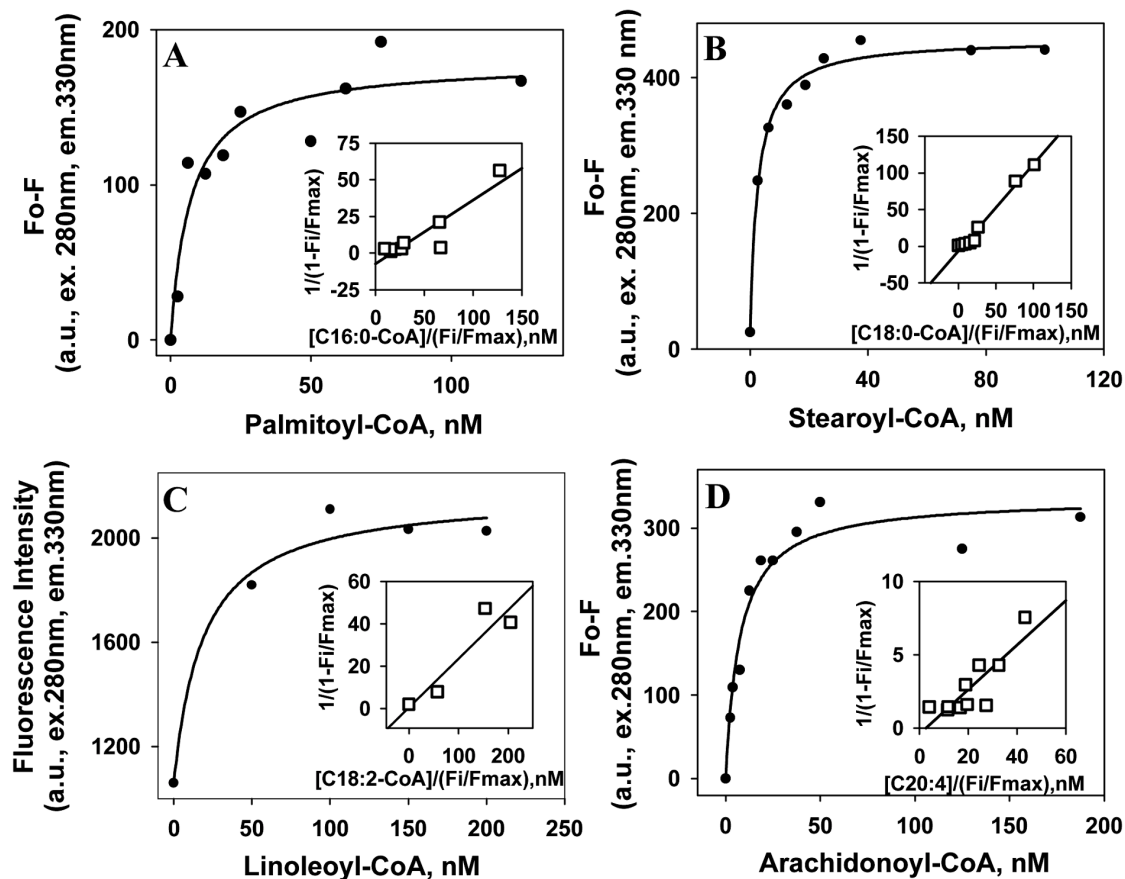


FIG. 3.8 . **Binding of long chain fatty acyl-CoAs to HNF-4 $\alpha$ LBD.** *Panel A:* Titration of 170 nM HNF-4 $\alpha$ LBD with palmitoyl-CoA. Inset: linear plot of the binding curve fits to one exponential. *Panel B:* Titration of 170 nM HNF-4 $\alpha$ LBD with stearoyl-CoA. Inset: linear plot of the binding curve fits to a single exponential. *Panel C:* Titration of HNF-4 $\alpha$ LBD (170 nM) with linoleoyl-CoA. Inset: linear plot of the binding curve fits to one exponential. *Panel D:* Titration of HNF-4 $\alpha$ LBD (170 nM) with arachidonoyl-CoA. Inset: linear plot of the binding curve fits to a single exponential.

### 3.3.6 Binding of Nonfluorescent, Long Chain Fatty Acyl-CoA to HNF-4 $\alpha$ LBD

The interaction of nonfluorescent, saturated and unsaturated naturally-occurring fatty acyl-CoAs with HNF-4 $\alpha$ LBD was examined. Palmitoyl-CoA (C-16 acyl chain) and stearoyl-CoA (C-18 acyl chain) were representative, highly-prevalent, straight-chain saturated fatty acyl CoAs while linoleoyl-CoA (C-18 acyl chain with 2 double bonds) and arachidonoyl-CoA (C-20 acyl chain with 4 unconjugated double bonds) were representative polyunsaturated, kinked-chain, fatty acyl-CoAs typically found in tissues.

When excited at 280 nm, HNF-4 $\alpha$ LBD Trp emission at 333 nm was significantly quenched in the presence of palmitoyl-CoA (Fig. 3.8A), stearoyl-CoA (Fig. 3.8B), linoleoyl-CoA (Fig. 3.8C), and arachidonoyl-CoA (Fig. 3.8D). HNF-4 $\alpha$ LBD exhibited hyperbolic, saturation binding curves with each of these fatty acyl-CoAs. Furthermore, linearization of each binding curve (shown in the insets of Fig. 3.8A, B, C, D, respectively) indicated the presence of a single binding site for each of these fatty acyl-CoAs. The binding affinities calculated from the latter linear plots showed that HNF-4 $\alpha$ LBD exhibited very high affinity for palmitoyl-CoA, stearoyl-CoA, linoleoyl-CoA, and arachidonoyl-CoA as evidenced by  $K_d$ 's of 1.7 nM, 3.8 nM, 4.4 nM and 4.0 nM, respectively (Table 3.4).

In summary, the very high affinity ( $K_d$ s of 1.7-4.4 nM) of HNF-4 $\alpha$ LBD for non-fluorescent, naturally-occurring fatty acyl CoAs showed that fatty acyl CoA binding to HNF-4 $\alpha$ LBD was not just a unique property of *cis*-parinaroyl-CoA. Furthermore, the two-order of magnitude higher  $K_d$ s of HNF-4 $\alpha$ LBD for *cis*-parinaroyl CoA ( $K_d$ s near 250 nM, depending on the type of assay, Table 3.2) suggested that presence of the conjugated tetraene double bonds in *cis*-parinaroyl CoA reduced HNF-4 $\alpha$ LBD's affinity for 18-carbon, naturally-occurring fatty acyl-CoA.

### 3.3.7 Binding Specificity of HNF-4 $\alpha$ LBD: Free Fatty Acids

In order to further assess the binding specificity of HNF-4 $\alpha$ LBD, the binding of two long-chain free fatty acids was examined: NBD-stearic acid (a fluorescently labeled,

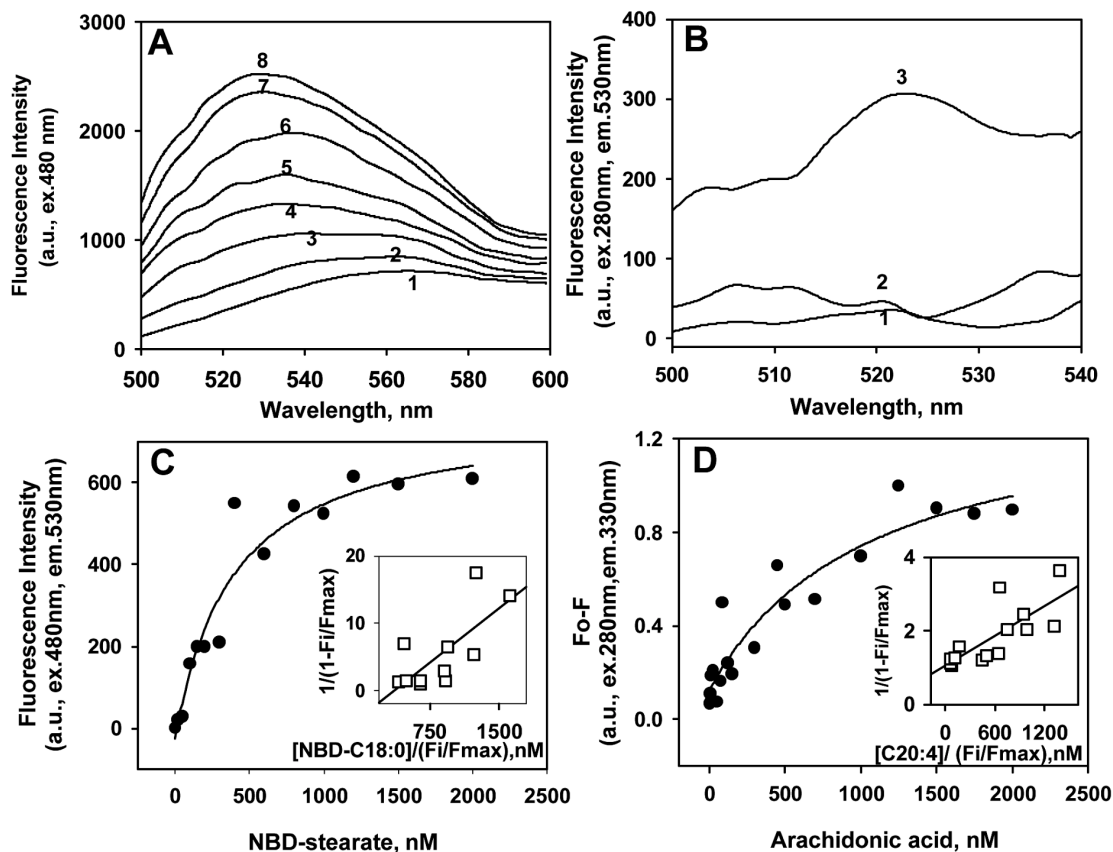


FIG. 3.9. **Binding of long chain free fatty acids to HNF-4 $\alpha$ LBD.** *Panel A:* Emission fluorescence spectra of NBD-stearic acid (250 nM) when titrated with increasing concentrations of HNF-4 $\alpha$ LBD; protein was added in following concentrations: 1, 0 nM; 2, 42.5 nM; 3, 85 nM; 4, 128 nM; 5, 170 nM; 6, 255 nM; 7, 340 nM; 8, 390 nM. *Panel B:* Sensitized emission of NBD-stearic acid upon excitation of Tyr/Trp of HNF-4 $\alpha$ LBD at 280 nm; 1, NBD-stearic acid only; 2, NBD-stearic acid plus 43 nM HNF-4 $\alpha$ LBD; 3, NBD-stearic acid plus 400 nM HNF-4 $\alpha$ LBD. *Panel C:* Binding of NBD-stearic acid to HNF-4 $\alpha$ LBD measured as increase in NBD-stearic acid fluorescence at 530 nm upon excitation at 480 nm. Inset: linear plot of the binding curve fits to a single exponential. *Panel D:* Binding of arachidonic acid to HNF-4 $\alpha$ LBD measured as quenching in Tyr/Trp fluorescence of HNF-4 $\alpha$ LBD, upon excitation at 280 nm. Inset: linear plot of the binding curve fits to a single exponential.



synthetic, 18-carbon saturated fatty acid) and arachidonic acid (a nonfluorescent, naturally-occurring, 20-carbon polyunsaturated fatty acid). In aqueous buffer, NBD-stearic acid fluoresced weakly with maximal emission near 562 nm (Fig. 3.9A, spectrum 1). However, when a constant amount of NBD-stearic acid was titrated with increasing concentrations of HNF-4 $\alpha$ LBD (Fig. 3.9A, spectra 2-8), three types of changes in the NBD-stearic acid fluorescence emission occurred. First, NBD-stearic acid fluorescence emission maximum exhibited a 32 nm blue shift from 562 nm in the absence of HNF-4 $\alpha$ LBD, to 530 nm at saturation with HNF-4 $\alpha$ LBD (Fig. 3.9A). When compared to a calibration curve of NBD-stearic acid in solvents with increasing dielectric constants (169), the maximal emission wavelength of NBD-stearic acid bound to HNF-4 $\alpha$ LBD corresponded to a dielectric constant near 2, indicating that the HNF-4 $\alpha$ LBD-bound NBD-stearic acid was localized in a highly hydrophobic microenvironment. Second, excitation of HNF-4 $\alpha$ LBD protein at 280 nm resulted in a small, but visible increase in the NBD-stearic acid fluorescence emission at 530 nm, due to FRET between HNF-4 $\alpha$ LBD (donor) and NBD-stearate (acceptor) (Fig. 3.9B). Third, NBD-stearic acid exhibited a saturable increase in fluorescence emission intensity with increasing HNF-4 $\alpha$ LBD (Fig. 3.9A). Titration of a constant amount of HNF-4 $\alpha$ LBD with increasing concentrations of NBD-stearic acid followed by measurement of the increase in the NBD-stearic acid fluorescence emission intensity at 530 nm (upon excitation at 480 nm), resulted in a hyperbolic, saturable, binding curve (Fig. 3.9C). The linear plot of this curve demonstrated a single binding site (Fig. 3.9C, inset) and allowed calculation of a  $K_d$  of 93 nM for NBD-stearic acid.

Since the affinity of HNF-4 $\alpha$ LBD for NBD-stearic acid ( $K_d$  of 93 nM) was 5-7 fold higher than for the other fluorescent fatty acid examined, *i.e.* *cis*-parinaric acid ( $K_d$  of 538-642 nM, Table 3.2), it was important to determine if this binding was dependent on the presence of the fluorophores (NBD, conjugated tetraene) present in these free fatty acids. Therefore, the affinity of HNF-4 $\alpha$ LBD for a non-fluorescent fatty acid, arachidonic acid, was determined. Increasing arachidonic acid also decreased the HNF-4 $\alpha$ LBD Trp emission at 333 nm (upon excitation at 280 nm) and resulted in a

hyperbolic, saturable binding curve (Fig. 3.9D). The linear plot of this curve resolved a single binding site with weak affinity as evidenced by  $K_d$  of 742 nM (Fig. 3.9D, inset).

In summary, unlike the very high affinity of HNF-4 $\alpha$ LBD for non-fluorescent fatty acyl CoAs ( $K_d$ s of 1-5 nM), HNF-4 $\alpha$ LBD only weakly bound non-fluorescent free fatty acid ( $K_d$  of 742 nM). However, the presence of fluorophores in the free fatty acid

TABLE 3.4  
*Specificity of HNF-4 $\alpha$ LBD for non-fluorescent ligands.*

Ligand	$K_d$ , (nM)	$n^a$
Long chain fatty acyl-CoAs		
C16:0-CoA	1.7	1.01
C18:0-CoA	3.8	1.18
C18:2-CoA	4.4	-
C20:4-CoA	4.0	1.38
Long chain free fatty acid		
C20:4	742.0	0.49
Peroxisome proliferators		
Medica-16-CoA	2.6	1.45
Medica-16	33.6	1.57
Bezafibroyl-CoA	29.3	1.63
Bezafibrate	57.1	1.55

<sup>a</sup>  $n$ , the number of binding sites was determined from Hill plot, as described in Experimental Procedures.

increased this affinity by 5-7 fold. These data suggested that HNF-4 $\alpha$ LBD's ligand binding specificity, especially for molecules that were not fatty acyl-CoAs, might be highly dependent on the individual structure of the potential ligand examined.

### 3.3.8 HNF-4 $\alpha$ LBD Binds Peroxisome Proliferators as CoA-thioesters or Free Fatty Acids

Because the structures of peroxisome proliferators such as Medica 16 and bezafibrate show some similarities to fatty acids (Table 3.1), the interaction of their CoA-thioesters with HNF-4 $\alpha$ LBD and full length HNF-4 $\alpha$  was recently examined (116). However, a radioligand competition assay yielded only low affinities for these drugs, i.e.  $K_{ds}$  in the mM range (116). Since results with direct fluorescence binding assays presented herein showed that the radioligand binding assay underestimated the affinities of HNF-4 $\alpha$ LBD for fatty acyl-CoAs by 3-orders of magnitude, HNF-4 $\alpha$ LBD binding parameters for Medica 16-CoA, bezafibroyl-CoA, as well as for the free acid forms of these PPs were examined by exciting HNF-4 $\alpha$ LBD Trp/Tyr at 280 nm and determining the effect on HNF-4 $\alpha$ LBD Trp emission at 333 nm.

Medica 16-CoA, unlike all the other ligands tested, induced an increase in fluorescence emission intensity of Tyr/Trp of HNF-4 $\alpha$ LBD. A titration curve of the Medica 16-CoA concentrations versus the Tyr/Trp fluorescence intensities fitted to a hyperbola, illustrating saturation binding (Fig. 3.10A). A reciprocal plot showed a straight line, consistent with a single binding site (Fig. 3.10A, inset), which yielded a  $K_d$  of 2.6 nM (Table 3.4). Medica 16 in free acid form quenched HNF-4 $\alpha$ LBD Trp fluorescence emission intensity. Again, the titration curve for Medica 16 in free acid form fitted a saturation binding curve (Fig. 3.10B), which when linearized indicated a single binding site (Fig. 3.10B, inset) with  $K_d$  value of 33.6 nM (Table 3.4). Titration of HNF-4 $\alpha$ LBD with bezafibroyl-CoA induced quenching in the intrinsic fluorescence of the protein, resulting in a saturation binding curve (Fig. 3.10C) which in a double reciprocal plot suggested a single binding site (Fig. 3.10C, inset) and yielded a  $K_d$  of 29.3 nM (Table 3.4). For bezafibrate in free acid form, linear plot of the binding curve (Fig. 3.10D) yielded a slightly higher  $K_d$  (57.1 nM) (Table 3.4).

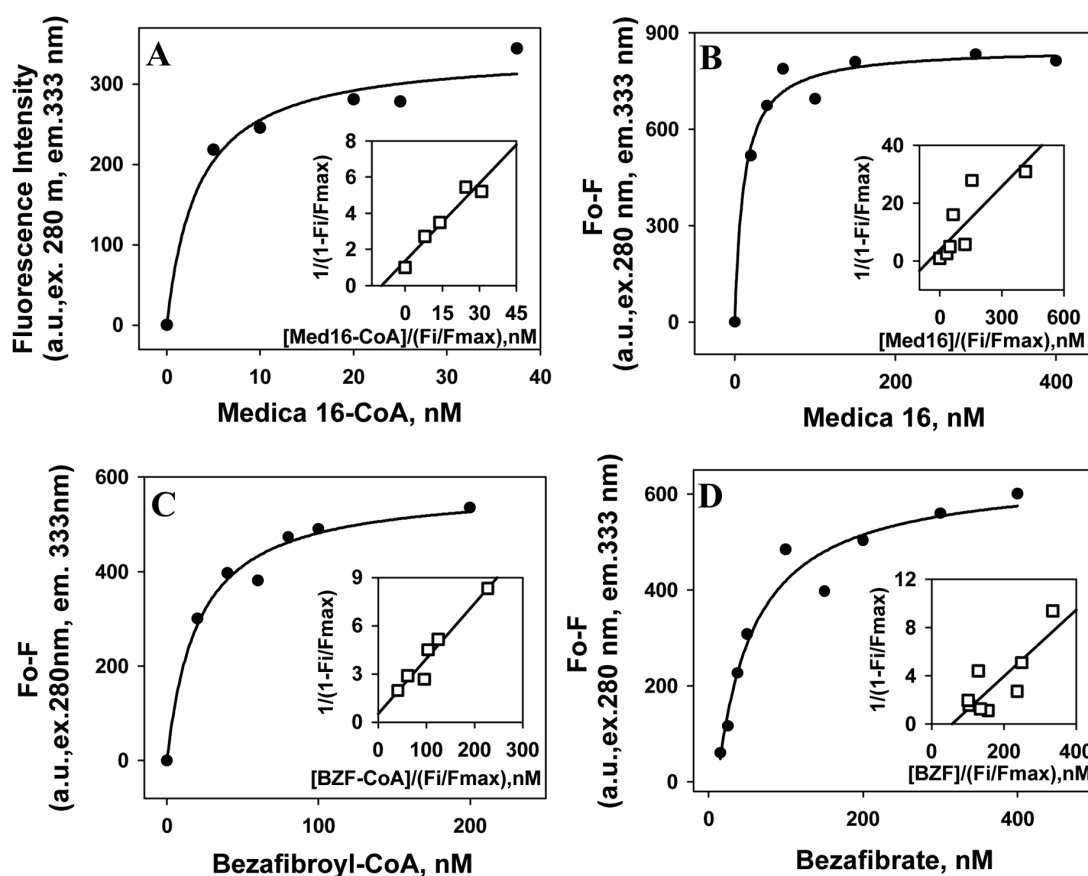


FIG. 3.10. **Binding of peroxisome proliferators as CoA thioesters or free fatty acids, to HNF-4 $\alpha$ LBD.** *Panel A:* Titration of 170 nM HNF-4 $\alpha$ LBD with Medica-16-CoA, measured as quenching in Tyr/Trp fluorescence of HNF-4 $\alpha$ LBD upon excitation at 280 nm. Inset: linear plot of the binding curve fits to one exponential. *Panel B:* Titration of 170 nM HNF-4 $\alpha$ LBD with Medica-16, measured as increase in Tyr/Trp fluorescence of HNF-4 $\alpha$ LBD. Inset: linear plot of the binding curve fits to a single exponential. *Panel C:* Titration of 170 nM HNF-4 $\alpha$ LBD with bezafibroyl-CoA, measured as quenching in Tyr/Trp fluorescence of HNF-4 $\alpha$ LBD upon excitation at 280 nm. Inset: linear plot of the binding curve fits to one exponential. *Panel D:* Titration of 170 nM HNF-4 $\alpha$ LBD with bezafibrate, measured as quenching in Tyr/Trp fluorescence of HNF-4 $\alpha$ LBD upon excitation at 280 nm. Inset: linear plot of the binding curve fits to one exponential.

In summary, HNF-4 $\alpha$ LBD has high affinity ( $K_d$ s as low as 2.6 nM) for certain classes of peroxisome proliferator drugs, especially in their CoA thioester form. The

order of affinities of the peroxisome proliferator drugs tested was Medica-16-CoA > Medica-16 > Bezafibroyl-CoA > Bezafibrate.

### *3.3.9 Secondary Structure of HNF-4 $\alpha$ LBD and Effects of Fatty Acyl-CoAs: Circular Dichroism*

One mechanism whereby ligands are thought to affect the function of nuclear binding proteins is to induce a conformational change in the protein to allow further events important for transcription to occur. The observation that non-fluorescent ligands induced significant alterations in HNF-4 $\alpha$ LBD Trp fluorescence emission (regardless of whether Trp/Tyr or Trp alone were excited) (Figs. 3.8, 3.10) suggested that fatty acyl-CoAs altered the secondary structure and conformation of HNF-4 $\alpha$ LBD. This possibility was further tested using circular dichroism.

The far UV circular dichroic spectrum of HNF-4 $\alpha$ LBD exhibited two minima, at 208 nm and 220 nm and one maximum at 195 nm (Fig. 3.11, filled circles). Spectrum analysis using the CDstr program as described in Methods, indicated that the polypeptide structure of HNF-4 $\alpha$ LBD was comprised of 18.6% total helix, 27.3%  $\beta$ -strands, 1.5% turns and 38.7% other types of secondary structures (Table 3.5). Palmitoyl-CoA, a 16-carbon chain length, saturated fatty acyl-CoA, significantly changed the circular dichroic spectrum of HNF-4 $\alpha$ LBD such that the minima at 208 nm and 220 nm significantly decreased to lower molar ellipticity values (Fig. 3.11, open triangles). Accordingly, a higher total helix percentage of 22% was calculated for HNF-4 $\alpha$ LBD in the presence of palmitoyl-CoA (Table 3.5). Interestingly, arachidonoyl-CoA, a 20-carbon chain length, polyunsaturated fatty acyl-CoA also altered the secondary structure of HNF-4 $\alpha$ LBD, but oppositely to palmitoyl-CoA. The molar ellipticity values of the minima at 208 and 220 nm exhibited by HNF-4 $\alpha$ LBD in the presence of arachidonoyl-CoA were higher (Fig. 3.11, open squares) than in the absence of the fatty acyl-CoA (Fig. 3.11, filled circles). This change was reflected in the helical and the  $\beta$ -strand structure percentages: nearly 3-fold lower percentages of helical structures, in

total only 6.4% (Table 3.5), but higher amount of turns (6.3%) and  $\beta$ -strands (35.7%) (Table 3.5) in the presence of arachidonoyl-CoA.

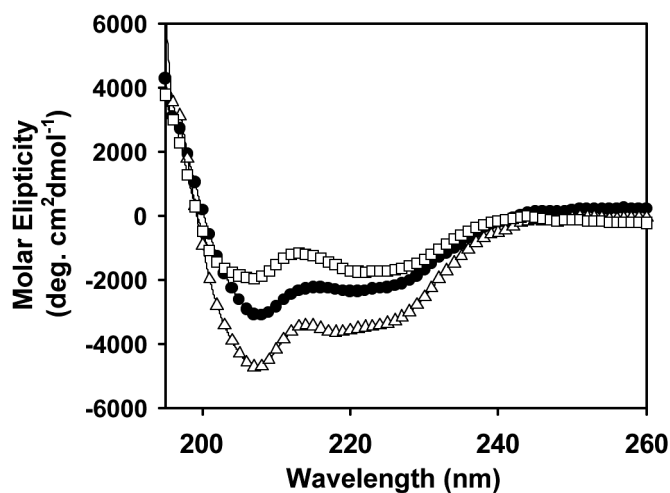


FIG. 3.11 **Circular dichroic spectral changes induced by fatty acyl-CoAs in HNF-4 $\alpha$ LBD.** The far UV CD spectrum of 2  $\mu$ M HNF-4 $\alpha$ LBD in the absence (filled circles) and in the presence of 50 mM arachidonoyl-CoA (empty squares) or palmitoyl-CoA (empty triangles).

In summary, fatty acyl-CoA binding significantly altered the secondary structure of HNF-4 $\alpha$ LBD with the direction of change highly dependent on the specific type of fatty acyl CoA.

### 3.4 DISCUSSION

Since hepatic nuclear factor-4 $\alpha$  (HNF-4 $\alpha$ ) regulates expression of liver genes involved in both lipid and carbohydrate metabolism, investigations on its structure and mechanism of action impacts on our understanding of diabetes, obesity, and atherosclerosis. Despite this importance of HNF-4 $\alpha$ , almost nothing is known regarding either its structure, especially that of the ligand binding domain (i.e. HNF-4 $\alpha$ LBD), or

how structure relates to function. In fact, until recently HNF-4 $\alpha$  was considered an orphan nuclear receptor. However, in 1998 Hertz *et al.* (45) demonstrated that various long chain fatty acyl-CoA (LCFA-CoA) thioesters bound to recombinant rat HNF-4 $\alpha$  and affected its transcriptional activity, depending on their chain length and degree of saturation. While this exciting discovery first suggested that fatty acyl-CoAs may be the natural ligand for this nuclear receptor, the radioligand competition assay used to demonstrate binding of fatty acyl-CoAs to HNF-4 $\alpha$  and HNF-4 $\alpha$ LBD yielded low affinities, i.e.  $K_d$ 's in the mM range (45). Consequently, it has been suggested that this low affinity represents nonspecific binding and is insufficient for HNF-4 $\alpha$  to significantly bind and be modulated by LCFA-CoAs in the nucleus (186). However, a significant potential problem with the radioligand competition assays is that they can seriously underestimate the affinities of binding proteins (18) or transcription factors (*e.g.*, PPAR $\alpha$ , (195)) for lipidic ligands. The purpose of the present investigation has been to resolve this issue of whether HNF-4 $\alpha$ LBD binds fatty acyl-CoAs with mM or nM  $K_d$ s, to determine the ligand specificity of HNF-4 $\alpha$ LBD, and examine if fatty acyl-CoA binding alters the structure/conformation of HNF-4 $\alpha$ LBD. As shown for the first time herein: (i) Forster fluorescence resonance energy transfer demonstrated close molecular interaction between fatty acyl-CoA and HNF-4 $\alpha$ LBD; (ii) A series of three independent, direct fluorescence binding assays showed that HNF-4 $\alpha$ LBD bound fatty acyl-CoAs with high affinity,  $K_d$ s as low as 1 nM; (iii) Fatty acyl-CoA binding induced significant changes in HNF-4 $\alpha$ LBD conformation as evidenced by intrinsic fluorescence and circular dichroism. The significance of these findings is detailed as follows:

First, the synthesis of *cis*-parinaroyl-CoA as ligand with excitation overlapping the emission of HNF-4 $\alpha$ LBD allowed for the first time demonstration of their close molecular interaction and determination of the intermolecular distance between the fluorescent ligand and its binding domain. FRET showed that the average intermolecular distance between HNF-4 $\alpha$ LBD Trp and bound *cis*-parinaroyl-CoA was in the range

TABLE 3.5  
*Effect of CoA thioesters of long chain saturated and unsaturated fatty acids on the secondary structure of HNF-4 $\alpha$ LBD.*

Ligand	$\alpha$ -Helix (H, %)	$3_{10}$ - Helix (G, %)	$3_1$ -helix (P %)	Total $\alpha$ - helix (H J %) <sup>c</sup>	$\beta$ -Strand (E, %)	Turns (T, %)	Others (O, %)
None	3.3 $\pm$ 0.003	6.0 $\pm$ 0.006	9.3 $\pm$ 0.021	7.7 $\pm$ 0.001	27.3 $\pm$ 0.025	1.5 $\pm$ 0.017	38.7 $\pm$ 0.032
C16:0-CoA <sup>a</sup>	6.0 $\pm$ 0.002	6.5 $\pm$ 0.001	9.5 $\pm$ 0.007	12.0 $\pm$ 0.002	27.5 $\pm$ 0.007	11.5 $\pm$ 0.007	39.0 $\pm$ 0.014
C20:4-CoA <sup>b</sup>	3.0 $\pm$ 0.010	2.3 $\pm$ 0.015	1.1 $\pm$ 0.058	6.0 $\pm$ 0.004	35.7 $\pm$ 0.100	6.3 $\pm$ 0.025	43.0 $\pm$ 0.017

<sup>a</sup>C16:0-CoA is palmitoyl-CoA.

<sup>b</sup>C20:4-CoA is arachidonoyl-CoA.

<sup>c</sup>”Total  $\alpha$ -helix (HJ%)” does not represent the sum of  $\alpha$ ,  $3_{10}$  and  $3_1$  helix. Instead, “Total  $\alpha$ -helix (HJ%)” is calculated using a different standard protein structure database with the same program as described in Experimental Procedures



of 23 Å (no ligand-induced conformational change in HNF-4 $\alpha$ LBD) to 42 Å (ligand-induced conformational change in HNF-4 $\alpha$ LBD). These are average intermolecular distances since HNF-4 $\alpha$ LBD contains 2 Trp residues (64). As further studies with non-fluorescent fatty acyl CoAs and circular dichroism supported the conclusion that fatty acyl-CoAs induce conformational changes in HNF-4 $\alpha$ LBD, these data are consistent with the intermolecular distance between bound fatty acyl-CoA and HNF-4 $\alpha$ LBD Trp being  $\leq$  42 Å. Further, the results demonstrate that fatty acyl-CoA binding with HNF-4 $\alpha$ LBD represent direct, molecular interaction rather than nonspecific coaggregation.

Second, three types of direct fluorescence binding assays showed that previous radioligand competition assays underestimated the binding affinities of HNF-4 $\alpha$ LBD for fatty acyl-CoAs. Instead, the direct fluorescence binding assays showed that HNF-4 $\alpha$ LBD bound fatty acyl-CoAs with high affinities as indicated by  $K_d$ s as low as 1 nM. This underestimation is characteristic of lipidic radioligand competition binding assays which typically yield  $K_d$ 's that are 2-3 orders of magnitude higher (i.e. lower affinity) than  $K_d$ 's determined by direct fluorescence or titration microcalorimetry binding assays (rev. in(18)). In contrast, the direct fluorescence binding assays took advantage of three different intrinsic properties of ligand or protein including the fluorescence of cis-parinaroyl-CoA, the intrinsic fluorescence of HNF-4 $\alpha$ LBD, or the FRET sensitized emission of HNF-4 $\alpha$ LBD bound cis-parinaroyl-CoA. None of these direct fluorescence ligand binding assay required separation of bound from free ligand. Taken together, the present study demonstrates that i) HNF-4 $\alpha$ LBD exhibits saturable fatty acyl-CoA binding, (ii) HNF-4 $\alpha$ LBD has one ligand binding site, (iii) the ligand binding site of HNF-4 $\alpha$ LBD has  $K_d$ s for LCFA-CoAs (*e.g.*, palmitoyl-CoA, stearoyl-CoA, linoleoyl-CoA, arachidonyl-CoA) in the very low nM range (1.6–4 nM), (iv) The respective free acids may bind, albeit with a significantly lower affinity ( $K_d$ s for C20:4-CoA and C20:4 differ by about 200 fold).

Third, fatty acyl-CoA binding was shown to differentially alter the structure of HNF-4 $\alpha$ LBD. This was supported by two types of evidence: (i) A wide variety of fatty acyl-CoAs and peroxisome proliferator-CoAs significantly quenched HNF-4 $\alpha$ LBD Trp fluorescence emission at 333 nm. (ii) Two LCFA-CoAs, a saturated one, C16:0-CoA and a polyunsaturated one, C20:4-CoA, were tested for ability to induce changes in the secondary structure of HNF-4 $\alpha$ LBD. Although both ligands quenched HNF-4 $\alpha$ LBD Trp fluorescence emission, they differentially altered circular dichroic spectra of HNF-4 $\alpha$ LBD (Fig. 3.11). Very significant was the finding that palmitoyl-CoA increased the  $\alpha$ -helix and turn content while arachidonoyl-CoA decreased the content of  $3_{10}$ -helix and  $3_1$ -helix, while increasing  $\beta$ -strands and turns. These very different changes induced by palmitoyl- vs arachidonoyl-CoAs in the secondary structure of HNF-4 $\alpha$ LBD correlated to the opposite effect of saturated and polyunsaturated fatty acyl-CoAs in functional assays (45).

Fourth, the proposed role of LCFA-CoA as natural ligands of HNF-4 $\alpha$  (45) was challenged by Bogan et al. (187) on the grounds of (i) computer modeling of HNF-4 $\alpha$ LBD structure based on its 22% and 37% overall identity with the progesterone and RXR receptors LBD, respectively, and in particular its homology with helix 1 and the F domain of progesterone receptor LBD; this modeling predicted a ligand binding pocket of around 320  $\text{\AA}^3$  as compared with a volume of 850  $\text{\AA}^3$  apparently required for the CoA-thioester; (ii) previously reported  $\mu\text{M}$   $K_d$ s for LCFA-CoA binding to HNF-4 $\alpha$  as compared with nM  $K_d$ s for the more abundant cytosolic fatty acyl CoA binding protein such as ACBP ( $K_d$  of 7 nM (22)), FABP ( $K_d$ s of 41–60 nM, (153)), and SCP-2 ( $K_d$  of 4.5 nM (191),(6)); (iii) lack of induced conformational changes in HNF-4 $\alpha$  as deduced from limited proteolysis (187). It is worth noting however that: (i) circular dichroic data presented here indicates a higher percentage of  $\beta$ -strand (27.3%) than helical secondary structure (3.3%  $\alpha$ -helix, 6.0%  $3_{10}$ -helix and 9.3%  $3_1$ -helix) and is inconsistent with the predicted modeling. Furthermore, FRET results indicate direct interaction of LCFA-CoA with the ligand binding site of HNF-4 $\alpha$ . (ii) While HNF-4 $\alpha$  is

localized in the nucleus (64), (197), ACBP and L-FABP are essentially localized outside the nucleus (rev. in (198), (18)) and SCP-2 is not detected in the nucleus (rev. in (198)). More important, the binding data presented here indicates 1–4 nM  $K_{dS}$  for LCFA-CoA binding to HNF-4 $\alpha$ , being in the range of other acyl-CoA binding proteins as well as in the range of unbound free fatty acyl-CoA concentrations estimated in the nucleus(185). It is possible, however, that these extranuclear fatty acyl-CoA binding proteins may alter the distribution of fatty acyl-CoAs to the nucleus. Alternately, some L-FABP (6) (199), (121), and ACBP (185) detected within the nucleus may compete with HNF-4 $\alpha$  for fatty acyl-CoA binding therein. (iii) This study reports direct evidence for ligand-induced conformational change verified by differential quenching of HNF-4 $\alpha$ LBD Trp fluorescence emission as well as by differential changes in helical content due to ligand binding. This evidence is consistent with previously reported protection from limited proteolysis of HNF-4 $\alpha$  by C14:0-CoA (116). Taken together, the results presented here support the original proposal by Hertz *et al.* (45) that LCFA-CoAs may serve as endogenous ligands for HNF-4 $\alpha$ .

This report further substantiates earlier findings by Hertz *et al.* (45) that CoA thioesters of hypolipidemic peroxisome proliferators such as Medica homologues or fibrate drugs bind to HNF-4 $\alpha$  or HNF-4 $\alpha$ LBD and suppress its transcriptional activity. It further confirms that Medica 16-CoA is a more effective ligand than bezafibroyl-CoA (order of magnitude difference in  $K_{dS}$ ). Similarly to LCFA-CoAs,  $K_{dS}$  for the CoA-thioesters of hypolipidemic peroxisome proliferators measured by quenching of HNF-4 $\alpha$ LBD Trp fluorescence emission were in the nM range as compared with  $\mu$ M  $K_{dS}$  previously reported using radioligand competition assays (116). However, in contrast to the free acid forms of LCFA which show low binding affinity to HNF-4 $\alpha$ LBD ( $K_{dS}$  of 421–742 nM), binding affinities for the free acid forms of hypolipidemic peroxisome proliferators were in the low nM range (34–57 nM), albeit significantly lower as compared with the respective CoA-thioesters. The capacity of hypolipidemic peroxisome proliferators bound in their free acid form to suppress the

transcriptional activity of HNF-4 $\alpha$  still remains to be investigated. It is worth noting however that HNF-4 $\alpha$  transcriptional activity was not suppressed by amphipathic carboxylates which due to a structural constraint did not endogenously yield the respective CoA-thioester.

Suppression of HNF-4 $\alpha$  activity by the CoA-thioesters of hypolipidemic peroxisome proliferators in the nM range may indicate that HNF-4 $\alpha$  serves as target for their therapeutic activity. This is consistent with HNF-4 $\alpha$  involvement in controlling the expression of genes encoding proteins with role in production and clearance of plasma lipoproteins (*e.g.*, MTP, apo B, apo C-III and others (181)). Since the human liver is not responsive to PPAR $\alpha$  (rev. in (45), (201)), the hypolipidemic activity induced by hypolipidemic PPAR $\alpha$  agonists in humans must be independent of PPAR $\alpha$ . In contrast, in rodents, activation of PPAR $\alpha$  by hypolipidemic peroxisome proliferators may result in HNF4 $\alpha$  displacement from DR-1 response elements shared by both transcription factors (114). Suppression of HNF-4 $\alpha$  function in transactivation by the CoA-thioesters of hypolipidemic peroxisome proliferators offers an hypolipidemic mode of action of peroxisome proliferators in humans independent of liver PPAR $\alpha$  and its proliferative-carcinogenic activity.

In conclusion, multiple fluorescence spectroscopic and circular dichroism approaches strongly demonstrate that fatty acyl-CoAs and certain peroxisome proliferator-CoAs are specific ligands for HNF-4 $\alpha$ LBD and that fatty acyl-CoA binding induces significant changes in HNF-4 $\alpha$ LBD secondary and overall conformational structure. While naturally-occurring fatty acids only weakly bind HNF-4 $\alpha$ LBD, some synthetic fluorescent fatty acids as well as certain peroxisome proliferators also bind as free acids to HNF-4 $\alpha$ LBD but with lower affinities than the respective acyl-CoAs. These data demonstrate for the first time that fatty acyl-CoAs and certain peroxisome proliferator drug thioesters may be natural and pharmacological HNF-4 $\alpha$ LBD ligands at physiological concentrations.

**CHAPTER IV**  
**PHYSICAL AND FUNCTIONAL INTERACTION OF**  
**ACYL-CoA BINDING PROTEIN (ACBP) AND HEPATOCYTE**  
**NUCLEAR FACTOR-4 $\alpha$  (HNF-4 $\alpha$ )**

4.1 INTRODUCTION

Acyl-CoA binding protein (ACBP) is a ubiquitous intracellular lipid binding protein whose physiological function remains to be determined (rev. (20)(185)(202)). Until recently, ACBP was thought primarily as a cytosolic protein unique among the soluble intracellular lipid proteins in that it exhibits very high affinity ( $K_{ds}$  of 0.5-10 nM) with essentially exclusive specificity for long chain fatty acyl-CoAs (LCFA-CoAs), (20) (22) (203) (204) (205). This ability of ACBP to exclusively bind LCFA-CoA led postulation of three types of potential functions for ACBP:

First, ACBP may be involved in directly presenting LCFA-CoAs to lipid metabolic enzymes. A variety of studies *in vitro* suggest that ACBP extracts LCFA-CoAs from membranes (202) to increase the intracellular LCFA-CoA pool for transport (rev. (185) to acyltransferase enzymes involved in phospholipid synthesis in the endoplasmic reticulum (206),(207) lysophosphatidic acid synthesis in mitochondria (208) cholesteryl ester synthesis in the endoplasmic reticulum (203) and fatty acid oxidation in mitochondria (208).

Second, ACBP controls the activities of a variety of lipid metabolic enzymes (e.g. acetyl CoA carboxylase) and intracellular signaling proteins (e.g. protein kinase C) whose activities are regulated by LCFA-CoAs in the cytosol (rev. in (204), (209)).

Third, recent data demonstrating the presence of significant amounts of ACBP in nuclei of cells transfected with ACBP expression vectors suggest that ACBP may also be involved in the action of LCFA-CoA dependent nuclear binding proteins that regulate transcription of genes involved in lipid and glucose metabolism (186),(123). Several members of the nuclear receptor superfamily including the thyroid hormone receptor, TR (56), hepatocyte nuclear receptor 4 $\alpha$  (HNF-4 $\alpha$ ), (45)(209) and peroxisome

proliferator-activated receptor- $\alpha$  and  $\delta$  (PPAR- $\alpha$ , $\delta$ ) interact with LCFA-CoAs (47) (210). The relative order of affinities of these nuclear receptors for LCFA-CoAs is HNF-4 $\alpha$  ( $K_{ds}$  of 1.5-4 nM)  $\gg$  TR ( $K_{ds}$  of 120 nM)  $\gg$  PPAR $\alpha$  (displaces Wy14643). On this basis, it appears that only HNF-4 $\alpha$  binds LCFA-CoAs with affinities in the physiological range of LCFA-CoA levels in the nucleus (209). HNF-4 $\alpha$  is a nuclear receptor with major role in hepatocyte differentiation during liver development, regulating the transcription of numerous target genes involved in lipid transport and metabolism (211),(212). Recently, a conditional gene knockout of HNF-4 $\alpha$  in mouse confirmed that HNF-4 $\alpha$  is an important *in vivo* regulator of genes involved in lipid homeostasis, such as apolipoproteins (Apo-AI,-II,-IV, Apo-B, Apo-CII,-III, and Apo-E), microsomal triglyceride transfer protein (MTP), cholesterol 7 $\alpha$ -hydroxylase (CYP7A), liver-fatty acid binding protein (L-FABP) and PPAR- $\alpha$  (66). A study in which 9000 genes were analyzed by cDNA microarray technology in human hepatoma cells that over-expressed HNF-4 $\alpha$  demonstrated that 26 out of the 45 HNF-4 $\alpha$ -sensitive genes were related to lipid metabolism (67).

Although both ACBP and HNF-4 $\alpha$  bind LCFA-CoAs with nanomolar affinities and have been reported to modulate lipid metabolism, it is not known if (i) ACBP interacts directly with HNF-4 $\alpha$  at the molecular level, (ii) ACBP interacts directly with HNF-4 $\alpha$  at the cellular level, and (iii) ACBP expression influences HNF-4 $\alpha$  transcriptional functions. Circular dichroism and coimmunoprecipitation of recombinant mouse ACBP and HNF-4 $\alpha$  ligand binding domain (LBD) *in vitro* clearly indicated that the two proteins interacted with formation of a complex. Confocal microscopy, immunocolocalization and fluorescence resonance energy transfer (FRET) imaging showed that ACBP and HNF-4 $\alpha$  interact within the nucleus of intact cells. A mammalian two-hybrid assay confirmed that there is physical association between ACBP and HNF-4 $\alpha$  in the nucleus of living cells. An HNF-4 $\alpha$  luciferase reporter assay as well as LSCM of individual cells showed that ACBP overexpression in COS-7 and rat hepatoma cells enhanced HNF-4 $\alpha$  transactivation was ACBP concentration-dependent.

In summary, these results for the first time demonstrate a physical and functional association between ACBP, a LCFA-CoA binding protein, and the nuclear LCFA-CoA binding receptor HNF-4 $\alpha$ .

## 4.2 EXPERIMENTAL PROCEDURES

### 4.2.1 *Materials*

Recombinant mouse ACBP was produced and purified as described (203). HNF- $\alpha$ -LBD was obtained as described earlier (45) (209). Fetal bovine serum (FBS), bovine serum albumin (BSA), Protein A-Sepharose 4CL, and FITC-goat anti-rat-IgG were purchased from Sigma Chemical Company (St. Louis, MO). Lab-Tek Coverglass slides were purchased from Fisher Scientific, Pittsburgh, PA. Mouse-anti-firefly luciferase monoclonal was purchased from Novus Biologicals (Littleton, CO). Texas-Red- goat anti-rabbit IgG was from Molecular Probes (Eugene, OR) and FluoroLink Cy5 labelled goat anti-mouse IgG was from Amersham Pharmacia (Piscataway, NJ). TOTO-3, a dimeric cyanine fluorophore, was from Molecular Probes (Eugene, OR). All reagents and solvents used were of the highest grade available and were cell culture tested as necessary.

### 4.2.2 *Circular Dichroism (CD) of ACBP and HNF-4 $\alpha$ LBD*

Far UV circular dichroic spectra of HNF-4 $\alpha$ LBD (1.44  $\mu$ M) and ACBP (2  $\mu$ M) in 2 mM Tri-HCl, pH 8 containing 0.5% glycerol and 0.05 mM DTT were measured separately and in a 1:1(v/v) mixture. The CD measurements were performed with a J-710 Spectropolarimeter (Jasco, Baltimore, MD) using a 1 mm cuvette. Spectra were recorded from 250 to 195 nm at 50 nm/min with a time constant of 1 s and a bandwidth of 2 nm. For each CD profile an average of ten scans was obtained. Percentages of various secondary structures in HNF-4 $\alpha$ LBD, ACBP, and [HNF-4 $\alpha$ LBD + ACBP] were calculated from CD spectra by using the CDstr program (195) (213). The CD spectrum of [ACBP + HNF-4 $\alpha$ -LBD] was compared to a theoretical spectrum obtained by

summing the spectra of the HNF-4 $\alpha$ LBD and ACBP recorded separately for each protein in a concentration equal to that in the mixture.

#### *4.2.3 ACBP and HNF-4 $\alpha$ LBD Antisera for Coimmunoprecipitation, Western Blotting, and Immunocytochemistry*

Rabbit polyclonal anti-mouse ACBP antiserum was obtained as described previously (202) (206). Rat polyclonal anti-mouse ACBP antisera were prepared according to AAALAC guidelines. Briefly, recombinant mouse ACBP (20  $\mu$ g) was emulsified in Freund's complete adjuvant (200  $\mu$ l) diluted 1:1 in PBS (200  $\mu$ l). A pre-bleed was taken prior to injection of the inoculum into a shaved area on the dorsum of a female rabbit (Hazleton Research Products, Denver, PA) as described earlier. After 6 weeks a test bleed was taken and a booster dose (20  $\mu$ g SCP-2, 200  $\mu$ l Freund's incomplete adjuvant, 200  $\mu$ l PBS) was administered. Fourteen days later the rabbit was exsanguinated. The resultant polyclonal antibodies were purified by affinity chromatography on protein-A-sepharose. The specificity of appropriate dilutions of the purified anti-ACBP antibodies for Western blotting was determined as described earlier western blotting performed as described earlier (206). Anti-ACBP antisera did not cross-react with HNF-4 $\alpha$ -LBD, HNF-4 $\alpha$ , or any intracellular lipid binding protein tested (SCP-2, L-FABP, I-FABP). Rabbit polyclonal anti-rat HNF-4 $\alpha$ -LBD antisera were prepared according to AAALAC guidelines. Briefly, recombinant HNF-4 $\alpha$ -LBD (20  $\mu$ g) was emulsified in Freund's complete adjuvant (200  $\mu$ l) diluted 1:1 in PBS (200  $\mu$ l). After 6 weeks a test bleed was taken and a booster dose (20  $\mu$ g SCP-2, 200  $\mu$ l Freund's incomplete adjuvant, 200  $\mu$ l PBS) was administered. Fourteen days later the rabbit was exsanguinated. The resultant polyclonal antibodies were purified by affinity chromatography on protein-A-sepharose. The specificity of appropriate dilutions of the purified anti-HNF-4 $\alpha$ -LBD antibodies for Western blotting was determined. For fluorescence resonance energy transfer (FRET) determined by laser scanning confocal microscopy, pure fractions of ACBP and HNF-4 $\alpha$  were prepared using an Econo-Pac



Protein kit from Bio-Rad (Hercules, CA) as described earlier (214), (215). The pure fractions of IgG from rabbit anti-HNF4 $\alpha$ -LBD and anti-ACBP antisera were then Cy3-labelled (anti-HNF-4 $\alpha$  IgG) or Cy5-labelled (anti-ACBP IgG) using a Fluorolink-antibody Cy3 and Cy5 labelling kit from Amersham (Piscataway, NJ) according to manufacturer's instructions.

#### 4.2.4 *Coimmunoprecipitation of ACBP and HNF-4 $\alpha$ LBD*

The ability of a polyclonal anti-mouse ACBP or a polyconal anti-HNF-4 $\alpha$ -LBD antiserum to immunoprecipitate both proteins from an *in vitro* mixture of recombinant ACBP and HNF-4 $\alpha$ -LBD. A mixture of ACBP (1mM) and HNF-4 $\alpha$ -LBD (1mM) was prepared in 20 mM Tris-HCl, pH 8, 0.3 M NaCl, 10% glycerol and 1 mM DTT (this buffer was used in order to preserve HNF-4 $\alpha$ -LBD in a soluble, non-aggregated form). The two proteins in the mixture were allowed to interact and eventually form complexes for 2 hours at room temperature. In two separate tubes, 200  $\mu$ l (ACBP + HNF-4 $\alpha$ -LBD) mix were precipitated with 20  $\mu$ l anti-ACBP and 20  $\mu$ l anti-HNF-4 $\alpha$ -LBD antiserum, respectively. Precipitation was allowed overnight at 4°C. Protein A-Sepharose 4CL was blocked for nonspecific binding with a solution containing 2% gelatin, in RIPA buffer (50 mM Tris, pH 8, 150 mM NaCl, 1% nonidet P-40, 0.5% deoxycholate, 0.1% SDS) (5) and added to precipitate ACBP/HNF-4 $\alpha$ -LBD complexes with incubation for 2 hours at 4C. After extensive washings of the beads with 500 mM NaCl in RIPA buffer, the beads were solubilized in 2x sample buffer for further SDS-PAGE separation and western blotting.

#### 4.2.5 *Western Blotting of ACBP and HNF-4 $\alpha$*

Protein concentration was determined by BCA Protein Assay (Pierce, Rockford, IL). SDS-PAGE and protein transfer on nitrocellulose membranes were performed as described (216) (217). Primary antibodies used in western blotting were rat anti-mouse ACBP and rabbit anti-rat-HNF-4 $\alpha$ -LBD polyclonal antibodies prepared as described above. Specific proteins were visualized either by a colorimetric method utilizing

alkaline-phosphatase-conjugated goat anti-rabbit IgG and BCIP/NBT substrate (Sigma Chemical Co, St. Louis, MO) or by a chemiluminescent method employing HR-peroxidase-conjugated goat anti-rabbit IgG and luminol/hydrogen peroxide substrates (Amersham Pharmacia Biotech, Piscataway, NJ).

#### 4.2.6 *Cell Culture*

COS-7 cells, CRL-1651 were purchased from American Type Culture Collection (ATCC, Manassas, VA). Rat hepatoma cells T-7 were obtained from Dr. Baum's laboratory (University of Chicago, Chicago, IL). The cells were grown in 4-well LabTek chamber slides in DMEM culture medium containing 10% fetal bovine serum (FBS).

#### 4.2.7 *Preparation of Cells for Indirect Immunofluorescence Microscopy*

COS-7 and rat hepatoma cells were grown in 4-well LabTek chamber slides as above upto 80% confluency, fixed with 70:30 acetone/ethanol (v/v) for 30 min at  $-20^{\circ}\text{C}$ , and blocked against nonspecific binding with 10% FBS in Hank's solution for 1 h at room temperature. The cells were then incubated with primary antibodies for 1 h at room temperature, followed by incubation with secondary antibodies for another 1 h at room temperature. After extensive washing of unbound antibodies with Hank's solution, the cells were mounted by the use of Slow Fade kit (Molecular Probes, Eugene, OR). Rabbit-anti-rat-HNF-4 $\alpha$  polyclonal, rat-anti-mouse ACBP polyclonal, and mouse-anti-firefly luciferase monoclonal antisera were used as primary antibodies. Texas-Red- goat anti-rabbit IgG, FITC-goat anti-rat-IgG, and FluoroLink Cy5-labelled goat anti-mouse IgG were used as secondary antibodies. In some experiments the nuclear areas of cells was defined by staining the DNA with TOTO-3, adimeric cyanine fluorophore from Molecular probes (Eugene, OR). Specificity of immunostaining was determined by deleting the primary antibody and using either one or both secondary antibodies. Several dilutions (1:20 to 1:200) of each primary and secondary antibody were tested and optimized. This minimized nonspecific adsorption of fluorescent antibodies,

optimized separation of the fluorescent signals, and optimized fluorophore concentration to preclude self-quenching.

#### 4.2.8 *Laser Scanning Confocal Microscopy (LSCM) and Image Analysis*

LSCM was performed on a MRC-1024 fluorescence imaging system (Bio-Rad, Hercules, CA) consisting of an Axiovert 135 microscope (Zeiss, New York, NY) equipped with three independent low-noise photomultiplier tube channels. The excitation light ( $\lambda=488, 568, \text{ and } 647$ ) from a 15mW krypton-argon laser was delivered to the sample through x63 Zeiss Plan-Fluor oil immersion objective, numerical aperture 1.45. Texas Red and Cy3 were excited at 568 nm and their emission detected through a HQ 585/40 bandpass filter. FITC was excited with 488 nm light and its emission selected through a 540/30 filter. TOTO-3 (DNA stain) and Cy5 were excited with 647nm light and their emission selected through a 680/32 bandpass filter. The conventional colors of emitted light were red (for Texas Red and Cy3), green (for FITC) and blue (for Cy5 and TOTO-3). Images were acquired and analyzed using LaserSharp (from Bio-Rad) and MetaMorph Image Analysis (from Advanced Scientific Imaging, Merieux, LA) softwares .

#### 4.2.9 *Fluorescence Resonance Energy Transfer (FRET) Microscopy*

In order to estimate the intermolecular distance between ACBP and HNF-4 $\alpha$  molecules that were detected colocalized in confocal microscopy images, FRET between Cy3-labelled anti-HNF-4 $\alpha$  IgG and Cy5-labelled anti-ACBP IgG was determined as described earlier (214)(215). Rat hepatoma cells were processed as for immunofluorescence microscopy, except that only primary antibodies that had been Cy3 and Cy5 labeled were used. Qualitatively, FRET from Cy3 to Cy5 was demonstrated by detection of sensitized emission of Cy5 (through the 680/32 bandpass filter) upon excitation of Cy3 at 568 nm, after correction of some bleedthrough of Cy3 emission through the same filter as follows. Fluorescence emission through 680/32 filter was recorded before and after photobleaching Cy5 at 647 nm for 3 minutes (the duration of

photobleaching was optimized such that a good decrease in Cy5 fluorescence was obtained without affecting the emission intensity of Cy3). The image recorded after photobleaching Cy5 was the bleedthrough of Cy3 emission through PMT3 (with 680/32 bandpass filter). Fluorescence intensity of emission through this 680/32 filter before photobleaching Cy5 (FRET acceptor), being the sum resulted from sensitized emission of Cy5 and the bleedthrough of Cy5, was always higher than the one taken after Cy5 photobleaching, clearly indicating FRET from Cy3 to Cy5. Quantitative measurements for FRET efficiency estimation were carried out as described (215) FRET efficiency was calculated according to:

$$E = (I_{post} - I_{pre}) / I_{post} \quad (\text{Eq. 4.1})$$

where E is FRET efficiency,  $I_{post}$  is the acceptor (Cy3) fluorescence intensity after Cy5 photobleach, and  $I_{pre}$  is the acceptor (Cy3) fluorescence intensity before Cy5 photobleach. The calculated E was further used to estimate R, the intermolecular distance between Cy3 and Cy5 (distance ultimately dictated in this experiment by the proximity between ACBP and HNF-4 $\alpha$ ), according to:

$$E = 1 / (1 + (R/R_0)^6) \quad (\text{Eq. 4.2})$$

where  $R_0$ , the distance for which a 50% FRET efficiency occurs, is known to be 50A for the Cy3 / Cy5 FRET pair.

#### 4.2.10 DNA Constructs and Plasmids Used in Transfection Assays

COS-7 and rat hepatoma cells were transfected with the following expression and reporter plasmids. A set of sense and antisense mouse ACBP expression vectors was constructed by inserting the 276 bp ACBP cDNA into a XhoI cloning site of pCI-neo mammalian expression vector purchased from Promega (Madison, WI). For an efficient repression of ACBP expression an antisense ACBP vector was constructed using a pUC plasmid that contained the mouse pgk-1 gene promoter, as described (218). The HNF-4 $\alpha$  expression vector pLEN4S, with the 3kb rat HNF-4 $\alpha$ 1 cDNA under a human metallothionein-II promoter and human growth hormone 3'-untranslated region was a gift from Dr. F. Sladek (University of California, Riverside, CA). From the same lab we

received the ApoBLuc reporter vector, containing 4 inserts of the 85-47 HNF-4 $\alpha$  responsive elements in the ApoB gene promoter in front of the firefly luciferase cDNA. For monitoring the transfection efficiencies, pRL-CMV (Promega, Madison, WI), the expression vector for Renilla luciferase was cotransfected with the other expression vectors.

#### *4.2.11 Functional Interaction of ACBP with HNF-4 $\alpha$ in Intact Cells: Transactivation Assay*

COS-7 and rat hepatoma cells grown in 6-well culture plates were transfected with 1  $\mu$ g each of pLEN4S (HNF-4 $\alpha$  expression vector), pCI-sACBP (sense ACBP expression vector) or pgk-aACBP (antisense ACBP RNA expression vector), and ApoBLuc (reporter plasmid) per well. pRL-CMV (0.05  $\mu$ g per well) was always co-transfected as internal standard for estimating the transfection efficiency. When no pCI-ACBP was used, empty vector (pCI-neo/pgk) in appropriate amount was added. Transfections were performed with Lipofectamine 2000 reagent from Invitrogen (Carlsbad, CA) according to manufacturer's instructions.

The firefly luciferase activity, normalized to Renilla luciferase (as internal control for transfection efficiency), was determined by using the dual-luciferase reporter assay system from Promega (Madison, WI). Luminescence was read and measured with a Microlite ML3000 Microtiter plate luminometer equipped with BioLinx assay management software (Dynatech Laboratories, Inc., Chantilly, VA).

#### *4.2.12 Functional Interaction of ACBP with HNF-4 $\alpha$ in Intact Cells: Mammalian Two-Hybrid Assay*

The interaction of ACBP with HNF-4 $\alpha$  in intact cells was also examined by a mammalian two-hybrid system CheckMate Mammalian Two-Hybrid System from Promega, (Madison, WI). The rat recombinant HNF-4 $\alpha$  cDNA was from Dr. J. Bartana (Hebrew University Medical School, Jerusalem, Israel). The mouse recombinant ACBP cDNA was prepared as described (202). Full length HNF-4 $\alpha$  and ACBP cDNA

fragments were amplified by PCR using primer sets containing specific restriction cloning sites: i) for ACBP, 29mer 5'-CTGGATCCGTATGTCTCAGGCTGAATTTG-3' and 33mer 5'-GGTCTAGATTATATTCCGTATTTCTTCTTTAGC-3'; ii) for HNF-4 $\alpha$ : 30mer 5'-CAGGATCCACATGGACATGGCTGACTACAG-3' and 28mer 5'-GCTCTAGACTAGATGGCTTCCTGCTTGG-3'. PCR fragments were restriction digested with BamHI/XbaI and ligated to pACT and pBIND vectors to produce pACT/HNF-4 $\alpha$  and pBIND/ACBP, pACT/ACBP and pBIND/HNF-4 $\alpha$ . The four constructs were purified and sequenced at their 5' junctions to verify that the introduced cDNAs were in the correct reading frame. Two separate sets of experiments were performed to ensure there was no vector preference for either cDNA. COS-7 cells, were cotransfected with pACT/HNF-4 $\alpha$ , pBIND/ACBP in a first set of experiments, and with pACT/ACBP, pBIND/HNF-4a in a second set, together with the firefly luciferase reporter plasmid pG5luc, using Lipofectamine 2000 (from Invitrogen, Carlsbad, CA). Renilla luciferase plasmid, pRL-CMV (Promega, Madison, WI) was used as internal control to monitor transfection efficiency at all times. Transfected COS-7 cells were cultured 24 hours, harvested and lysed. Renilla and firefly luciferase activities were measured by using Dual Reporter Assay System (Promega, Madison, WI) and a ML3000 Microtiter Plate luminometer equipped with BioLinx assay management software (Dynatech Laboratories Inc., Chantilly, VA).

### 4.3 RESULTS

#### 4.3.1 ACBP/HNF-4 $\alpha$ Complex Formation *in Vitro*: Circular Dichroism

To determine if ACBP and HNF-4 $\alpha$ LBD physically interact to alter conformation, circular dichroism (CD) was used to determine the secondary structure of these proteins were obtained individually and in combination. The shape of the far UV CD spectrum of ACBP indicated the presence of high amount of  $\alpha$ -helix (Fig.1, solid triangles). Quantitative analysis of multiple CD spectra of ACBP showed that ACBP contains nearly half of its polypeptide chain as  $\alpha$ -helix (48%) structure, with very little  $\beta$ -sheet (2%) in its secondary structure. In contrast, CD spectra of HNF-4 $\alpha$ LBD indicated that  $\alpha$ -

helix structures represented only a minor component of this protein (Fig. 4.1, solid circles). This was confirmed by quantitative analysis of multiple CD spectra which showed HNF-4 $\alpha$ LBD as predominantly  $\beta$ -strand structure (27.3%) with low content of  $\alpha$ -helices (3.3%) (Table 4.1).

The significant differences in CD spectra of pure ACBP versus pure HNF-4 $\alpha$ LBD provided a means for detecting direct interaction between ACBP and HNF-4 $\alpha$ LBD measured as conformational change. Theoretically, if does not ACBP interact with HNF-4 $\alpha$ LBD, then a mixture of the two proteins should show a CD spectrum equally intermediate between pure ACBP and pure HNF-4 $\alpha$ LBD. On the contrary, the experimental data showed that (ACBP + HNF-4 $\alpha$ LBD) exhibited a CD spectrum that was not equally intermediate between pure ACBP and pure HNF-4 $\alpha$ LBD (Fig. 4.1, open circles).

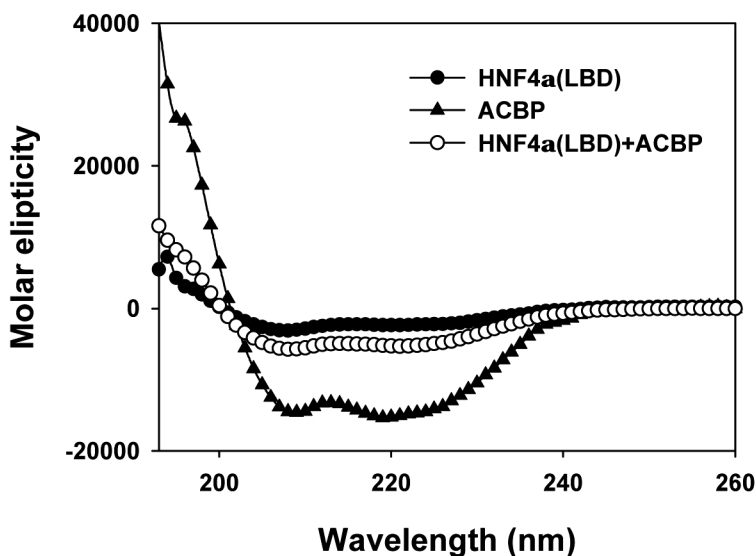


FIG. 4.1. **Circular dichroic spectrum of ACBP in the presence of HNF-4 $\alpha$ LBD indicates complex formation.** Far UV CD spectra of ACBP (black triangles), HNF-4 $\alpha$ LBD (black circles) and a mixture of ACBP and HNF-4 $\alpha$ LBD (white circles).

TABLE 4.1

*Secondary structure of ACBP, HNF-4 $\alpha$ LBD and complexes of these two proteins.*

Proteins	$\alpha$ -Helix (H*, %)	$3_{10}$ - Helix (G*, %)	$3_1$ -helix (P*, %)	$\beta$ -Strand (E*, %)	Turns (T*, %)	Others (O*, %)
ACBP	48.0 $\pm$ 0.14	10.5 $\pm$ 0.07	3.5 $\pm$ 0.06	2.0 $\pm$ 0.08	10.0 $\pm$ 0.06	25.5 $\pm$ 0.13
HNF-4 $\alpha$	3.3 $\pm$ 0.03	6.0 $\pm$ 0.08	9.3 $\pm$ 0.02	27.3 $\pm$ 0.25	1.5 $\pm$ 0.17	38.7 $\pm$ 0.32
HNF-4 $\alpha$ +ACBP	14.7 $\pm$ 0.05	3.7 $\pm$ 0.05	10.7 $\pm$ 0.08	21.3 $\pm$ 0.15	10.3 $\pm$ 0.21	39.7 $\pm$ 0.23
Predicted	25.7 $\pm$ 0.08	8.3 $\pm$ 0.08	7.1 $\pm$ 0.06	11.7 $\pm$ 0.30	3.6 $\pm$ 0.20	32.1 $\pm$ 0.25

\*Different types of secondary structure:  $\alpha$ -helix (H),  $3_{10}$ -helix (G),  $\beta$ -strand (E), turn (T), poly(L-proline)II type  $3_1$ -helix (P) are denoted as in (219).



The CD spectrum of (ACBP + HNF-4 $\alpha$ LBD) was much closer to that of pure HNF-4 $\alpha$ LBD, suggesting a significant conformational change. Quantitative analysis of multiple CD spectra of (ACBP + HNF-4 $\alpha$ LBD) which showed that the amount of  $\alpha$ -helix (14.7%) in the (ACBP + HNF-4 $\alpha$ LBD) mixture was 14.7%, much lower than predicted from the theoretical non-interactive CD spectrum (25.7%) (Table 4.1). In contrast, (ACBP + HNF-4 $\alpha$ LBD) exhibited much higher  $\beta$ -strand structures (21.3%) than predicted from the theoretical noninteractive CD spectrum (11.7%) (Table 4.1). These data were consistent with ACBP binding directly with HNF-4 $\alpha$ LBD to form an ACBP/HNF-4 $\alpha$ LBD complex *in vitro*. This interaction was detectable as a change in protein conformation resulting in altered protein secondary structure.

#### 4.3.2 ACBP/HNF-4 $\alpha$ Complex Formation in Vitro: Coimmunoprecipitation

To further investigate the possibility that ACBP binds HNF-4 $\alpha$ LBD to form an ACBP/HNF-4 $\alpha$ LBD complex, a mixture of (ACBP + HNF-4 $\alpha$ LBD) was treated with either anti-ACBP or anti-HNF-4 $\alpha$ LBD antibodies. If an ACBP/HNF-4 $\alpha$ LBD complex formed, then either antibody should immunoprecipitate the complex. ACBP was detected by western blotting of the immune precipitate obtained with anti-HNF-4 $\alpha$ LBD (Fig. 4.2, panel A). Similarly, HNF-4 $\alpha$  was detected by western blotting of the immune precipitate obtained with anti-ACBP (Fig. 4.2, panel B). Thus, ACBP and HNF-4 $\alpha$ LBD interacted directly to form an immunoprecipitable complex *in vitro*.

#### 4.3.3 Colocalization of ACBP and HNF-4 $\alpha$ within the Nuclei of Fixed Hepatoma Cells

To determine if ACBP and HNF-4 $\alpha$ LBD were in close proximity in intact cells, rat hepatoma cells expressing both proteins were double immunolabeled and examined by laser scanning confocal microscopy (LSCM). Rat hepatoma cells were fixed, coimmunolabeled with rabbit anti-HNF4 $\alpha$  and rat anti-ACBP primary antisera,

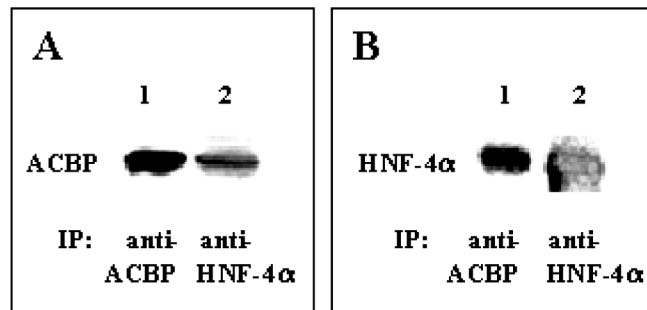


FIG. 4.2. **Coimmunoprecipitation of ACBP and HNF-4 $\alpha$ LBD from an *in vitro* mixture.** *Panel A*, western blot for ACBP of an immunoprecipitate obtained with anti-ACBP (lane 1) or anti-HNF-4 $\alpha$ LBD (lane 2). *Panel B*, western blot for HNF-4 $\alpha$  of the immunoprecipitate obtained with anti-ACBP (lane 1) or anti-HNF-4 $\alpha$ -LBD (lane 2).

followed by treatment with Texas-Red- goat anti-rabbit (to detect HNF-4 $\alpha$ ) and FITC-goat anti-rat (to detect ACBP) IgG secondary antibodies, as described in Methods. HNF4 $\alpha$  was distributed strongly throughout rat hepatoma nuclei with more intense staining near the nuclear envelope (Fig. 4.3A). HNF-4 $\alpha$  was only weakly detected diffusely outside nuclei (Fig. 4.3A). In contrast, although ACBP was stained most intensely in the perinuclear region and throughout the cytoplasm (Fig. 4.3B). However, smaller amounts of ACBP were also detected as more diffuse punctate regions within the nucleus (Fig. 4.3B). Superposition of simultaneously acquired red and green fluorescence images indicated the regions where the two labels were most colocalized, yellow pixels (Figure 4.3C). The yellow pixels with the highest degree of colocalization (i.e. the pixels with high fluorescence intensity of both red and green fluorophores) were also shown as a separate panel (Fig. 4.3D). This indicated that both ACBP and HNF-4 $\alpha$  were strongly colocalized in the perinuclear region and as punctate structures within the nuclei of rat hepatoma cells (Fig. 4.3D).

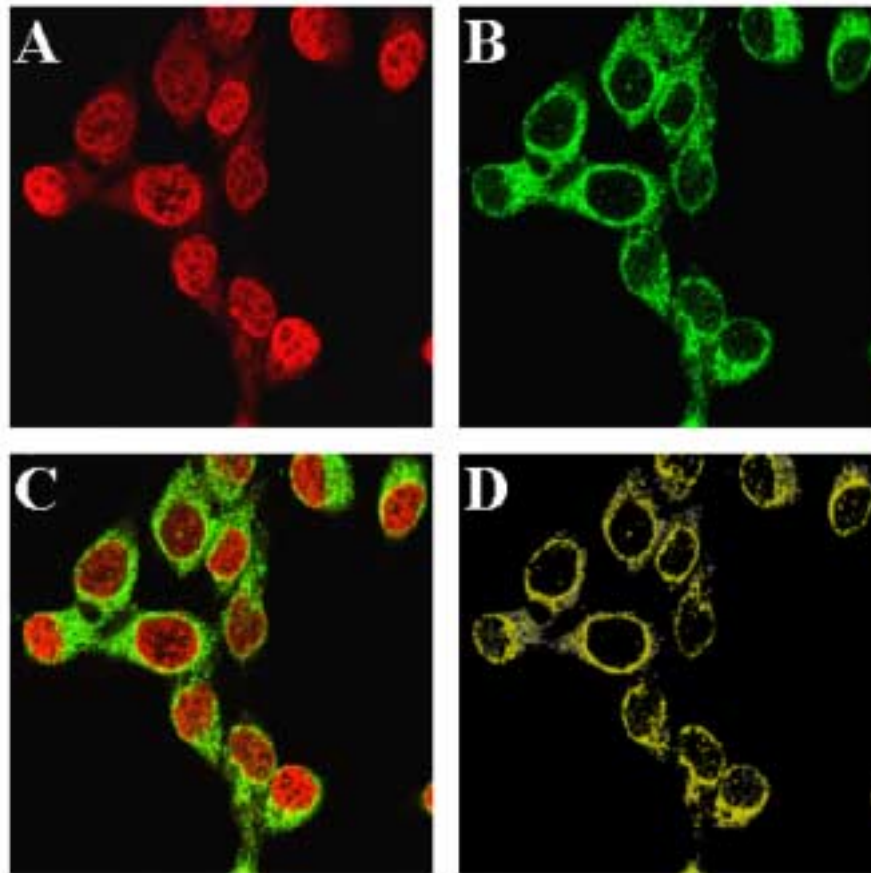
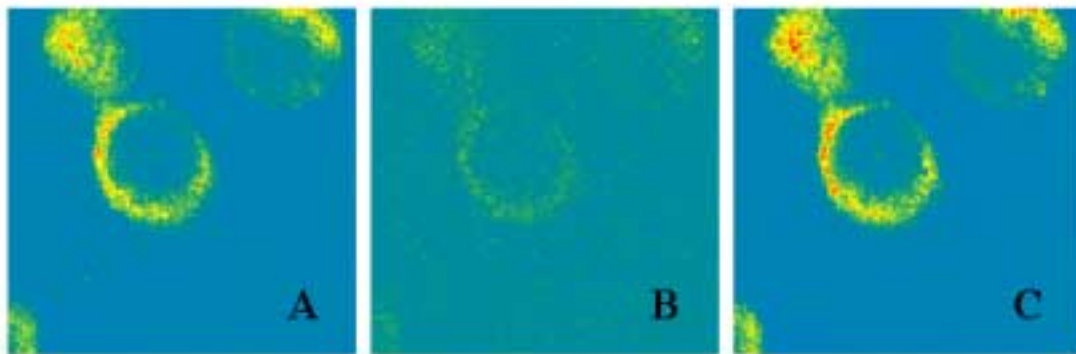


FIG. 4.3. **LSCM colocalization of ACBP and HNF-4 $\alpha$  in fixed hepatoma cells.** *A*, fluorescence image of HNF-4 $\alpha$  labeled indirectly with Texas Red; *B*, green fluorescence image of ACBP labeled indirectly with FITC; *C*, the overlay of HNF-4 $\alpha$  and ACBP fluorescence images in *A* and *B*; the arrows indicate regions where overlapped red and green pixels appear yellow; *D*, selected pixels with high fluorescence intensity for both red and green labels are shown in yellow.

Although the limit of resolution of LSCM is about 2 microns, the significant colocalization of the two proteins is consistent with the possibility that ACBP and HNF-4 $\alpha$  are distributed to potentially interact physically in intact cells.

#### 4.3.4 ACBP/HNF-4 $\alpha$ Intermolecular Distance in Fixed Cells: Fluorescence Resonance Energy Transfer (FRET) Microscopy

To increase the resolution of LSCM, the intermolecular distance between ACBP and HNF-4 $\alpha$  within hepatoma cell nuclei was determined by fluorescence resonance energy transfer (FRET).



**FIG. 4.4. ACBP/HNF-4 $\alpha$  association in nuclei of fixed cells: FRET microscopy.** Rat hepatoma cells were labeled with Cy3-anti-HNF-4 $\alpha$  and Cy5-anti-ACBP as described in “Experimental Procedures”. *A*, Cy3 (FRET donor) was excited at 568 nm and its emission detected through a HQ598/40 bandpass filter; *B*, Cy3 (FRET donor) was excited at 568 nm and the sensitized emission of Cy5 (FRET acceptor) was measured through a 680/30 bandpass filter; *C*, same as in *A*, but after photobleaching of Cy5 (FRET acceptor) at 647 nm. The increase in donor fluorescence intensity (*C*, red pixels) after acceptor photobleaching allowed calculation of FRET efficiency and determination of the ACBP and HNF-4 $\alpha$  intermolecular distance (53 A).

FRET efficiency between Cy3-labeled anti-HNF-4 $\alpha$  and Cy5-labeled anti-ACBP was measured as described in Methods. Detection of Cy5 (FRET acceptor) sensitized emission through a 680/32 bandpass filter upon excitation of Cy3 (FRET donor) at 568 nm was the first indication of FRET transfer (Fig. 4.4B). To determine the energy transfer efficiency, the Cy5 (FRET Cy3 (FRET donor) fluorescence emission was then detected through a HQ598/40 bandpass filter with excitation at 568 nm) (Fig. 4.4C). As indicated by the larger amount of red/yellow pixels, Cy3 (FRET donor)

fluorescence emission at 568 nm after photobleaching at 647 nm (Fig. 4.4C) was significantly greater than fluorescence emission of Cy3 (FRET donor) at 568 nm before photobleaching (Fig. 4.4A). Quantitative analyses of these intensities as described in Methods, allowed calculation of an intermolecular distance of 53 Å between ACBP and HNF4 $\alpha$ . This indicated a close molecular association of ACBP and HNF-4 $\alpha$  within the peripheral region of hepatoma cell nuclei.

#### 4.3.5 *ACBP/HNF-4 $\alpha$ Structural Interaction in Living Cells: Mammalian Two-Hybrid Assay*

To examine whether ACBP structurally interacted with HNF-4 $\alpha$  in living cells, a mammalian two-hybrid assay was performed. ACBP and HNF-4 $\alpha$  cDNAs were ligated to pACT (DNA binding component) and pBIND (transcription complex component) and assayed for transactivation as described in Methods. In both combination sets, i.e. when either ACBP was on the DNA binding component and HNF-4 $\alpha$  on the transcription side (experiment A) or vice-versa (experiment B) the transactivation was higher than negative controls (Fig. 4.5, groups 2 and 3) and not as great as the positive control (Fig. 4.4, group 4). These data demonstrated ACBP interacted directly with HNF-4 $\alpha$  in the nucleus of living cells.

#### 4.3.6 *Expression of ACBP and HNF-4 $\alpha$ in COS-7 and Hepatoma Cells*

To begin to establish the functional significance of ACBP interaction with HNF-4 $\alpha$ , it was necessary to utilize transfected cells to vary the content of ACBP and HNF4 $\alpha$ . Two types of cells (COS-7 and rat hepatoma) were used. COS-7 cells do not express a detectable amount of HNF4 $\alpha$  as indicated by the absence of a HNF-4 $\alpha$  band at 55000 Da in western blots (Fig. 4.6A, lane 1). COS-7 have only low levels of ACBP as detected by a band at 10000 Da in western blots of COS-7 cell homogenate (Fig. 4.6A, lane 1) and by indirect immunofluorescence microscopy (Fig. 4.7). Comparison with standards revealed that 0.08 % of protein in COS7 cells was ACBP. The expression level of ACBP was increased 6-fold in COS-7 cells transfected with sense ACBP

expression vector, pCI-sACBP (Fig. 4.6A, lane 2). Conversely, ACBP expression level was decreased up to 90% by transfection of COS-7 cells with antisense ACBP vector,

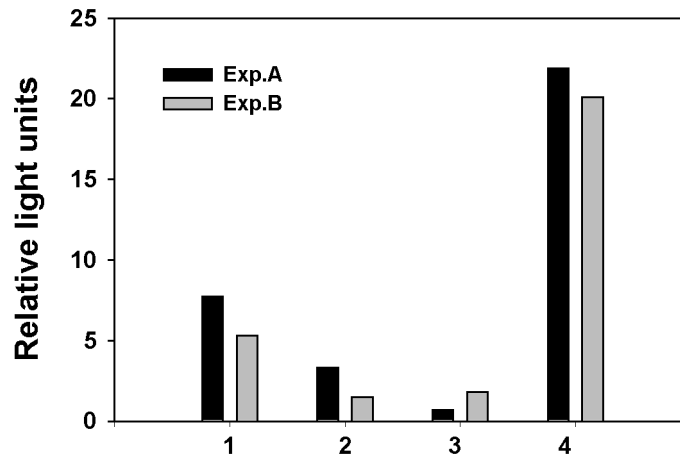


**FIG. 4.5. Mammalian two-hybrid assay of ACBP/HNF-4 $\alpha$  interaction.** In this assay the level of firefly luciferase expression is directly proportional with the affinity between ACBP and HNF-4 $\alpha$ . Firefly luciferase activity has been normalized to Renilla luciferase activity and expressed in relative light units. 1, COS-7 cells were transfected with pACT/ACBP and pBIND/HNF-4 $\alpha$  (experiment A) or with pACT/HNF-4 $\alpha$  and pBIND/ACBP (experiment B); 2, negative control, COS-7 cells were transfected with pACT and pBIND/HNF-4 $\alpha$  (experiment A) or pBIND/ACBP (experiment B); 3, negative control, COS-7 cells were transfected with pBIND and pACT/ACBP (experiment A) or pACT/HNF-4 $\alpha$  (experiment B); 4, positive control, COS-7 cells were transfected with pACT/myoD and pBIND/ID (experiments A,B).

pgk-aACBP (Fig. 4.6A, lane 5). Both ACBP overexpression and antisense-induced underexpression were maintained in COS-7 cells cotransfected with HNF4 $\alpha$  expression vector, pLEN4s (Fig. 4.6A, lanes 3-5). Comparison of ACBP levels in cells cotransfected with HNF4 $\alpha$  expression vector (pLEN4s) revealed that HNF-4 $\alpha$  was highly expressed in cells cotransfected with the antisense ACBP vector (Fig. 4.6A, lane 5), but only at a lower level in cells cotransfected with sense ACBP expression vector (Fig. 4.6A, lane 4). This may indicate that the expression of ACBP in COS-7 cells has a negative effect on HNF-4 $\alpha$  expression level.

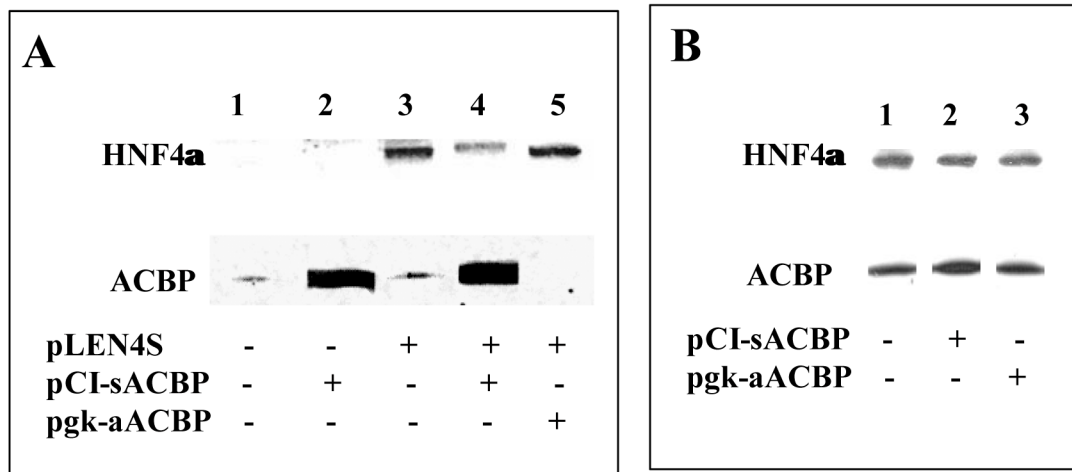


**FIG. 4.6. ACBP and HNF-4 $\alpha$  expression in transfected cells: western blotting.** *Panel A*, ACBP and HNF-4 $\alpha$  bands detected in COS-7 cells, nontransfected (lane 1) or transfected with pLEN4S (HNF-4 $\alpha$  expression vector), pCI-sACBP (ACBP expression vector) and pgk-aACBP (ACBP antisense RNA expression plasmid) (lanes 2-5). *Panel B*, ACBP and HNF-4 $\alpha$  bands detected in rat hepatoma cells nontransfected (lane 1) or transfected with pCI-sACBP, pgk-aACBP (lanes 2-3).

These western blotting data were confirmed by indirect immunofluorescence microscopy. COS-7 cells either nontransfected (Fig. 4.7A) or transfected with HNF-4 $\alpha$  expression vector, pLEN4s (Fig. 4.7B), sense ACBP expression vector, pCI-sACBP (Figs. 4.7D-F) and antisense ACBP vector, pgk-aACBP (Fig. 4.7C) were fixed and labeled with Texas Red (red fluorescence) for HNF-4 $\alpha$  and with FITC (green fluorescence) for ACBP. The ACBP level is detectable in nontransfected COS-7 cells, increased in numerous cells upon transfection with pCI-sACBP alone or together with HNF-4 $\alpha$  expression vector and decreased in cells cotransfected with antisense ACBP vector, pgk-aACBP. Interestingly, by confocal microscopy it was observed that in these transient transfections only up to 20% of the cells actually express the transfected proteins; in cells cotransfected with HNF4 $\alpha$  and sense ACBP expression vectors, only few cells expressed both proteins, many of them expressing only one of them (Figs.

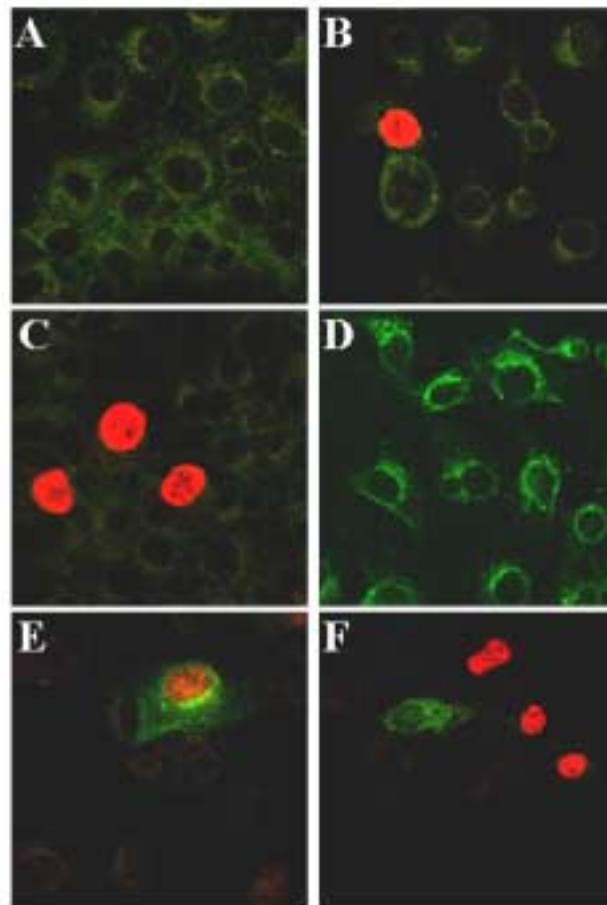


**FIG. 4.7. ACBP and HNF-4 $\alpha$  expression in transfected cells: LSCM imaging.** Nontransfected (control) and transfected COS-7 cells were labeled with Texas red and FITC so that ACBP was detected as green fluorescence and HNF-4 $\alpha$  as red fluorescence. A, nontransfected (control) COS-7 cells; B, COS-7 cells transfected with pLEN4S (HNF-4 $\alpha$  expression plasmid); C, COS-7 cells co-transfected with pLEN4S (HNF4 $\alpha$  expression vector) and pgk-aACBP (ACBP antisense RNA expression vector); D, COS-7 cells transfected with pCI-sACBP (ACBP expression vector); E, COS-7 cells co-transfected with pLEN4S and pCI-sACBP, and the two proteins were expressed in same cell; F, COS-7 cells co-transfected with pLEN4S and pCI-sACBP and the two proteins were expressed separately.

4.7E-F). Thus, the overexpression of ACBP in COS-7 as determined by western blotting represents the total amount of ACBP expressed in transfected cells, but not necessarily



ACBP simultaneously overexpressed with HNF-4 $\alpha$  in same cells. Only about 4% of transfected cells coexpressed both HNF4- $\alpha$  and ACBP.

Western blots of ACBP and HNF-4 $\alpha$  in rat hepatoma cells showed a high level of these proteins in nontransfected cells (0.6 % ACBP, 0.5% HNF-4 $\alpha$ ; Fig. 4.6B, lane 1). Transfection of rat hepatoma cells with the sense ACBP expression vector increased the ACBP protein expression by 2 fold, while the transfection of antisense ACBP vector, pgk-aACBP did not significantly decrease of ACBP expression (Fig. 4.6B, lanes 4,2,3). Confocal microscopy images confirmed these findings (data not shown).

#### *4.3.7 Intracellular Distribution of ACBP and HNF-4 $\alpha$ in Transfected COS-7 and Rat Hepatoma Cells Overexpressing ACBP and HNF-4 $\alpha$*

In order to determine the intracellular localization of the two proteins (ACBP, HNF-4 $\alpha$ ) ectopically expressed, COS-7 cells cotransfected with HNF-4 $\alpha$  and ACBP expression vectors were processed for laser scanning confocal microscopy (LSCM) as described in Methods. Triple fluorescent labeling was performed by the use of Texas-Red (for HNF-4 $\alpha$ ), FITC (for ACBP) and TOTO-3 (DNA stain). Three fluorescence images (each dye through a separate photomultiplier) were simultaneously acquired and analyzed for colocalization. In COS-7 cells expressing high levels of both ACBP and HNF-4 $\alpha$ , ACBP was spread throughout the cell while HNF4- $\alpha$  was localized mostly within the nucleus, (Figs. 4.8A-C). Quantitative analysis of colocalization analysis showed 61% of ACBP inside the nucleus (overlapping with the DNA stain TOTO-3), and 96% of HNF-4 $\alpha$  within the nucleus (Figs. 4.8D-E). ACBP and HNF-4 $\alpha$  were significantly codistributed since 57% of ACBP and 60% of HNF4- $\alpha$  within a single cell colocalized (Fig. 4.8F). When the pixels with highest green and red fluorescence intensities were selected, the region where ACBP and HNF-4 $\alpha$  colocalized the most was observed (Fig. 4.8I). This region was located inside the nucleus, at the peripheral zone of the nucleus.

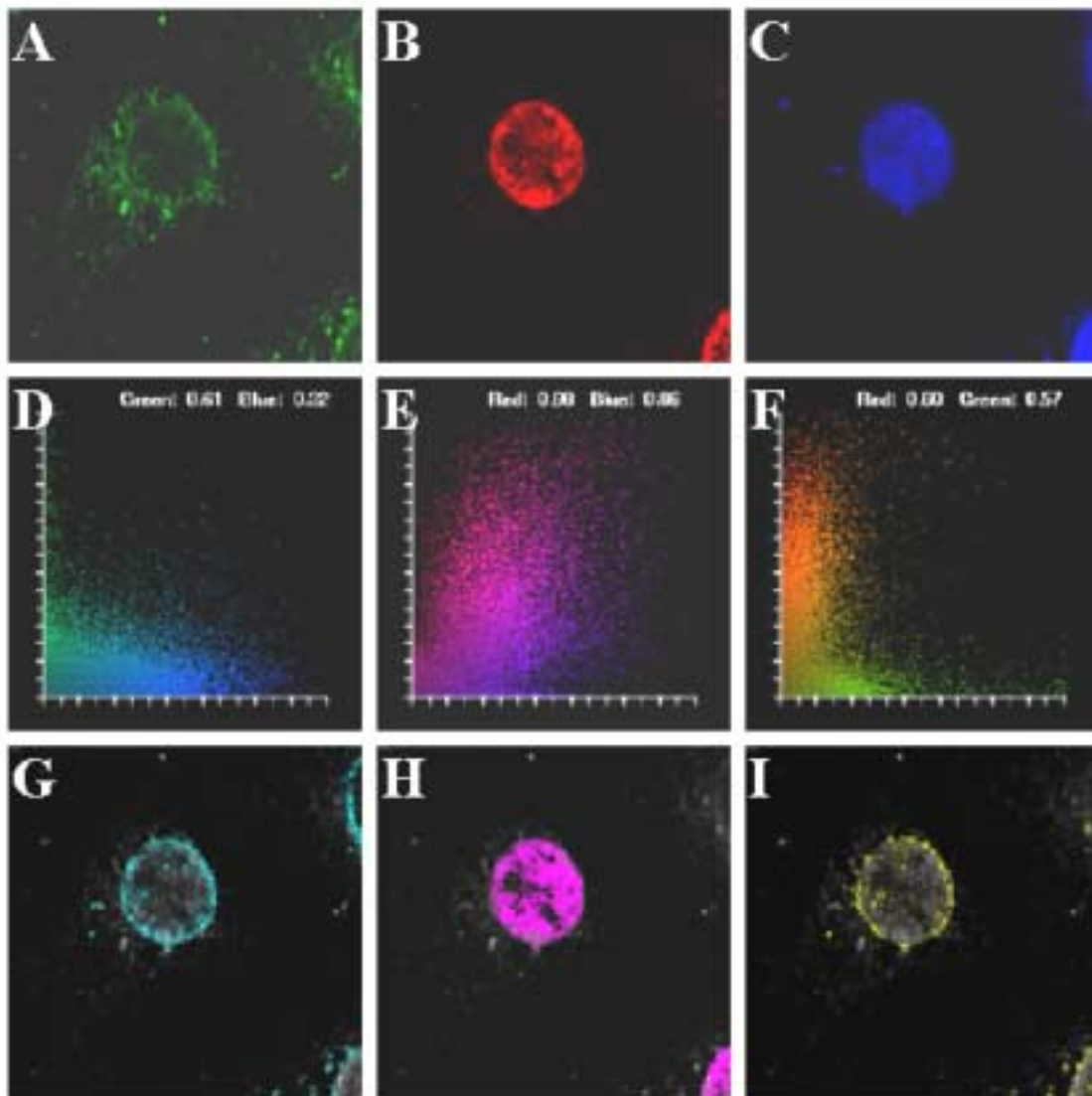


FIG. 4.8. **Intracellular distribution of ACBP and HNF-4 $\alpha$  in transfected COS-7 cells: LSCM colocalizations.** COS-7 cells transfected with expression plasmids for ACBP and HNF-4a were labeled with three different fluorophors and processed for LSCM as described in Experimental Procedures. *A*, ACBP (green fluorescence); *B*, HNF-4 $\alpha$  (red fluorescence); *C*, DNA (conventionally blue fluorescence); *D*, *E*, *F*, green/blue (ACBP/DNA), red/blue (HNF4 $\alpha$ /DNA) and green/red (ACBP/HNF-4 $\alpha$ ) colocalization fluorographs, respectively; *G*, *H*, *I*, selected pixels with highest colocalization of green/blue (ACBP/DNA), red/blue (HNF-4 $\alpha$ /DNA) and green/red (ACBP/HNF-4 $\alpha$ ) fluorescence intensities, respectively.

The ACBP pixels that colocalized the most with DNA (i.e. TOTO-3) pixels was also located at the periphery within the nucleus (Fig. 4.8G).

Hepatoma cells transfected with ACBP expression vector were also analyzed for colocalization of three labels (conventional fluorescent colors: red for HNF-4 $\alpha$ , green for ACBP, and blue for DNA) ( Figs. 4.9A-C). Interestingly, a higher overlapping of ACBP (80%) and DNA (67%) was determined (Fig. 4.9D, 4.9G) than in COS-7 cells. In rat hepatoma cells, most of the HNF-4 $\alpha$  (94%) was colocalized with the DNA stain TOTO-3 (93%), as expected (Figs. 4.9E, 4.9H). A higher colocalization was also found for ACBP (93%) and HNF-4 $\alpha$  (83%) in rat hepatoma cells than in COS-7 cells (Figs. 4.9F, 4.9I). The most colocalized pixels were located within the nucleus, at the peripheral zone of the nuclei. A few distinct colocalized ACBP and HNF-4 $\alpha$  pixels were also found within the central zone of the nucleus as well as outside nuclei, within the cytoplasm.

#### 4.3.8 *Functional Significance of ACBP Expression on HNF-4 $\alpha$ Transcriptional Activity: Transactivation Assays*

From molecular studies *in vitro*, in fixed cells, and in intact cells, it was evident that ACBP and HNF-4 $\alpha$  can form a complex by physical association. In cultured cells frequent ACBP/ HNF-4 $\alpha$  complexes were detected inside the nuclei, at the peripheral zone, close to the nuclear membrane. These findings led to the question whether this association between ACBP and HNF-4 $\alpha$  was functionally significant. Therefore, the influence of ACBP over- and underexpression upon HNF-4 $\alpha$ -mediated transactivation of a reporter vector, consisting of firefly luciferase gene under HNF-4 $\alpha$  response elements from ApoB gene promoter, was studied. Since COS-7 express no HNF-4 $\alpha$ , they were cotransfected with pLEN4S (HNF-4 $\alpha$  expression vector), pCI-sACBP (ACBP expression vector) and ApoBLuc (reporter plasmid) as described in Experimental Procedures. COS-7 cells overexpressing ACBP exhibited a 3.5-fold increase in transcription of luciferase under HNF-4 $\alpha$ -response element ApoB promoter (Fig. 4.10A).

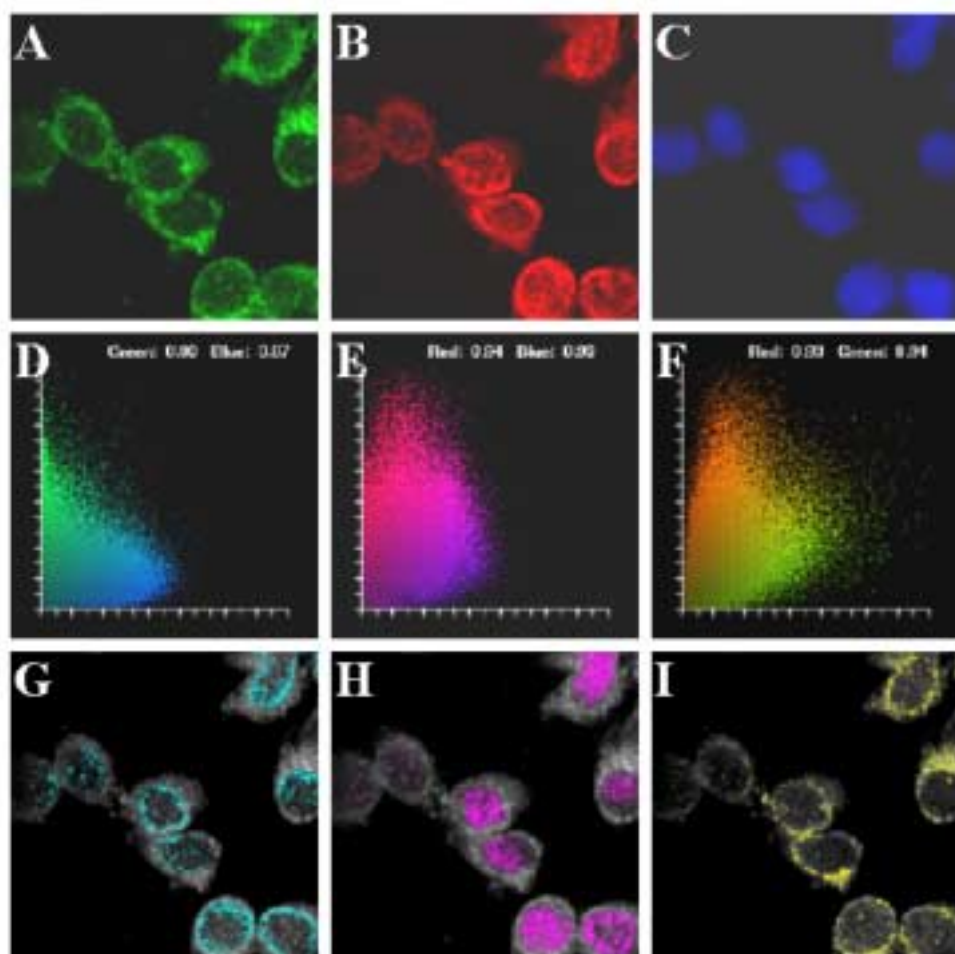


FIG. 4.9. **Intracellular distribution of ACBP and HNF4 $\alpha$  in hepatoma cells: LSCM colocalizations.** Rat hepatoma cells were labeled with three different fluorophors for ACBP, HNF-4 $\alpha$  and DNA and colocalization studies were carried out as described in Experimental Procedures. *A*, ACBP (green fluorescence); *B*, HNF-4 $\alpha$  (red fluorescence); *C*, DNA (conventionally blue fluorescence); *D*, *E*, *F*, green/blue (ACBP/DNA), red/blue (HNF4 $\alpha$ /DNA) and green/red (ACBP/HNF-4 $\alpha$ ) colocalization fluorographs, respectively; *G*, *H*, *I*, selected pixels with highest colocalization of green/blue (ACBP/DNA), red/blue (HNF-4 $\alpha$ /DNA) and green/red (ACBP/HNF-4 $\alpha$ ) fluorescence intensities, respectively.

To determine the effect of ACBP overexpression in a cell line that normally expressed significant amounts of HNF-4 $\alpha$ , rat hepatoma cells were cotransfected only with pCI-sACBP (ACBP expression vector) and ApoBLuc (reporter plasmid) as described in Methods. Due to the presence of high level of ACBP in non-transfected and mock transfected rat hepatoma cells (see above), the level of luciferase transactivation under HNF-4 $\alpha$  control was 10 fold higher in hepatoma cells that had not been transfected with the ACBP overexpression vector as compared to that in COS-7 cells transfected with HNF4 $\alpha$  and ACBP vectors (Fig. 4.10A). Thus, the endogenous level of ACBP in rat hepatoma cells was very effective in enhancing luciferase transcription (Fig.4.10A). Transfection of rat hepatoma cells to overexpress ACBP about 2-fold, resulted in a 1.8-fold increase in luciferase transcription (Fig. 4.10A). A dose response of the ACBP expression versus luciferase activity was determined in COS-7 cells (Fig. 4.10B). Luciferase transactivation in COS-7 cells was directly proportional to transfection with increasing amounts of pCI-sACBP, the overexpression vector for ACBP (Fig. 4.10B, sense ACBP). Conversely, luciferase transactivation in COS-7 cells was inversely proportional to transfection with increasing amounts of antisense ACBP vector, pgk-aACBP (Fig.4.10B, antisense-ACBP). Thus, ACBP stimulated HNF-4 $\alpha$ -mediated transactivation proportional to the level of ACBP expression in the COS-7 and rat hepatoma cells.

#### *4.3.9 Functional Significance of ACBP Expression on HNF-4 $\alpha$ Transcriptional Activity: LSCM Imaging of Luciferase Transactivation in Individual Cells*

As indicated in the preceding sections, transient cotransfection of cells with multiple vectors allowed for only qualitative comparison of transactivation with ACBP expression level. To more accurately assess transactivation, a new technical approach used to estimate the influence of ACBP on HNF-4 $\alpha$ -regulated transactivation. Transfected rat hepatoma cells were fixed and triple fluorescent labeled to simultaneously detect HNF4 $\alpha$ , ACBP and luciferases. Thus, cells transfected with pCI-sACBP (ACBP overexpression vector) and ApoBLuc (luciferase reporter vector) were

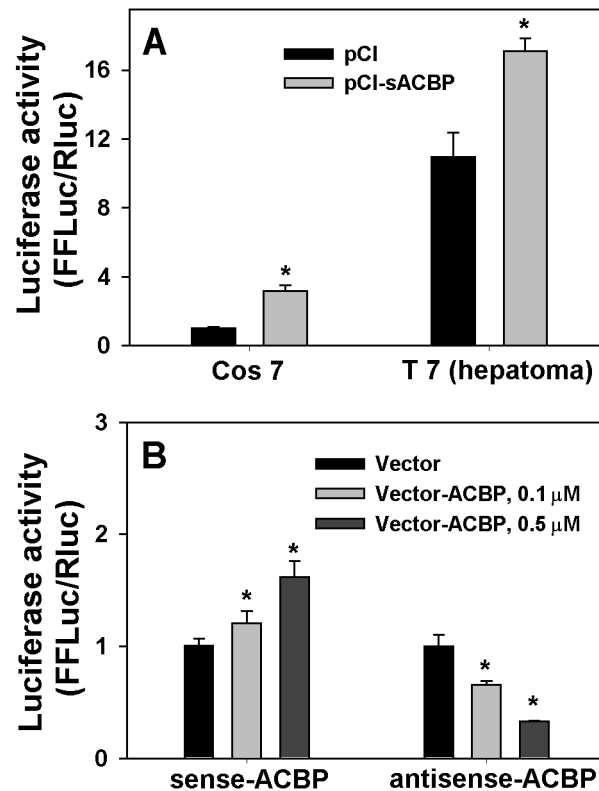


FIG. 4.10. **ACBP stimulates HNF-4 $\alpha$ -mediated transactivation.** *Panel A:* COS-7 and rat hepatoma cells were co-transfected with expression vectors and luciferase reporter plasmid as described in Experimental Procedures. The transcription activity (relative light units) in cells over-expressing ACBP (pCI-sACBP) was significantly higher than in cells transfected with empty vector (pCI). *Panel B,* COS-7 cells transfected with increasing amounts of sense ACBP expression vector (pCI-sACBP) or anti-sense ACBP plasmid (pgk-aACBP) indicated decrease in HNF-4 $\alpha$ -mediated transactivation in a dose response manner.

labeled with Texas-Red for HNF-4 $\alpha$ , FITC for ACBP and Cy5 for luciferase (Fig. 4.11A-C). By image analysis, many individual cells were assayed for their content in HNF4 $\alpha$ , ACBP and luciferase and then the correlation curves for the three protein expression levels were studied (Fig. 4.11D-E). A plot of ACBP versus luciferase expression (Fig. 4.11D) revealed a very high correlation coefficient ( $r^2$ , 0.936)

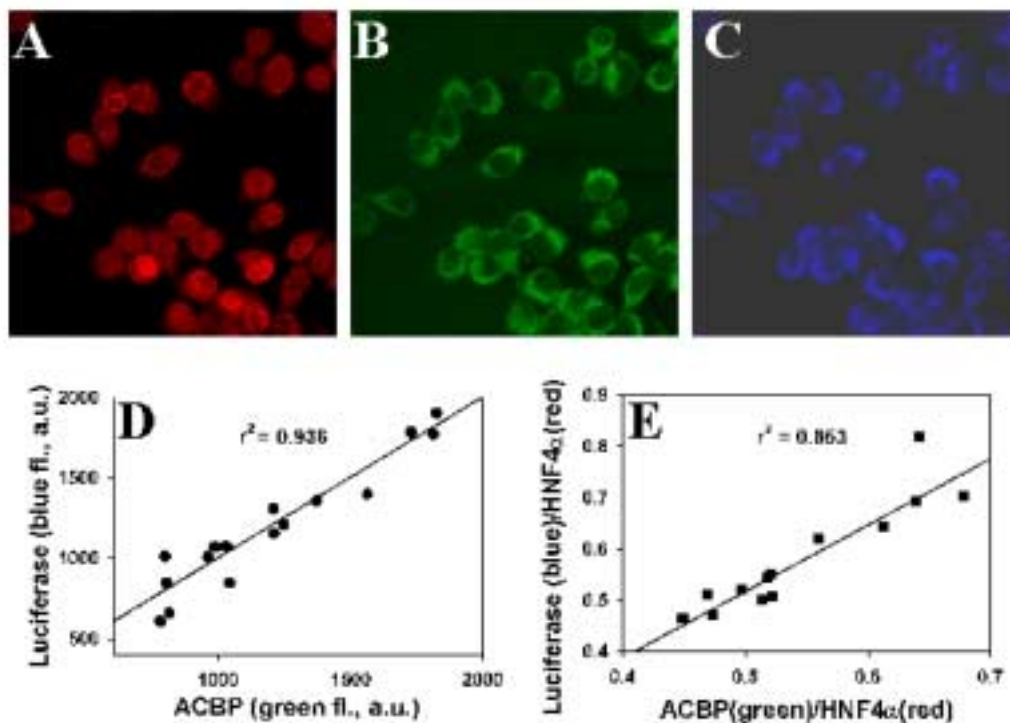


FIG. 4.11. **LSCM imaging of HNF-4 $\alpha$ -mediated luciferase transactivation in individual hepatoma cells.** Rat hepatoma cells transfected with ApoBLuc reporter plasmid and pCI-sACBP (ACBP expression vector) were labeled with Texas Red (red fluorescence, *A*) for HNF-4 $\alpha$ , FITC (green fluorescence, *B*) for ACBP and Cy5 (conventionally blue fluorescence, *C*) for luciferase, as described in Experimental Procedures. *D*, Correlation plot for luciferase (blue fluorescence intensity) and ACBP (green fluorescence intensity) expression. *E*, Correlation plot of HNF-4 $\alpha$ -normalized ACBP fluorescence intensities versus HNF-4 $\alpha$ -normalized luciferase fluorescence intensities. The plots allowed calculation of correlation coefficients of 0.936 and 0.853, indicating that ACBP stimulates HNF-4 $\alpha$ -mediated luciferase transactivation.

suggesting that cells with higher amounts of ACBP exhibited higher level of luciferase (and implicitly had a higher HNF-4 $\alpha$ -mediated transactivation). As both luciferase versus HNF-4 $\alpha$  and ACBP versus HNF-4 $\alpha$  showed very good correlation ( $r^2$ , 0.899 and 0.856, respectively), we normalized luciferase and ACBP to HNF-4 $\alpha$  and then assayed the degree of correlation again. Interestingly, for ratios of ACBP/HNF-4 $\alpha$  lower than 0.7, a good correlation coefficient has been found, i.e.  $r^2$  of 0.856 (Fig. 4.11E). For ratios

of ACBP/HNF-4 $\alpha$  higher than 0.7, the correlation did not hold. As both ACBP and HNF-4 $\alpha$  had been reported to bind fatty acyl-CoAs with very high affinities (in the low nanomolar range), the ratio between the two proteins may be a very important factor in the way ACBP influences HNF-4 $\alpha$  activity.

#### 4.4 DISCUSSION

Long-chain fatty acid-CoA thioesters (LCFA-CoAs) are known as the activated form of fatty acids, ready to enter metabolic pathways such as  $\beta$ -oxidation in mitochondria and peroxisomes, esterification with formation of triglycerides and phospholipids in microsomes. Beside their role in metabolism, LCFA-CoAs were found to act as signalling molecules mediating transcriptional regulation of genes involved in lipid metabolism and transport and related to metabolic disorders like obesity and diabetes (91) (185) (219)(220).

Two proteins that bind LCFA-CoAs with high affinity and specificity, and have been shown to influence genes with role in lipid and glucose metabolism are ACBP and HNF-4 $\alpha$ . ACBP was reported to be localized not only in cytosol but also in the nuclei of CV-1 and 3T3-L1 cells and to induce a significant decrease in PPAR- $\gamma$ -mediated transactivation (123). However, acyl-CoAs were shown to antagonize the effects of peroxisome proliferators on PPAR- $\alpha$  but not  $\gamma$  or  $\delta$  (47). LCFA-CoAs were detected in nuclei of rat liver cells (186) and proved to be specific ligands for nuclear proteins like HNF-4 $\alpha$  and TR (45) (56) (209).

HNF-4 $\alpha$  had been known as an orphan receptor until 1998 when Hertz *et al.* (45) demonstrated that LCFA-CoAs bound to HNF-4 $\alpha$  and influenced HNF-4 $\alpha$ -mediated transactivation inducing stimulation or inhibition depending on the LCFA-CoA chain length and saturation (45). Using a radiolabeled binding assay, Hertz *et al.* reported low affinity ( $\mu$ M range) of HNF-4 $\alpha$  for acyl-CoA ligands, which questioned the physiological significance of this binding, as the acyl-CoAs were reported in cell nuclei in nanomolar concentrations (20) . By the use of more sensitive fluorescence binding



assays and FRET spectroscopy methods we demonstrated that HNF-4 $\alpha$ -ligand binding domain (HNF-4 $\alpha$ -LBD) binds long chain fatty acid-CoAs (LCFA-CoAs) with nanomolar affinities (209). A strong debate on the matter of LCFA-CoAs being endogenous ligands of HNF-4 $\alpha$  is still in place as there are reports on the HNF-4 $\alpha$ -binding site volume being smaller than LCFA-CoAs volume, from structural modelling data (187). However, two very recent reports on the HNF-4 $\alpha$  x-ray crystal structure demonstrate that two conformations of the HNF-4 $\alpha$  monomers are possible, a closed and an open one, and each one can accommodate the long hydrophobic chains of a fatty acid molecules (221)(222). Chemical analysis of HNF-4 $\alpha$  preps by gas chromatography detected fatty acids associated with the protein, especially C16:0, C14:0, C16:1 and numerous fatty acids specific for bacteria in which the recombinant HNF-4 $\alpha$  was prepared (221). No search for the CoA-derivatives of these fatty acids has been carried out. The drastic methods by which the HNF-4 $\alpha$  crystals were obtained (long times of incubations in the presence of DTT) and processed for chemical analysis, rendered the detection of HNF-4 $\alpha$ -associated LCFA-CoA thioesters impossible. In our view, the large amounts of bacterial fatty acids (e.g., C17:0cyclo, C18:1 $\omega$ 7c) associated with recombinant HNF-4 $\alpha$  prepared by Dhe-Paganon's group suggest that fatty acids (remnants of their CoA thioesters) were bound as ligands and not cofactors. A very strict specificity of proteins for their cofactors is known for any other alloprotein, while a certain variety of ligands within a specific group is often seen at lipid binding proteins. Both x-ray crystallography groups interpreted their data in the sense that the free fatty acids are constitutive, structural cofactors but not ligands to HNF-4 $\alpha$  protein. However, the detection of a LCFA in the HNF-4 $\alpha$  monomer binding site by x-ray crystal structure analysis may be a step forward to prove by other methods than our fluorescence binding assays that fatty acyl-CoAs are specific ligands of HNF-4 $\alpha$ .

In the present work we demonstrate that there is a direct, physical interaction between ACBP and HNF-4 $\alpha$ . First, *in vitro* studies by circular dichroism and co-immunoprecipitation demonstrated that recombinant mouse ACBP and rat HNF-4 $\alpha$ -

ligand binding domain when mixed together, interact and form a complex with altered conformation (Fig. 4.1, 4.2). Furthermore, at cellular level, indirect immunofluorescence microscopy showed that ACBP and HNF-4 $\alpha$  colocalized in rat hepatoma and COS-7 cells transfected with expression vectors for ACBP and HNF-4 $\alpha$ , mostly at the peripheral region of nuclei (Fig. 3, 8 and 9). An ACBP/HNF-4 $\alpha$  intermolecular distance of 53 Å was calculated from FRET microscopy data in rat hepatoma cells in which ACBP and HNF-4 $\alpha$  were labeled with Cy3- anti-ACBP and Cy5-anti-HNF-4 $\alpha$  IgGs (Fig. 4.4). A mammalian two-hybrid assay with ACBP and HNF-4 $\alpha$  cDNAs ligated to pACT and pBIND, also demonstrated a moderate binding of the two proteins (Fig. 4.5).

A quantitative estimation of ACBP located inside the nuclei of COS-7 cells transfected with ACBP and HNF-4 $\alpha$  expression vectors, and in rat hepatoma cells, was performed for the first time by triple fluorescent labeling and LSCM (confocal microscopy; Fig. 4.8 and 4.9). The highest level of ACBP/HNF-4 $\alpha$  colocalization was detected at the peripheral zone of nuclei, proximal to the nuclear membrane. It is not known how LCFA-CoAs are carried from cytosol into nuclei. A possible explanation is that LCFA-CoA/ACBP complexes pass through the nuclear membrane pores. For mitochondria and peroxisomes, it has been demonstrated that cytosolic LCFA-CoAs have to be hydrolyzed to free LCFAs, which are then passed through the membrane and re-esterified to CoA-derivatives by intra-mitochondrial and peroxisomal LCFA-CoA synthases. A similar transfer mechanism can be presumed for nuclei, but no nuclear LCFA-CoA synthases were identified so far (223). At least 5 different LCFA-CoA synthases have been characterized in liver, bound to mitochondrial-associated membranes, peroxisomes or microsomes (223). Free LCFA-CoAs are very unstable, being quickly hydrolyzed and it is the role of ACBP to bind LCFA-CoAs and form LCFA-CoA pools within different compartments of the cells. Thus, in either of the two possible mechanisms, ACBP is needed in the nucleus to maintain a certain pool of LCFA-CoAs.

Functional studies in COS-7 cells co-transfected with HNF-4 $\alpha$ , ACBP expression vectors and ApoBLuc reporter plasmid indicated that ACBP had a stimulatory effect on

HNF-4 $\alpha$ -mediated transactivation (Fig. 4.10A). Rat hepatoma cells, transfected only with reporter plasmid had a 10 fold higher transactivation activity compared with HNF-4 $\alpha$  and ACBP- expressing COS-7 cells, suggesting that the presence of both HNF-4 $\alpha$  and ACBP in all cells (compared to 4% COS-7 transfected cells) contributed to a stronger rate of luciferase transcription. An over-expression of ACBP in rat hepatoma cells resulted in a significant increase in HNF-4 $\alpha$ -mediated transactivation (Fig. 4.10A). In COS-7 cells, a dose response in HNF-4 $\alpha$  mediated transactivation over a range of ACBP sense and anti- sense expression vectors was obtained, demonstrating that the more ACBP was in the cells the higher the HNF-4 $\alpha$ -mediated transactivation was found (Fig. 4.10B).

A different approach was carried out in order to test the effect of ACBP on HNF-4 $\alpha$ -mediated transactivation: COS-7 cells transfected with the ACBP, HNF-4 $\alpha$  and ApoBLuc plasmids were assayed for the level of expression of all three proteins, *i.e.* ACBP, HNF-4 $\alpha$  and luciferase by using triple fluorescent labeling. Individual cells were analyzed for the expression of the three proteins and then correlation curves have been plotted, demonstrating that cells with higher amounts of ACBP expressed more luciferase (Fig. 4.11).

This stimulatory effect of ACBP on HNF-4 $\alpha$ -mediated transactivation could be explained by the ability of ACBP to concentrate and form a nuclear pool of LCFA-CoAs in close proximity of HNF-4 $\alpha$ . Even though both proteins display very high affinities for LCFA-CoAs *in vitro* and might be competing for a common ligand, it is known that in other cases (e.g. carnityl-palmitoyl-transferase) ACBP-bound LCFA-CoAs rather than free LCFA-CoAs are preferentially taken further into a transport or metabolic pathways (34).

Interestingly, the stimulatory effect of ACBP on HNF-4 $\alpha$  transactivation function is in agreement with acyl-CoA and ACBP inhibitory effects on PPAR $\alpha$  (previously reported in (47)(123) as a cross-talk of HNF-4 $\alpha$ /PPAR $\alpha$  has been demonstrated (114) to regulate apoC-III gene through common DR-1 consensus elements in its promoter. Thus, the overall process includes apoC-III transcription stimulation when preponderant fatty

acyl-CoA/ACBP activate HNF-4 $\alpha$  to bind to DR-1 response elements, in balance with the opposite effect, i.e. apoC-III transcription down-regulation when free fatty acid/FABP stimulate PPAR $\alpha$ /RXR heterodimers to displace HNF4 $\alpha$  homodimers from DR-1 cis-elements.

In conclusion, this study demonstrates a physical and functional interaction of ACBP with HNF-4 $\alpha$ , suggesting that ACBP is a coregulator of genes targeted by HNF-4 $\alpha$ .

## V SUMMARY AND CONCLUSIONS

Studies on ligand binding properties and cellular functions of three different proteins, steroidogenic acute regulatory protein (StAR), hepatocyte nuclear factor-4 $\alpha$  (HNF-4 $\alpha$ ) and acyl-CoA binding protein (ACBP) were carried out leading to several significant conclusions.

### *5.1 Steroidogenic Acute Regulatory Protein (StAR) Binds Cholesterol with High Affinity and Modulates the Dynamics of Mitochondrial Membrane Domains*

StAR mediates the rate-limiting step of steroidogenesis, delivery of cholesterol to the inner mitochondrial membrane. However, the mechanism whereby cholesterol translocation is accomplished has not been resolved. Recombinant StAR proteins lacking the first N-terminal 62 amino acids comprising the mitochondrial targeting sequence were used to determine if StAR binds cholesterol and alters mitochondrial membrane cholesterol domains to enhance sterol transfer.

I) A fluorescent NBD-cholesterol binding assay revealed 2 sterol binding sites ( $K_d$ s near 32 nM) while the inactive A218V N-62 StAR mutant had only a single binding site with 8-fold lower affinity.

II) NBD-cholesterol spectral shifts and fluorescence resonance energy transfer (FRET) from StAR tryptophan residues to NBD-cholesterol showed (i) close molecular interaction between these molecules ( $R_{2/3}=33 \text{ \AA}$ ), and (ii) sensitized NBD-cholesterol emission from only one of the two sterol binding sites.

III) Circular dichroism showed that cholesterol binding induced a change in StAR secondary structure.

IV) A fluorescent sterol transfer assay that did not require separation of donor and acceptor mitochondrial membranes demonstrated that StAR enhanced mitochondrial sterol transfer as much as 100-fold and induced/increased the formation of rapidly transferable cholesterol domains in isolated mitochondrial membranes. StAR was 67-

fold more effective in transferring cholesterol from mitochondria of steroidogenic MA-10 cells than from human fibroblast mitochondria. In contrast, sterol carrier protein-2 (SCP-2) was only 2.2-fold more effective in mediating sterol transfer from steroidogenic cell mitochondria.

Taken together these data showed that StAR is a cholesterol binding protein, preferentially enhances sterol transfer from steroidogenic cell mitochondria, and interacts with mitochondrial membranes to alter their sterol domain structure and dynamics.

### *5.2 Ligand Specificity and Conformational Dependence of the Hepatocyte Nuclear Factor-4 $\alpha$ (HNF-4 $\alpha$ )*

HNF-4 $\alpha$  controls the expression of genes encoding proteins involved in lipid and carbohydrate metabolism. Fatty acyl-CoA thioesters have recently been proposed to be naturally occurring ligands of HNF-4 $\alpha$  and to regulate its transcriptional activity as function of their chain length and degree of unsaturation (45). However, the apparent low affinities ( $\mu\text{M}$   $K_{\text{d}}$ s) obtained with a radiolabeled fatty acyl-CoA ligand binding assay raised questions regarding the physiological significance of this finding. Furthermore, it is not known whether interaction with fatty acyl-CoA alters the structure of HNF-4 $\alpha$ . These issues were examined using rat recombinant HNF-4 $\alpha$  ligand binding domain (HNF-4 $\alpha$ LBD) in conjunction with photon counting fluorescence and circular dichroism.

I) Fluorescence resonance energy transfer (FRET) between HNF-4 $\alpha$ LBD tryptophan (Trp) and *cis*-parinaroyl-CoA (cPNA-CoA) yielded an intermolecular distance of  $\leq 42\text{\AA}$ , thus pointing to direct molecular interaction rather than nonspecific coaggregation.

II) Quenching of HNF-4 $\alpha$ LBD intrinsic Trp fluorescence by fatty acyl CoAs (*e.g.*, pamitoyl-, stearoyl-, linoleoyl-, arachidonoyl-CoAs) yielded a single binding site with  $K_{\text{d}}$ s of 1.6–4.0 nM. These affinities were 2–3 orders of magnitude higher than those previously derived by radiolabeled fatty acyl-CoA ligand binding assay.

III) Binding of fatty acyl-CoAs was specific as the binding affinities of the respective free fatty acids (FFA) or free CoA ( $K_{ds}$  of 421–742 nM) were significantly lower.

IV) Circular dichroism demonstrated that the HNF-4 $\alpha$ LBD secondary structure was significantly and differentially altered by fatty acyl-CoA binding. The opposite effects of saturated versus polyunsaturated fatty acyl-CoAs on HNF-4 $\alpha$ LBD secondary structure correlated with their opposite regulatory effects on HNF-4 $\alpha$  function.

V) The CoA thioesters of some hypolipidemic peroxisome proliferators bind with high affinity ( $K_{ds}$  as low as 2.6 nM) to HNF-4 $\alpha$ LBD thus indicating that HNF-4 $\alpha$  may serve as target for these drugs.

In summary, these data demonstrate for the first time high affinity binding to HNF-4 $\alpha$  of fatty and xenobiotic acyl-CoAs in the physiological range, resulting in significantly altered HNF-4 $\alpha$  conformation.

### 5.3 *Studies on Physical and Functional Interaction of Acyl-CoA Binding Protein (ACBP) and Hepatocyte Nuclear Factor-4 $\alpha$ (HNF-4 $\alpha$ )*

Although ACBP has been detected in the nucleus, it is not known whether ACBP may directly and/or functionally interact with a nuclear LCFA-CoA binding protein such as HNF-4 $\alpha$  to regulate transcription. Four lines of evidence showed that ACBP physically interacted with HNF-4 $\alpha$  *in vitro* and in intact cells:

I) Circular dichroism detected significant changes in secondary structure in a mixture of HNF-4 $\alpha$  and ACBP.

II) Specific antisera to ACBP or HNF-4 $\alpha$  coimmunoprecipitated both proteins.

III) Double immunolabeling and laser scanning confocal microscopy (LSCM) of rat hepatoma cells and transfected COS-7 cells significantly colocalized ACBP and HNF-4 $\alpha$  in the nucleus of cultured hepatoma cells, distributed in the perinuclear region close to the nuclear membrane.

IV) LSCM fluorescence resonance energy transfer (FRET) determined an intermolecular distance of 53 Å between ACBP and HNF-4 $\alpha$  in rat hepatoma cell nuclei.

V) The functional significance of ACBP interaction with HNF-4 $\alpha$  was evidenced by mammalian two-hybrid and transactivation assays.

VI) Transfection assays showed that increasing ACBP overexpression in COS-7 or rat hepatoma cells enhanced transactivation of a HNF-4 $\alpha$ -dependent luciferase reporter plasmid by 3.5 and 1.8-fold, respectively, while treatment with antisense ACBP expression vectors resulted in dose-dependent inhibition.

VII) LSCM examination of individual rat hepatoma cells, triple fluorescent labeled to detect HNF-4 $\alpha$ , ACBP and luciferase (transfected with a reporter plasmid), showed a high correlation ( $r^2$ , 0.936) between the level of luciferase and the level of ACBP expression.

In summary, ACBP not only physically interacted with HNF-4 $\alpha$  *in vitro* and in intact cells, but ACBP expression level directly correlated with HNF-4 $\alpha$ -mediated transactivation.



## REFERENCES

1. Schroeder, F., Gallegos, A. M., Atshaves, B. P., Storey, S. M., McIntosh, A. L., Petrescu, A. D., Huang, H., Starodub, O., Chao, H., Yang, H., Frolov, A., and Kier, A. B. (2001) *Exp. Biol. Med. (Maywood.)* **226**, 873-890
2. Simons, K. and Ikonen, E. (2000) *Science* **290**, 1721-1726
3. Frolov, A., Petrescu, A., Atshaves, B. P., So, P. T., Gratton, E., Serrero, G., and Schroeder, F. (2000) *J. Biol. Chem.* **275**, 12769-12780
4. Hao, M. and Maxfield, F. R. (2000) *J. Biol. Chem.* **275**, 15279-15286
5. Uittenbogaard, A., Ying, Y., and Smart, E. J. (1998) *J. Biol. Chem.* **273**, 6525-6532
6. Schroeder, F., Frolov, A., Schoer, J., Gallegos, A., Atshaves, B. P., Stelowich, N. J., Scott, A. I., and Kier, A. B. (1998) in *Intracellular Cholesterol Trafficking*, (Chang T.Y. and Freeman D.A., eds.) pp.213-234, Kluwer Academic Publishers, Norwell, MA.
7. Gallegos, A. M., Atshaves, B. P., Storey, S., Schoer, J., Kier, A. B., and Schroeder, F. (2002) *Chem. Phys. Lipids* **116**, 19-38
8. Neufeld, E. B., Wastney, M., Patel, S., Suresh, S., Cooney, A. M., Dwyer, N. K., Roff, C. F., Ohno, K., Morris, J. A., Carstea, E. D., Incardona, J. P., Strauss, J. F., III, Vanier, M. T., Patterson, M. C., Brady, R. O., Pentchev, P. G., and Blanchette-Mackie, E. J. (1999) *J. Biol. Chem.* **274**, 9627-9635
9. Schmitz, G., Kaminski, W. E., and Orso, E. (2000) *Curr. Opin. Lipidol.* **11**, 493-501
10. Hayden, M. R., Clee, S. M., Brooks-Wilson, A., Genest, J., Jr., Attie, A., and Kastelein, J. J. (2000) *Curr. Opin. Lipidol.* **11**, 117-122
11. Stocco, D. M. and Clark, B. J. (1996) *Endocr. Rev.* **17**, 221-244
12. Cherradi, N., Rossier, M. F., Vallotton, M. B., Timberg, R., Friedberg, I., Orly, J., Wang, X. J., Stocco, D. M., and Capponi, A. M. (1997) *J. Biol. Chem.* **272**,

7899-7907

13. Arakane, F., Sugawara, T., Nishino, H., Liu, Z., Holt, J. A., Pain, D., Stocco, D. M., Miller, W. L., and Strauss, J. F., III (1996) *Proc. Natl. Acad. Sci. U.S.A* **93**, 13731-13736
14. Kallen, C. B., Billheimer, J. T., Summers, S. A., Stayrook, S. E., Lewis, M., and Strauss, J. F., III (1998) *J. Biol. Chem.* **273**, 26285-26288
15. Tsujishita, Y. and Hurley, J. H. (2000) *Nat. Struct. Biol* **7**, 408-414
16. Arakane, F., King, S. R., Du, Y., Kallen, C. B., Walsh, L. P., Watari, H., Stocco, D. M., and Strauss, J. F., III (1997) *J. Biol. Chem.* **272**, 32656-32662
17. Christenson, L. K. and Strauss, J. F., III (2000) *Biochim. Biophys. Acta* **1529**, 175-187
18. McArthur, M. J., Atshaves, B. P., Frolov, A., Foxworth, W. D., Kier, A. B., and Schroeder, F. (1999) *J. Lipid Res.* **40**, 1371-1383
19. Storch, J. and Thumser, A. E. (2000) *Biochim. Biophys. Acta* **1486**, 28-44
20. Gossett, R. E., Frolov, A. A., Roths, J. B., Behnke, W. D., Kier, A. B., and Schroeder, F. (1996) *Lipids* **31**, 895-918
21. Hubbell, T., Behnke, W. D., Woodford, J. K., and Schroeder, F. (1994) *Biochemistry* **33**, 3327-3334
22. Frolov, A. and Schroeder, F. (1998) *J. Biol. Chem.* **273**, 11049-11055
23. Thumser, A. E., Voysey, J. E., and Wilton, D. C. (1994) *Biochem. J.* **301**, 801-806
24. Frolov, A., Cho, T. H., Billheimer, J. T., and Schroeder, F. (1996) *J. Biol. Chem.* **271**, 31878-31884
25. Wanders, R. J., Denis, S., Wouters, F., Wirtz, K. W., and Seedorf, U. (1997) *Biochem. Biophys. Res. Commun.* **236**, 565-569
26. Guidotti, A., Forchetti, C. M., Corda, M. G., Konkell, D., Bennett, C. D., and Costa, E. (1983) *Proc. Natl. Acad. Sci. U.S.A* **80**, 3531-3535
27. Mogensen, I. B., Schulenberg, H., Hansen, H. O., Spener, F., and Knudsen, J. (1987) *Biochem. J.* **241**, 189-192

28. Knudsen, J., Hojrup, P., Hansen, H. O., Hansen, H. F., and Roepstorff, P. (1989) *Biochem. J.* **262**, 513-519
29. Rosendal, J., Ertbjerg, P., and Knudsen, J. (1993) *Biochem. J.* **290 ( Pt 2)**, 321-326
30. Mandrup, S., Sorensen, R. V., Helledie, T., Nohr, J., Baldursson, T., Gram, C., Knudsen, J., and Kristiansen, K. (1998) *J. Biol. Chem.* **273**, 23897-23903
31. Franch, J., Knudsen, J., Ellis, B. A., Pedersen, P. K., Cooney, G. J., and Jensen, J. (2002) *Diabetes* **51**, 449-454
32. Yang, Y., Pritchard, P. H., Bhuiyan, J., Secombe, D. W., and Moghadasian, M. H. (2001) *Lipids* **36**, 595-600
33. Brown, A. S. and Hall, P. F. (1991) *Biochem. Biophys. Res. Commun.* **180**, 609-614
34. Abo-Hashema, K. A., Cake, M. H., Lukas, M. A., and Knudsen, J. (2001) *Int. J. Biochem. Cell. Biol.* **33**, 807-815
35. Beato, M., Herrlich, P., and Schutz, G. (1995) *Cell* **83**, 851-857
36. Mangelsdorf, D. J. and Evans, R. M. (1995) *Cell* **83**, 841-850
37. Laudet, V. (1997) *J. Mol. Endocrinol.* **19**, 207-226
38. Maglich, J. M., Sluder, A., Guan, X., Shi, Y., McKee, D. D., Carrick, K., Kamdar, K., Willson, T. M., and Moore, J. T. (2001) *Genome Biol.* **2**, Research 0029
39. Giguere, V. (1999) *Endocr. Rev.* **20**, 689-725
40. Chawla, A., Repa, J. J., Evans, R. M., and Mangelsdorf, D. J. (2001) *Science* **294**, 1866-1870
41. McKenna, N. J., Lanz, R. B., and O'Malley, B. W. (1999) *Endocr. Rev.* **20**, 321-344
42. Aranda, A. and Pascual, A. (2001) *Physiol Rev.* **81**, 1269-1304
43. Iyemere, V. P., Davies, N. H., and Brownlee, G. G. (1998) *Nucleic Acids Res.* **26**, 2098-2104
44. Mietus-Snyder, M., Sladek, F. M., Ginsburg, G. S., Kuo, C. F., Ladas, J. A.,

- Darnell, J. E., Jr., and Karathanasis, S. K. (1992) *Mol. Cell. Biol.* **12**, 1708-1718
45. Hertz, R., Magenheim, J., Berman, I., and Bar-Tana, J. (1998) *Nature* **392**, 512-516
46. Rajas, F., Gautier, A., Bady, I., Montano, S., and Mithieux, G. (2002) *J. Biol. Chem.* **277**, 15736-15744
47. Elholm, M., Dam, I., Jorgensen, C., Krogsdam, A. M., Holst, D., Kratchmarova, I., Gottlicher, M., Gustafsson, J. A., Berge, R., Flatmark, T., Knudsen, J., Mandrup, S., and Kristiansen, K. (2001) *J. Biol. Chem.* **276**, 21410-21416
48. Evans, M., Park, Y., Pariza, M., Curtis, L., Kuebler, B., and McIntosh, M. (2001) *Lipids* **36**, 1223-1232
49. Duplus, E. and Forest, C. (2002) *Biochem. Pharmacol.* **64**, 893-901
50. Aoyama, T., Peters, J. M., Iritani, N., Nakajima, T., Furihata, K., Hashimoto, T., and Gonzalez, F. J. (1998) *J. Biol. Chem.* **273**, 5678-5684
51. Helledie, T., Grontved, L., Jensen, S. S., Kiilerich, P., Rietveld, L., Albrektsen, T., Boysen, M. S., Nohr, J., Larsen, L. K., Fleckner, J., Stunnenberg, H. G., Kristiansen, K., and Mandrup, S. (2002) *J. Biol. Chem.* **277**, 26821-26830
52. Rosen, E. D., Sarraf, P., Troy, A. E., Bradwin, G., Moore, K., Milstone, D. S., Spiegelman, B. M., and Mortensen, R. M. (1999) *Mol. Cell* **4**, 611-617
53. Ou, J., Tu, H., Shan, B., Luk, A., DeBose-Boyd, R. A., Bashmakov, Y., Goldstein, J. L., and Brown, M. S. (2001) *Proc. Natl. Acad. Sci. U.S.A* **98**, 6027-6032
54. Yoshikawa, T., Shimano, H., Yahagi, N., Ide, T., Amemiya-Kudo, M., Matsuzaka, T., Nakakuki, M., Tomita, S., Okazaki, H., Tamura, Y., Iizuka, Y., Ohashi, K., Takahashi, A., Sone, H., Osuga, J. J., Gotoda, T., Ishibashi, S., and Yamada, N. (2002) *J. Biol. Chem.* **277**, 1705-1711
55. Thurmond, D. C., Baillie, R. A., and Goodridge, A. G. (1998) *J. Biol. Chem.* **273**, 15373-15381
56. Li, Q., Yamamoto, N., Morisawa, S., and Inoue, A. (1993) *J. Cell. Biochem.* **51**, 458-464

57. de Urquiza, A. M., Liu, S., Sjoberg, M., Zetterstrom, R. H., Griffiths, W., Sjoval, J., and Perlmann, T. (2000) *Science* **290**, 2140-2144
58. Chen, W. S., Manova, K., Weinstein, D. C., Duncan, S. A., Plump, A. S., Prezioso, V. R., Bachvarova, R. F., and Darnell, J. E., Jr. (1994) *Genes Dev.* **8**, 2466-2477
59. Miquerol, L., Lopez, S., Cartier, N., Tulliez, M., Raymondjean, M., and Kahn, A. (1994) *J. Biol. Chem.* **269**, 8944-8951
60. Yamagata, K., Furuta, H., Oda, N., Kaisaki, P. J., Menzel, S., Cox, N. J., Fajans, S. S., Signorini, S., Stoffel, M., and Bell, G. I. (1996) *Nature* **384**, 458-460
61. Hani, E. H., Suaud, L., Boutin, P., Chevre, J. C., Durand, E., Philippi, A., Demenais, F., Vionnet, N., Furuta, H., Velho, G., Bell, G. I., Laine, B., and Froguel, P. (1998) *J. Clin. Invest.* **101**, 521-526
62. Navas, M. A., Munoz-Elias, E. J., Kim, J., Shih, D., and Stoffel, M. (1999) *Diabetes* **48**, 1459-1465
63. Suaud, L., Hemimou, Y., Formstecher, P., and Laine, B. (1999) *Diabetes* **48**, 1162-1167
64. Sladek, F. M., Zhong, W. M., Lai, E., and Darnell, J. E., Jr. (1990) *Genes Dev.* **4**, 2353-2365
65. Hadzopoulou-Cladaras, M., Kistanova, E., Evagelopoulou, C., Zeng, S., Cladaras, C., and Ladias, J. A. (1997) *J. Biol. Chem.* **272**, 539-550
66. Hayhurst, G. P., Lee, Y. H., Lambert, G., Ward, J. M., and Gonzalez, F. J. (2001) *Mol. Cell. Biol.* **21**, 1393-1403
67. Naiki, T., Nagaki, M., Shidoji, Y., Kojima, H., Imose, M., Kato, T., Ohishi, N., Yagi, K., and Moriwaki, H. (2002) *J. Biol. Chem.* **277**, 14011-14019
68. Pare, J. F., Roy, S., Galarneau, L., and Belanger, L. (2001) *J. Biol. Chem.* **276**, 13136-13144
69. Qian, A., Cai, Y., Magee, T. R., and Wan, Y. J. (2000) *Biochem. Biophys. Res. Commun.* **276**, 837-842
70. Bailly, A., Torres-Padilla, M. E., Tinel, A. P., and Weiss, M. C. (2001) *Nucleic*

*Acids Res.* **29**, 3495-3505

71. Stoffel, M. and Duncan, S. A. (1997) *Proc. Natl. Acad. Sci. U.S.A* **94**, 13209-13214
72. Gregori, C., Porteu, A., Lopez, S., Kahn, A., and Pichard, A. L. (1998) *J. Biol. Chem.* **273**, 25237-25243
73. Roth, U., Jungermann, K., and Kietzmann, T. (2002) *Biochem. J.* **365**, 223-228
74. Stafford, J. M., Waltner-Law, M., and Granner, D. K. (2001) *J. Biol. Chem.* **276**, 3811-3819
75. Bartoov-Shifman, R., Hertz, R., Wang, H., Wollheim, C. B., Bar-Tana, J., and Walker, M. D. (2002) *J. Biol. Chem.* **277**, 25914-25919
76. Metzger, S., Halaas, J. L., Breslow, J. L., and Sladek, F. M. (1993) *J. Biol. Chem.* **268**, 16831-16838
77. Ladas, J. A., Hadzopoulou-Cladaras, M., Kardassis, D., Cardot, P., Cheng, J., Zannis, V., and Cladaras, C. (1992) *J. Biol. Chem.* **267**, 15849-15860
78. Ginsburg, G. S., Ozer, J., and Karathanasis, S. K. (1995) *J. Clin. Invest.* **96**, 528-538
79. Murao, K., Bassyouni, H., Taylor, A. H., Wanke, I. E., and Wong, N. C. (1997) *Biochemistry* **36**, 301-306
80. De Fabiani, E., Mitro, N., Anzulovich, A. C., Pinelli, A., Galli, G., and Crestani, M. (2001) *J. Biol. Chem.* **276**, 30708-30716
81. Garuti, R., Croce, M. A., Piccinini, L., Tiozzo, R., Bertolini, S., and Calandra, S. (2002) *Gene* **283**, 133-143
82. You, M., Fischer, M., Cho, W. K., and Crabb, D. (2002) *Arch. Biochem. Biophys.* **398**, 79-86
83. Boesch, J. S., Miskimins, R., Miskimins, W. K., and Lindahl, R. (1999) *Arch. Biochem. Biophys.* **361**, 223-230
84. Hara, H. and Adachi, T. (2002) *Mol. Pharmacol.* **61**, 194-200
85. Jover, R., Bort, R., Gomez-Lechon, M. J., and Castell, J. V. (2001) *Hepatology* **33**, 668-675

86. Pineda, T., I, Jamshidi, Y., Flavell, D. M., Fruchart, J. C., and Staels, B. (2002) *Mol. Endocrinol.* 1013-1028
87. Torra, I. P., Chinetti, G., Duval, C., Fruchart, J. C., and Staels, B. (2001) *Curr. Opin. Lipidol.* **12**, 245-254
88. Horton, J. D., Goldstein, J. L., and Brown, M. S. (2002) *J. Clin. Invest.* **109**, 1125-1131
89. Edwards, P. A. and Ericsson, J. (1999) *Annu. Rev. Biochem* **68**, 157-185
90. Shimano, H. (2001) *Prog. Lipid Res.* **40**, 439-452
91. Jump, D. B. (2002) *Curr. Opin. Lipidol.* **13**, 155-164
92. Goldstein, J. L. and Brown, M. S. (1990) *Nature* **343**, 425-430
93. Brown, M. S. and Goldstein, J. L. (1997) *Cell* **89**, 331-340
94. Ericsson, J., Jackson, S. M., Lee, B. C., and Edwards, P. A. (1996) *Proc. Natl. Acad. Sci. U.S.A* **93**, 945-950
95. Guan, G., Dai, P., and Shechter, I. (1998) *J. Biol. Chem.* **273**, 12526-12535
96. Magana, M. M. and Osborne, T. F. (1996) *J. Biol. Chem.* **271**, 32689-32694
97. Lopez, J. M., Bennett, M. K., Sanchez, H. B., Rosenfeld, J. M., and Osborne, T. E. (1996) *Proc. Natl. Acad. Sci. U.S.A* **93**, 1049-1053
98. Tabor, D. E., Kim, J. B., Spiegelman, B. M., and Edwards, P. A. (1998) *J. Biol. Chem.* **273**, 22052-22058
99. Swinnen, J. V., Alen, P., Heyns, W., and Verhoeven, G. (1998) *J. Biol. Chem.* **273**, 19938-19944
100. Ericsson, J., Jackson, S. M., Kim, J. B., Spiegelman, B. M., and Edwards, P. A. (1997) *J. Biol. Chem.* **272**, 7298-7305
101. Horton, J. D. and Shimomura, I. (1999) *Curr. Opin. Lipidol.* **10**, 143-150
102. Edwards, P. A., Tabor, D., Kast, H. R., and Venkateswaran, A. (2000) *Biochim. Biophys. Acta* **1529**, 103-113
103. Sakakura, Y., Shimano, H., Sone, H., Takahashi, A., Inoue, N., Toyoshima, H., Suzuki, S., Yamada, N., and Inoue, K. (2001) *Biochem. Biophys. Res. Commun.* **286**, 176-183

104. Wolf, G. (1999) *Nutr. Rev.* **57**, 196-198
105. Rennert, H., Fischer, R. T., Alvarez, J. G., Trzaskos, J. M., and Strauss, J. F., III (1990) *Endocrinology* **127**, 738-746
106. Axelson, M. and Larsson, O. (1995) *J. Biol. Chem.* **270**, 15102-15110
107. Lin, D., Sugawara, T., Strauss, J. F., III, Clark, B. J., Stocco, D. M., Saenger, P., Rogol, A., and Miller, W. L. (1995) *Science* **267**, 1828-1831
108. Sugawara, T., Holt, J. A., Kiriakidou, M., and Strauss, J. F., III (1996) *Biochemistry* **35**, 9052-9059
109. Nomura, M., Nawata, H., and Morohashi, K. (1996) *J. Biol. Chem.* **271**, 8243-8249
110. Sugawara, T., Lin, D., Holt, J. A., Martin, K. O., Javitt, N. B., Miller, W. L., and Strauss, J. F., III (1995) *Biochemistry* **34**, 12506-12512
111. Xu, J., Nakamura, M. T., Cho, H. P., and Clarke, S. D. (1999) *J. Biol. Chem.* **274**, 23577-23583
112. Yahagi, N., Shimano, H., Hasty, A. H., Amemiya-Kudo, M., Okazaki, H., Tamura, Y., Iizuka, Y., Shionoiri, F., Ohashi, K., Osuga, J., Harada, K., Gotoda, T., Nagai, R., Ishibashi, S., and Yamada, N. (1999) *J. Biol. Chem.* **274**, 35840-35844
113. Marrapodi, M. and Chiang, J. Y. (2000) *J. Lipid Res.* **41**, 514-520
114. Hertz, R., Bishara-Shieban, J., and Bar-Tana, J. (1995) *J. Biol. Chem.* **270**, 13470-13475
115. Nakshatri, H. and Chambon, P. (1994) *J. Biol. Chem.* **269**, 890-902
116. Hertz, R., Sheena, V., Kalderon, B., Berman, I., and Bar-Tana, J. (2001) *Biochem. Pharmacol.* **61**, 1057-1062
117. Yamamoto, N., Li, Q. L., Mita, S., Morisawa, S., and Inoue, A. (2001) *Horm. Metab. Res.* **33**, 131-137
118. Dong, D., Ruuska, S. E., Levinthal, D. J., and Noy, N. (1999) *J. Biol. Chem.* **274**, 23695-23698
119. Budhu, A. S. and Noy, N. (2002) *Mol. Cell. Biol.* **22**, 2632-2641



120. Delva, L., Bastie, J. N., Rochette-Egly, C., Kraiba, R., Balitrand, N., Despouy, G., Chambon, P., and Chomienne, C. (1999) *Mol. Cell. Biol.* **19**, 7158-7167
121. Wolfrum, C., Borrmann, C. M., Borchers, T., and Spener, F. (2001) *Proc. Natl. Acad. Sci. U.S.A* **98**, 2323-2328
122. Adida, A. and Spener, F. (2002) *Prostaglandins Leukot. Essent. Fatty Acids* **67**, 91-98
123. Helledie, T., Antonius, M., Sorensen, R. V., Hertzelt, A. V., Bernlohr, D. A., Kolvraa, S., Kristiansen, K., and Mandrup, S. (2000) *J. Lipid Res.* **41**, 1740-1751
124. Schlegel, A., Wang, C., Katzenellenbogen, B. S., Pestell, R. G., and Lisanti, M. P. (1999) *J. Biol. Chem.* **274**, 33551-33556
125. Smart, E. J. and van der Westhuyzen, D. R. (1998) in *Intracellular Cholesterol Trafficking*, (Chang T.Y. and Freeman D.A., eds.), pp.253-272, Kluwer Academic Publishers, Norwell, MA
126. Fielding, C. J., Bist A., and Fielding P.E. (1998) in *Intracellular Cholesterol Trafficking*, (Chang T.Y. and Freeman D.A., eds.), pp. 273-288, Kluwer Academic Publishers, Norwell, MA
127. Neufeld, E. B. (1998) in *Intracellular Cholesterol Trafficking*, (Chang T.Y. and Freeman D.A., eds.) pp.93-121, Kluwer Academic Publishers, Norwell, MA
128. Chanderbhan, R. F., Kharroubi, A., Pastuszyn, A., Gallo, L. L., and Scallan, T. (1998) in *Intracellular Cholesterol Trafficking*, (Chang T.Y. and Freeman D.A., eds.), pp.97-212, Kluwer Academic Publisher, Norwell, MA
129. Pfeifer, S. M., Furth, E. E., Ohba, T., Chang, Y. J., Rennert, H., Sakuragi, N., Billheimer, J. T., and Strauss, J. F., III (1993) *J. Steroid Biochem. Mol. Biol.* **47**, 167-172
130. Choi, Y.-S. and Freeman, D. A. (1998) in *Intracellular Cholesterol Trafficking*, (Chang T.Y. and Freeman D.A., eds.), pp.109-121, Kluger Academic Publishers, Norwell, MA

131. Gallegos, A. M., Schoer, J. K., Starodub, O., Kier, A. B., Billheimer, J. T., and Schroeder, F. (2000) *Chem. Phys. Lipids* **105**, 9-29
132. Stocco, D. M. (1999) *Medicina (B Aires)* **59**, 538-539
133. Stocco, D.M. and Strauss, J. F. (1998) in *Intracellular Cholesterol Trafficking*, (Chang T.Y. and Freeman D.A., eds.), pp. 169-182, Kluger Academic Publishers, Norwell, MA
134. Stocco, D. M. (1996) in *The Leydig Cell*, (Payne, A. H., Hardy, M. P., and Russell, L. D., eds.) Cache River Press, Vienna, IL
135. Thomson, M. (1998) *Horm. Metab Res.* **30**, 16-28
136. Toren, D., Menon, K. M. L., Forchielli, E., and Dorfman, R. I. (1964) *Steroids* **3**, 381-390
137. Seedorf, U. (1998) in *Intracellular Cholesterol Trafficking*, (Chang T.Y. and Freeman D.A., eds.), pp. 233-252, Kluwer Academic Publishers, Norwell, MA
138. Seedorf, U., Raabe, M., Ellinghaus, P., Kannenberg, F., Fobker, M., Engel, T., Denis, S., Wouters, F., Wirtz, K. W., Wanders, R. J., Maeda, N., and Assmann, G. (1998) *Genes Dev.* **12**, 1189-1201
139. Stocco, D. M. (2000) *Biochim. Biophys. Acta* **1486**, 184-197
140. Bose, H. S., Sugawara, T., Strauss, J. F., III, and Miller, W. L. (1996) *N. Engl. J. Med.* **335**, 1870-1878
141. Caron, K. M., Soo, S. C., Wetsel, W. C., Stocco, D. M., Clark, B. J., and Parker, K. L. (1997) *Proc. Natl. Acad. Sci. U.S.A* 11540-11545
142. King, S. R., Ronen-Fuhrmann, T., Timberg, R., Clark, B. J., Orly, J., and Stocco, D. M. (1995) *Endocrinology* **136**, 5165-5176
143. Arakane, F., Kallen, C. B., Watari, H., Foster, J. A., Sepuri, N. B., Pain, D., Stayrook, S. E., Lewis, M., Gerton, G. L., and Strauss, J. F., III (1998) *J. Biol. Chem.* **273**, 16339-16345
144. Ponting, C. P. and Aravind, L. (1999) *Trends Biochem Sci.* **24**, 130-132

145. Mueller, E., Drori, S., Aiyer, A., Yie, J., Sarraf, P., Chen, H., Hauser, S., Rosen, E. D., Ge, K., Roeder, R. G., and Spiegelman, B. M. (2002) *J. Biol. Chem.* **277**, 41925-41930
146. Fischer, R. T., Stephenson, F. A., Shafiee, A., and Schroeder, F. (1984) *Chem. Phys. Lipids* **36**, 1-14
147. Fischer, R. T., Cowlen, M. S., Dempsey, M. E., and Schroeder, F. (1985) *Biochemistry* **24**, 3322-3331
148. Matsuura, J. E., George, H. J., Ramachandran, N., Alvarez, J. G., Strauss, J. F., III, and Billheimer, J. T. (1993) *Biochemistry* **32**, 567-572
149. Clark, B. J., Wells, J., King, S. R., and Stocco, D. M. (1994) *J. Biol. Chem.* **269**, 28314-28322
150. Lowry O.H., Rosebrough N.J., Farr A.L., and Randall, R. J. (1951) *J. Biol. Chem.* **193**, 264-275
151. Stolowich, N., Frolov, A., Petrescu, A. D., Scott, A. I., Billheimer, J. T., and Schroeder, F. (1999) *J. Biol. Chem.* **274**, 35425-35433
152. Segel, I. H. (1983) in *Enzyme Kinetics*, (Segel, I. H., ed.), pp.347-371, John Wiley & Sons, Inc., New York
153. Frolov, A., Cho, T. H., Murphy, E. J., and Schroeder, F. (1997) *Biochemistry* **36**, 6545-6555
154. Forster, T. (1967) in *Comprehensive Biochemistry*, (Florkin, M., and Statz, E. H., eds.), pp.61-77, Elsevier Science Publishing, Co. Inc., New York
155. Frolov, A., Miller, K., Billheimer, J. T., Cho, T. H., and Schroeder, F. (1997) *Lipids* **32**, 1201-1209
156. Lakowicz, J. R. (1999) in *Principles of Fluorescence Spectroscopy*, (Lakowicz, J. R., ed.), pp. 237-266, Plenum Publishing Corp., New York
157. Parker, C. A. (1968) in *Photoluminescence in Solution*, p.84, Elsevier Science Publishers B.V., Amsterdam
158. Wu, P. and Brand, L. (1994) *Anal. Biochem.* **218**, 1-13

159. Lakowicz, J. R. (1999) in *Principles in Fluorescence Spectroscopy*, (Lakowicz, J. R., ed.), pp. 367-394, Plenum Publishing Corp., New York
160. Schroeder, F., Frolov, A., Starodub, O., Atshaves, B. B., Russell, W., Petrescu, A., Huang, H., Gallegos, A. M., McIntosh, A., Tahotna, D., Russell, D. H., Billheimer, J. T., Baum, C. L., and Kier, A. B. (2000) *J. Biol. Chem.* **275**, 25547-25555
160. Jatzke, C., Hinz, H. J., Seedorf, U., and Assmann, G. (1999) *Biochim. Biophys. Acta* **1432**, 265-274
161. Frolov, A., Woodford, J. K., Murphy, E. J., Billheimer, J. T., and Schroeder, F. (1996) *J. Lipid Res.* **37**, 1862-1874
162. Frolov, A., Woodford, J. K., Murphy, E. J., Billheimer, J. T., and Schroeder, F. (1996) *J. Biol. Chem.* **271**, 16075-16083
163. Haberland, M. E. and Reynolds, J. A. (1973) *Proc. Natl. Acad. Sci. U.S.A* **70**, 2313-2316
164. Avdulov, N. A., Chochina, S. V., Igbavboa, U., Warden, C. S., Vassiliev, A. V., and Wood, W. G. (1997) *J. Neurochem.* **69**, 1746-1752
165. Avdulov, N. A., Chochina, S. V., Igbavboa, U., Warden, C. S., Schroeder, F., and Wood, W. G. (1999) *Biochim. Biophys. Acta* **1437**, 37-45
166. Liu, R., Siemiarczuk, A., and Sharom, F. J. (2000) *Biochemistry* **39**, 14927-14938
167. Bose, H. S., Baldwin, M. A., and Miller, W. L. (1998) *Biochemistry* **37**, 9768-9775
168. Schroeder, F., Myers-Payne, S. C., Billheimer, J. T., and Wood, W. G. (1995) *Biochemistry* **34**, 11919-11927
169. Liu, Z., Frolov, A., Schroeder, F., and Stocco, D. (1996) *Biol. Reprod.* **54**, 154(Abstr.549)
170. Schroeder, F., Jefferson, J.R., Powell, D., Incerpi, S., Woodford, J.K., Colles, S.M., Myers-Payne, S., Emge, T., Hubbell, T., Moncecchi, D., Prows, D.R., and Heyliger, C.E. (1993) *Mol. Cell. Biochem.* **123**, 73-83.

171. Schroeder, F., Butko, P., Hapala, I., and Scallen, T. J. (1990) *Lipids* **25**, 669-674
172. Woodford, J. K., Behnke, W. D., and Schroeder, F. (1995) *Mol. Cell. Biochem.* **152**, 51-62
173. Schroeder, F., Dempsey, M. E., and Fischer, R. T. (1985) *J. Biol. Chem.* **260**, 2904-2911
174. Woodford, J. K., Colles, S. M., Myers-Payne, S., Billheimer, J. T., and Schroeder, F. (1995) *Chem. Phys. Lipids* **76**, 73-84
175. Rosenblum, M. F., Huttler, C. R., and Strauss, J. F., III (1981) *Endocrinology* **109**, 1518-1527
176. Papadopoulos, V., Amri, H., Li, H., Boujrad, N., Vidic, B., and Garnier, M. (1997) *J. Biol. Chem.* **272**, 32129-32135
177. Sladek, F. (1994) *Liver Gene Expression*, VRG Landes Co., Austin, TX
178. Jiang, G., Nepomuceno, L., Hopkins, K., and Sladek, F. M. (1995) *Mol. Cell. Biol.* **15**, 5131-5143
179. Nakshatri, H. and Chambon, P. (1994) *J. Biol. Chem.* **269**, 890-902
180. Li, J., Ning, G., and Duncan, S. A. (2000) *Genes Dev.* **14**, 464-474
181. Zannis, V. I., Kan, H. Y., Kritis, A., Zanni, E., and Kardassis, D. (2001) *Front Biosci.* **6**, D456-D504
182. Shih, D. Q., Dansky, H. M., Fleisher, M., Assmann, G., Fajans, S. S., and Stoffel, M. (2000) *Diabetes* **49**, 832-837
183. Wang, H., Maechler, P., Antinozzi, P. A., Hagenfeldt, K. A., and Wollheim, C. B. (2000) *J. Biol. Chem.* **275**, 35953-35959
184. Carter, M. E., Gulick, T., Raisher, B. D., Caira, T., Ladas, J. A., Moore, D. D., and Kelly, D. P. (1993) *J. Biol. Chem.* **268**, 13805-13810
185. Knudsen, J., Jensen, M. V., Hansen, J. K., Faergeman, N. J., Neergaard, T. B., and Gaigg, B. (1999) *Mol. Cell. Biochem.* **192**, 95-103\
186. Elholm, M., Garras, A., Neve, S., Tornehave, D., Lund, T. B., Skorve, J., Flatmark, T., Kristiansen, K., and Berge, R. K. (2000) *J. Lipid Res.* **41**, 538-545

187. Bogan, A. A., Dallas-Yang, Q., Ruse, M. D., Jr., Maeda, Y., Jiang, G., Nepomuceno, L., Scanlan, T. S., Cohen, F. E., and Sladek, F. M. (2000) *J. Mol. Biol.* **302**, 831-851
188. Bar-Tana, J., Rose-Kahn, G., and Srebnik, M. (1985) *J. Biol. Chem.* **260**, 8404-8410
189. Kawaguchi, A., Yoshimura, T., and Okuda, S. (1981) *J. Biochem. (Tokyo)* **89**, 337-339
190. Juguelin, H. and Cassagne, C. (1984) *Anal. Biochem.* **142**, 329-335
191. Serrero, G., Frolov, A., Schroeder, F., Tanaka, K., and Gelhaar, L. (2000) *Biochim. Biophys. Acta* **1488**, 245-254
192. Nemezc, G., Hubbell, T., Jefferson, J. R., Lowe, J. B., and Schroeder, F. (1991) *Arch. Biochem. Biophys.* **286**, 300-309
193. Stryer, L. (1978) *Annu. Rev. Biochem.* **47**, 819-846
194. Petrescu, A. D., Gallegos, A. M., Okamura, Y., Strauss III, J. F., and Schroeder, F. (2001) *J. Biol. Chem.* **276**, 36970-36982
195. Compton, L. A. and Johnson, W. C., Jr. (1986) *Anal. Biochem.* **155**, 155-167
196. Lin, Q., Ruuska, S. E., Shaw, N. S., Dong, D., and Noy, N. (1999) *Biochemistry* **38**, 185-190
197. Ktistaki, E., Ktistakis, N. T., Papadogeorgaki, E., and Talianidis, I. (1995) *Proc. Natl. Acad. Sci. U.S.A* **92**, 9876-9880
198. Gossett, R., Kier, A. B., Schroeder, F., McConkey, D., Fadok, V., and Amoss, M. S., Jr. (1996) *J. Comp. Pathol.* **115**, 353-372
199. Gallegos, A. M., Atshaves, B. P., Storey, S. M., Starodub, O., Petrescu, A. D., Huang, H., McIntosh, A. L., Martin, G. G., Chao, H., Kier, A. B., and Schroeder, F. (2001) *Prog. Lipid Res.* **40**, 498-563
200. Bordewick, U., Heese, M., Borchers, T., Robenek, H., and Spener, F. (1989) *Biol. Chem. Hoppe Seyler* **370**, 229-238

201. Cattley, R. C., DeLuca, J., Elcombe, C., Fenner-Crisp, P., Lake, B. G., Marsman, D. S., Pastoor, T. A., Popp, J. A., Robinson, D. E., Schwetz, B., Tugwood, J., and Wahli, W. (1998) *Regul. Toxicol. Pharmacol.* **27**, 47-60
202. Chao, H., Martin, G. G., Russell, W. K., Waghela, S. D., Russell, D. H., Schroeder, F., and Kier, A. B. (2002) *Biochemistry* **41**, 10540-10553
203. Faergeman, N. J. and Knudsen, J. (1997) *Biochem. J.* **323** , 1-12
204. Wadum, M. C., Villadsen, J. K., Feddersen, S., Moller, R. S., Neergaard, T. B., Kragelund, B. B., Hojrup, P., Faergeman, N. J., and Knudsen, J. (2002) *Biochem. J.* **365**, 165-172
205. Jolly, C. A., Wilton, D. C., and Schroeder, F. (2000) *Biochim. Biophys. Acta* **1483**, 185-197
206. Gossett, R. E., Edmondson, R. D., Jolly, C. A., Cho, T. H., Russell, D. H., Knudsen, J., Kier, A. B., and Schroeder, F. (1998) *Arch. Biochem. Biophys.* **350**, 201-213
207. Rasmussen, J. T., Faergeman, N. J., Kristiansen, K., and Knudsen, J. (1994) *Biochem. J.* **299** , 165-170
208. Gaigg, B., Neergaard, T. B., Schneiter, R., Hansen, J. K., Faergeman, N. J., Jensen, N. A., Andersen, J. R., Friis, J., Sandhoff, R., Schroder, H. D., and Knudsen, J. (2001) *Mol. Biol. Cell* **12**, 1147-1160
209. Petrescu, A. D., Hertz, R., Bar-Tana, J., Schroeder, F., and Kier, A. B. (2002) *J. Biol. Chem.* **277**, 23988-23999
210. Jorgensen, C., Krogsdam, A. M., Kratchmarova, I., Willson, T. M., Knudsen, J., Mandrup, S., and Kristiansen, K. (2002) *Ann. N. Y. Acad. Sci.* **967**, 431-439
211. Kardassis, D., Falvey, E., Tsantili, P., Hadzopoulou-Cladaras, M., and Zannis, V. (2002) *Biochemistry* **41**, 1217-1228
212. Sauvaget, D., Chauffeton, V., Citadelle, D., Chatelet, F. P., Cywiner-Golenzner, C., Chambaz, J., Pincon-Raymond, M., Cardot, P., Le Beyec, J., and Ribeiro, A. (2002) *J. Biol. Chem.* **277**, 34540-34548
213. Johnson, W.C. (1999) *Proteins* **35**, 307-317

214. Wouters, F. S., Bastiaens, P. I., Wirtz, K. W., and Jovin, T. M. (1998) *EMBO J.* **17**, 7179-7189
215. Kenworthy, A. K. (2001) *Methods* **24**, 289-296
216. Laemmli, U. K. (1970) *Nature* **227**, 680-685
217. Gershoni, J. M. and Palade, G. E. (1982) *Anal. Biochem.* **124**, 396-405
218. Adra, C. N., Boer, P. H., and McBurney, M. W. (1987) *Gene* **60**, 65-74
219. Duplus, E., Glorian, M., and Forest, C. (2000) *J. Biol. Chem.* **275**, 30749-30752
220. Krishna, M., I and Das, U. N. (2001) *Nutrition* **17**, 126-151
221. Dhe-Paganon, S., Duda, K., Iwamoto, M., Chi, Y. I., and Shoelson, S. E. (2002) *J. Biol. Chem.* **277**, 37973-37976
222. Wisely, G. B., Miller, A. B., Davis, R. G., Thornquest, A. D., Jr., Johnson, R., Spitzer, T., Sefler, A., Shearer, B., Moore, J. T., Miller, A. B., Willson, T. M., and Williams, S. P. (2002) *Structure (Camb.)* **10**, 1225-1234
223. Coleman, R. A., Lewin, T. M., Van Horn, C. G., and Gonzalez-Baro, M. R. (2002) *J. Nutr.* **132**, 2123-2126



## APPENDIX

10/22/2002 02:05 3816347100 JBC PAGE 01/01  
 10/21/02 13:40 0970 882 4929 YIPP-SAFE 001

To: The American Society for Biochemistry  
 and Molecular Biology, Inc.  
 The Journal of Biological Chemistry

From: Anca D. Petrescu  
 Texas A&M University  
 CVML MS 4466  
 College Station, TX 77843  
 FAX: 979 8624929

October 21, 2002

I am a graduate student at Texas A&M University, Faculty of Toxicology and first author of two articles published in JBC, namely:

- Ligand Specificity and Conformational Dependence of the Hepatic Nuclear Factor-4 $\alpha$  (HNF-4 $\alpha$ ), AD Petrescu, R Hertz, J Bar-Tana, F Schroeder and AB Kiar, *JBC* 277 (No.27) 23988-23999, 2002.
- Steroidogenic Acute Regulatory Protein Binds Cholesterol and Modulates Mitochondrial Membrane Sterol Domain Dynamics, AD Petrescu, AM Gallegos, Y Okamura, JF Strauss III and F. Schroeder, *JBC* 276 (No.40), 36970-36982, 2001.

I would greatly appreciate if you allow me to reproduce the figures, tables and parts of the text of these two articles into my thesis dissertation : I am writing this thesis within my PhD program.

Thank you,

Anca Petrescu



PERMISSION GRANTED  
 as agent upon obtaining that of the author



OCT 22 2002

for the copyright owner  
 THE AMERICAN SOCIETY FOR BIOCHEMISTRY  
 & MOLECULAR BIOLOGY

## VITA

Name: Petrescu Anca Daniela  
Permanent address: 1300 Briar Cliff Dr. #101  
Bryan, TX 77802  
Education: B.S. in Biochemistry, University of Bucharest, Romania, 1979  
M.S. in Biochemistry, University of Bucharest, Romania, 1981  
Ph.D. in Toxicology, Texas A&M University, USA, 2003

### Publications:

1. **Petrescu AD**, Hertz R, Bar-Tana J, Schroeder F, Kier AB.: Ligand specificity and conformational dependence of the hepatic nuclear factor-4 $\alpha$  (HNF-4 $\alpha$ ). *J. Biol. Chem.* 277(27):23988-99, 2002.
2. Stolowich NJ, **Petrescu AD**, Huang H, Martin GG, Scott AI, Schroeder F. Sterol carrier protein-2: structure reveals function. *Cell Mol. Life Sci.* 59(2):193-212, 2002.
3. Schroeder F, Gallegos AM, Atshaves BP, Storey SM, McIntosh AL, **Petrescu AD**, Huang H, Starodub O, Chao H, Yang H, Frolov A, Kier AB.: Recent advances in membrane microdomains: rafts, caveolae, and intracellular cholesterol trafficking. *Exp. Biol. Med.* 226(10):873-90, 2001.
4. Gallegos AM, Atshaves BP, Storey SM, Starodub O, **Petrescu AD**, Huang H, McIntosh AL, Martin GG, Chao H, Kier AB, Schroeder F. Gene structure, intracellular localization, and functional roles of sterol carrier protein-2. *Prog. Lipid Res.* 40(6):498-563, 2001.
5. **Petrescu AD**, Gallegos AM, Okamura Y, Strauss JF 3rd, Schroeder F, : Steroidogenic acute regulatory protein binds cholesterol and modulates mitochondrial membrane sterol domain dynamics. *J. Biol. Chem.* 276(40):36970, 82, 2001.